Study on a Mixed-wettability Evaporator Surface of a Loop Thermosyphon

何, 洪斌

https://doi.org/10.15017/1866297

Study on a Mixed-wettability Evaporator Surface of a Loop Thermosyphon

Ph.D. Thesis

Hongbin He

Department of Mechanical Engineering

Graduate School of Engineering

Kyushu University

Japan

July 2017

Contents

Nomenclatures

A	evaporator surface area
c_p	specific heat
C_s	comprehensive effect parameter of heating surface
d	diameter
FR	filling ratio
h	heat transfer coefficient
k	thermal conductivity
la	Laplace coefficient
L_{lv}	latent heat
m	mass flow rate of condenser
Nu	Nusselt number
p	pitch
P	pressure
ΔP	pressure difference
Pr	Prandtl number
q	heat flux
Q	heat transfer rate
R	thermal resistance
Re	Reynolds number
T	temperature
ΔT	temperature difference
x	distance of two thermocouples

Greek symbols

ν	viscosity
σ	surface tension
ρ	density
λ	thermal conductivity

Subscripts

amb	ambient
boil	boiling
cond	condenser
in	input
l	liquid
loss	heat loss
out	outlet
safe	safety condition
sat	saturation
v	vapor
w	surface

Chapter 1 Introduction

1.1 Introduction

1.1.1 Background

In recent years, thermal management for electronic components such as CPU has become a serious problem. Heat dissipation has been increasing rapidly due to the growing trend of high performance computing [1]. It is well known that excess heat reduces the performance of these electronic chips and can ultimately destroy the delicate circuits, it will be necessary to design an effective high performance cooler for these kinds of high power electronic chips. Cooling system for high power electronic devices becomes increasingly more significant. Its role in the operation of these devices becomes critical sometimes concerning the safety, reliability, and life of the system. Traditional forced air cooling is limited and may be insufficient to meet the high demand of future electronics [2]. More applicable and reliable technologies of heat dissipation need to be developed to meet the challenges [3, 4]. It is well known that liquid cooling is superior to air cooling due to the heat capacity and the overall thermal resistance. Liquid cooling with phase change is a very promising way for thermal management of electronics because it achieves very high heat transfer coefficient compared to single phase cooling [5].

Consequently, it is imperative to develop the high performance cooling technologies to substitute the conventional air cooling systems. Heat pipes are widely used in many industrial applications [6 – 11]. They enable the transfer of high heat fluxes with low temperature gradients by using the latent heat of vaporization of a working fluid [12]. The diversity of the different kinds of heat pipes reflects the diversity of the conditions in which they are used. However, whatever the type of heat pipe, their normal behaviour is bounded by several operating limits that depend on various phenomena. Heat pipes are the object of thousands of scientific articles published in more than a hundred international journals. Despite the numerous studies on heat pipes for fifty years, the development of predictive tools for the design is still challenging, even for conventional technologies. It results in a real limitation in the spreading of heat pipes in the industry, as each new heat pipe has to be carefully designed for each specific application. Through a review of the recent works published on heat pipes, the author aims to understand the scientific key issues leading to this situation and to build the strategies that can be implemented to progress towards a better understanding of the different types of heat pipes.

1.1.2 Literature review

Fig. 1.1 Word cloud of the titles of articles about heat pipes [13].

During several years, the research field on heat pipes has changed substantially. Fig. 1.1 presents a word cloud realised from the titles of the articles published on heat pipes between 2012 and 2014 (about 800 papers). In this word cloud, the size of the words is proportional to the square root of the number of occurrence of each word.

Fig. 1.2 presents the distribution of the papers in the main journals. Despites the great number of journals publishing articles on heat pipes, about 40% of the papers was published in only 10 journals and almost all of them are dedicated to research on heat transfer. However, it is found that the heat pipes also interest the communities of solar and renewable energy applications, industrial applications and electronic cooling applications.

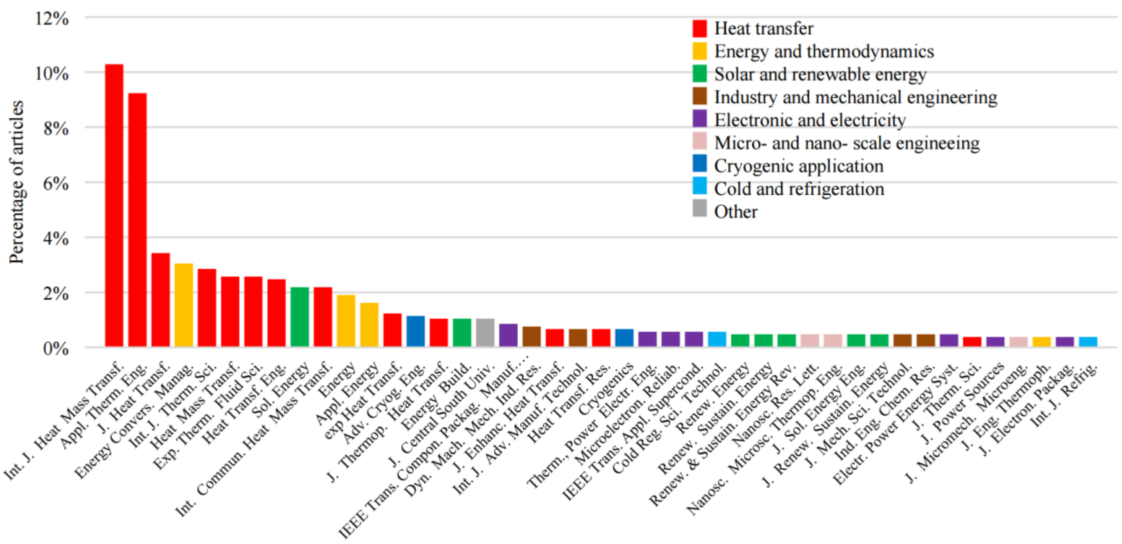

Fig. 1.2 Distribution of the papers of the international journals on heat pipes in recent years [13].

1.2 Heat pipe technologies

1.2.1 Conventional heat pipes

Heat pipes operating with a phase change process are known as heat-transfer devices with a high efficiency [14]. In 1972, the first heat pipe was designed and tested successfully by the scientists Gerasimov and Maydanik from the Ural Polytechnical Institute in Russia. It had a wick structure with capillary pumping of a working fluid. However, with the rapid development of sciences and technologies, heat pipes are becoming much more popular for electronics thermal management, heat transfer, cooling, air-conditioning and utilization of waste heat. Recent heat pipe including heat pipe panels, conventional heat pipes, pulsating heat pipe, miniature pipes, and sorption heat pipes were studied by many researchers [15 – 20].

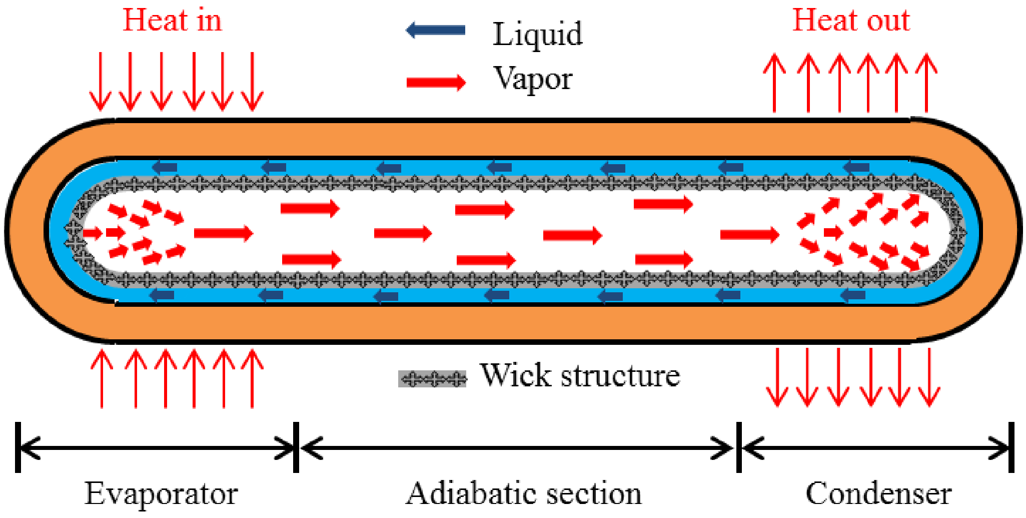

Fig. 1.3 Schematic of a cylindrical heat pipe.

As shown in Fig. 1.3, the main parts of a loop heat pipe are the evaporator and condenser. It is a passive cooling system with the heat removal by free air fans from an external radiator. The evaporator of a loop heat pipe maybe a flat or cylindrical, which is related to the shape, the heat source, the working fluids and the designing purpose. Conventional heat pipes have sintered wick structure inside as a convenient heat transfer devices [21]. It has a very excellent ability to transport a large amount of energy through long distance with a low temperature difference. The liquid is vaporized at the evaporator chamber, and vapor is condensed at the heat sink [22, 23].

Some of the advantages of the application of a loop heat pipe in electronic devices cooling system are summarized by Maydanik et al. as: 1) a much higher capacity at comparable dimensions; 2) operating at any orientation in the gravity field; 3) a considerable and low thermal resistance; 4) flexibility in packaging; 5) high heat flux over a considerable distance, and so on [24]. There were many research works on loop heat pipe for cooling electronic devices. V.G. Pastukhov et al. investigated an active cooler for CPU of desktop computers on the basis of copper-water loop heat pipes with the minimum value of total thermal resistance of 0.15 K/W. Heat transfer capacity of the cooler was 500 – 600W [25]. Ji Li et al. reported a copper-water compact loop heat pipe with a flat square evaporator with a thermal resistance as low as 0.042 K/W at the heat load of 628 W [26]. The significant contributions regarding to the improvement of the new capillary evaporator design was presented by Roger R. et al. They designed the capillary evaporator primary wick with circumferential grooves, which gave the lower evaporator temperature and high efficiency to collect the vapor [27].

1.2.2 Loop heat pipes

For loop heat pipes (LHPs), the sum of frictional and gravitational pressure drops are compensated by the capillary forces in the capillary structure placed at the evaporator only, as seen from Fig. 1.4.

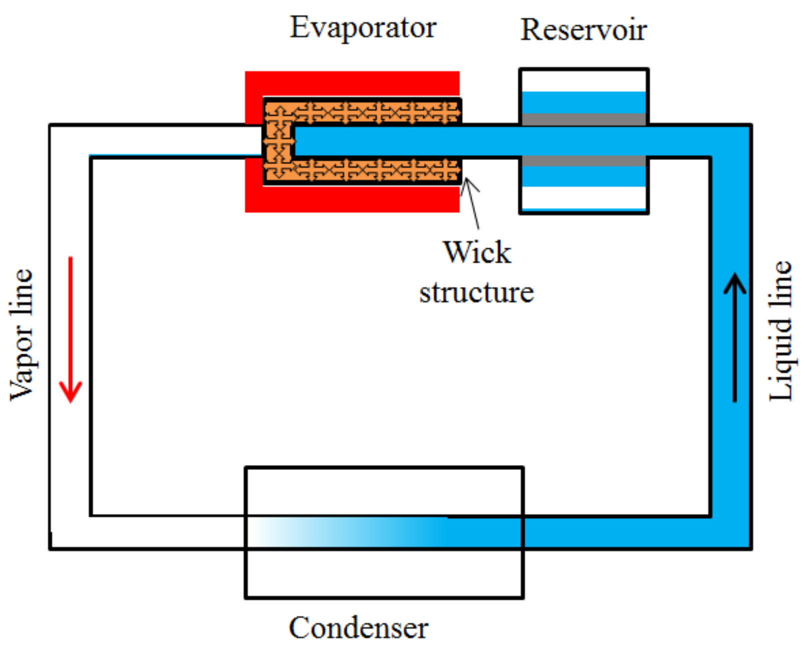

Fig. 1.4 Loop heat pipe.

It is developed from the conventional heat pipe. In a loop heat pipe, it consists of an evaporator, a condenser, a vapor line, a liquid line and a hydro-accumulator [28]. The heat flux dissipated at the evaporator outer wall is transferred to the wetted porous wick structure in the evaporator inner wall. The main part of the heat flux is consumed in the evaporation process at the porous wick surface, while the other part of the heat flux is transferred by the reservoir through the porous wick [29]. A slight pressure-head between the evaporator channels and the reservoir is induced by the vapor production in the evaporator channels. This slight pressure difference forces the vapor to flow in direction to the reservoir through the smooth transport lines. Thus, the heat flux dissipated by the heat source is efficiently transported by the vapor flow from the evaporator to the condenser heat exchanger. The heat flux is released to the heat exchanger involving the latent heat of condensation, as the vapor flow returns into the liquid state when in contact to the cold surface of the condenser. The loop heat pipe operation is then self-regulated in temperature according to the net heat balance in the reservoir. The evaporation process at the porous wick surface in contact to the evaporator channel generates liquid/vapor menisci in the porous wick. Such menisci induce a capillary force, which insures the liquid flow through the porous wick from the reservoir to the evaporation interface without any active pump [30]. The fluid loop is completed.

1.2.3 Pulsating heat pipes

Pulsating heat pipes (PHPs) are made of a single meandering tube placed between the heat source and the heat sink, which is developed in 1990. The diameter of the pipes, close to the fluid capillary length, leads to a distribution of the fluid within the tube into liquid plugs and vapor slugs. As shown in Fig. 1.5, it is a simple het pipe without wick structure relying on the motion of phase change [31]. A typical pulsating heat pipe is partially filled with the working fluid [32]. The violent vaporization of multiple liquid slugs in the evaporator, associated to the condensation of multiple vapor plugs at the condenser, generates self-sustained oscillations of the fluid [33]. It leads to an efficient heat transfer from the heat source to the heat sink, both by latent and sensible heat [31]. These systems are cheap and easy to manufacture, but their behaviour is difficult to predict and they are currently sparsely used in the industry. Vadim Tsoi et al. studied a plate-type thermosyphon with the inter-connected multi channels in the evaporation section, which is considered as a pulsating thermosyphon leading the the better thermal resistance [34].

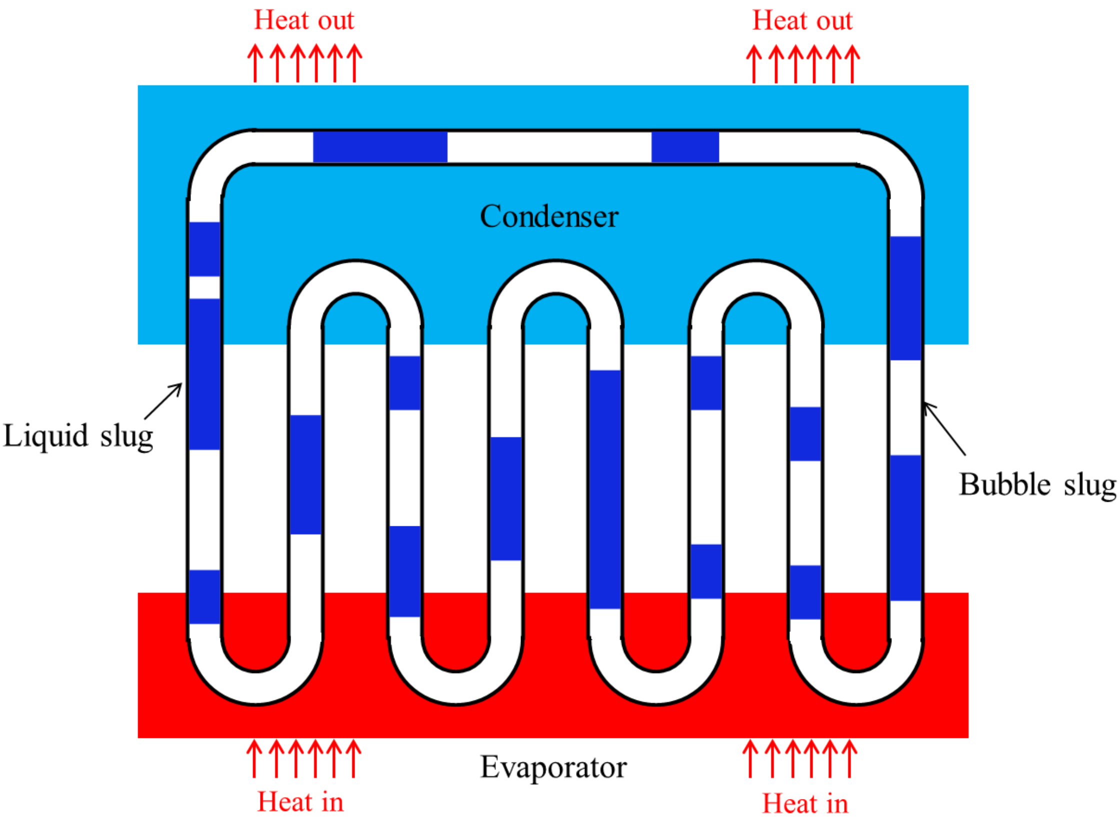

Fig. 1.5 Pulsating heat pipe.

However, at the present stage, the life time of the liquid pump and the possible leakage during the operation are two critical concerns to limit the commercial promotion of this technology in industry. In addition, the capillary structure of a loop heat pipe and its installation in the electronic equipment are very complicated and much more expensive compared to other conventional solutions. Other cooling system must be designed, which need to have the simple structure and high efficiency.

1.2.4 Conventional thermosyphons

As an effective and reliable heat removal technique, a loop thermosyphon (gravity assisted heat pipes), which has a simple structure and high heat transfer coefficient, is studied by many researchers. A large amount of heat is transferred by small temperature differences between the evaporator and condenser [35, 36]. Both the pressure head due to vapor generation and the large density ratio of liquid to vapor drive the coolant flow

[37, 38]. It is a reliable gravity-assisted wickless heat pipe. This feature can result in a convenient operation without wick structure and better heat transfer performance compared with conventional heat pipes [39, 40]. Vapor is condensed and changed into liquid flowing to the evaporator by gravity [41]. Thermosyphons may be separated into two kinds of shapes, conventional thermosyphons and loop thermosyphons [42]. The schematic of a thermosyphon is presented in Fig. 1.6. The conventional thermosyphon includes a cylinder vacuum pipe, which is filled with the working fluid partially [43, 44]. The liquid in the evaporation zone starts boiling with the supplied heat source. Then the vapor generated goes through into the condenser part where it condenses [45]. The heat goes out through the condenser wall to the external heat sink [46]. There is a counter-current between the movement of the liquid and vapor.

H. Jouhara et al. proposed an experimental investigation regarding to a smaller diameter (6 mm) copper thermosyphon for providing the heat dissipation 30 – 50 W approximately [47]. Y.J. Park et al. investigated a closed thermosyphon with various filling ratios, which was performed in the range of 50 – 600 W heating powers. The grooved surface improved the heat flux compared with those of smooth surface due to the excellent bubble nucleation on grooved surface [48]. The cryogenic thermosyphon under different cooling conditions and various filling ratios was designed by Z.Q. Long et al. They experimentally analysed the results to understand the mechanisms of heat transfer limit for various operating conditions [49]. X.F. Yang et al. investigated a loop thermosyphon using functionalized nanofluid (silica nanoparticles) as the working fluid to keep the long-term stability of the heat transfer performance owing to the covalent bonding Si-O-Si. Under three different operating pressures, the wall temperatures were very low with functionalized nanofluid compared with the water [50].

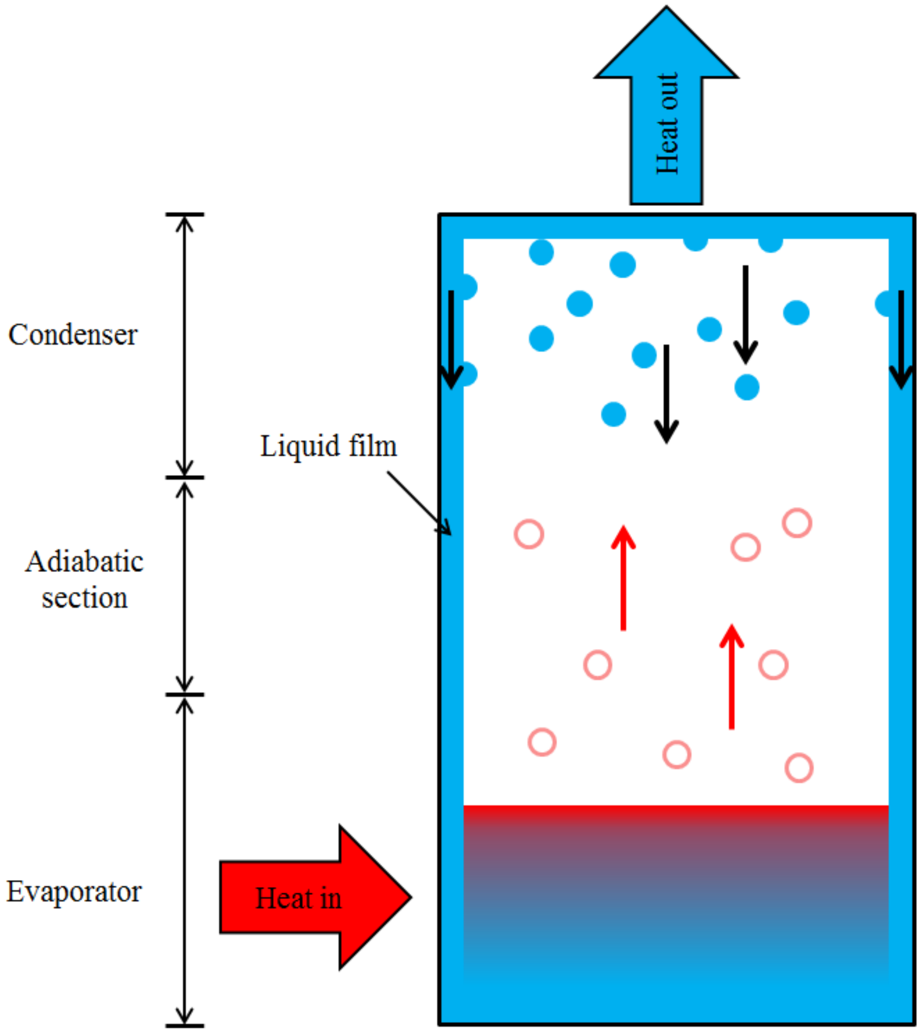

Fig. 1.6 Schematic of a conventional thermosyphon.

1.2.5 Loop thermosyphons

The closed two-phase loop thermosyphon is an attractive cooling system and widely used in various engineering application as a cooling system [51]. This apparatus has two pipes to connect two heat sources where heat is going from the hot source to the cold source by a long distance [52]. For the conventional thermosyphons, the vapor moves upward from the evaporation zone, where the pressure is high, then into the condenser, where the pressure is low. This phenomenon causes a limited heat transfer capacity due to the extra hydrodynamic resistance. This resistance increases with an increase of the heating power.

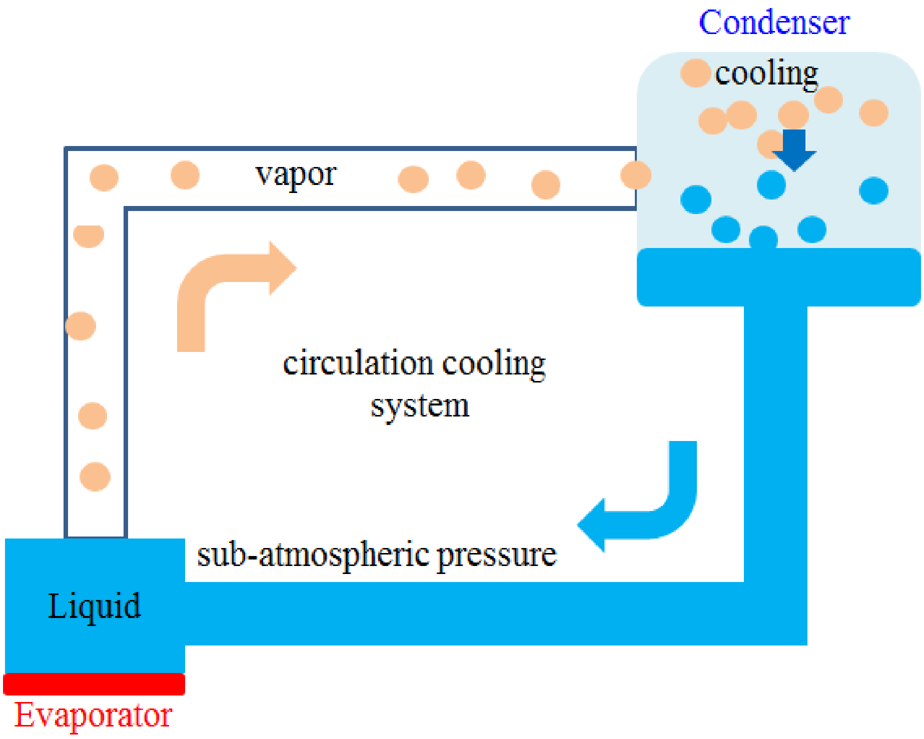

Fig. 1.7 Schematic of a two-phase loop thermosyphon.

The mentioned issue would be solved by the design in Fig. 1.7, which was proposed by Kapitanchuk et al. firstly in 1967 [53]. Lots of studies about this kind of thermosyphon have been carried out during the past few decades owing to the cost-effectiveness, high efficiency, and reliability [54]. The advantage is that it is easy to use the flexible pipes connecting the boiling and condenser chambers [55]. The condenser is arranged over the evaporator [56]. This kind of loop thermosyphon is capable of transferring heat with high heat flux over a very long distance, and maintaining an excellent temperature. Because the vapor flow and the liquid flow are separated, the counter flow is avoided [57, 58]. It is found to be an effective way to recover heat and utilize free energy. The critical heat flux is 1.2 – 1.5 times higher than those of the heat pipes with a wick structure [59]. H. Louahlia-Gualous et al. designed a loop thermosyphon with a micro-porous layer of the evaporator to cool electronic devices using water as the working fluid [60]. S.W. Chang et al. carried out a developed loop thermosyphon with series of experimental tests. The thermal network and thermodynamic cycle of the thermosyphon loop were analysed [61]. Ji Li et al.

proposed a unique insert-type closed thermosyphon working for a solar water heater, which had twice heating speed compared with the conventional one. It was a developed thermosyphon without any temperature overshooting, which got to a steady operating situation quickly [62]. P. Zhang et al. established an experimental setup about a loop thermosyphon and measured the flowing features, including the effect of different heights and temperatures. The results showed that the large temperature difference raised the liquid head and the results got better [63]. The overall transient performance was also by the researchers in the past years. The thermosyphon with water as the working fluid was analysed with emphasis on the dynamic behaviour and mass fluxes under the transient condition [64].

1.3 Influence factors of heat pipes

1.3.1 Boiling at sub-atmospheric pressure

Boiling, due to the large latent heat of vaporization, is a highly efficient means of energy transfer and therefore has a wide range of industrial applications as varied as water-cooled nuclear reactors, fossil fuel power plants, heat pipes and microchannels for electronics cooling, and chemical processes. In the case of pool boiling, where the heating surface is immersed in a large body of stagnant liquid, individual vapor bubbles emerge from distinct nucleation sites and ultimately grow detached from the heating evaporator surface owing to the buoyancy effect. The efficacy of boiling heat transfer is characterized by two important parameters, the heat transfer coefficient (HTC) and the critical heat flux (CHF).

As a typical boiling curve shows (Fig. 1.8), the boiling heat transfer involves processes of natural convection, nucleate boiling, transition boiling, and film boiling. In region I, heat is removed by natural convection from the surface to the liquid. When the wall superheat becomes sufficient to cause vapor nucleation at the heating evaporator surface, it is the nucleate boiling, region II-III, in Fig. 1.9. The first bubble nucleation is called the point of onset of nucleate boiling (ONB).

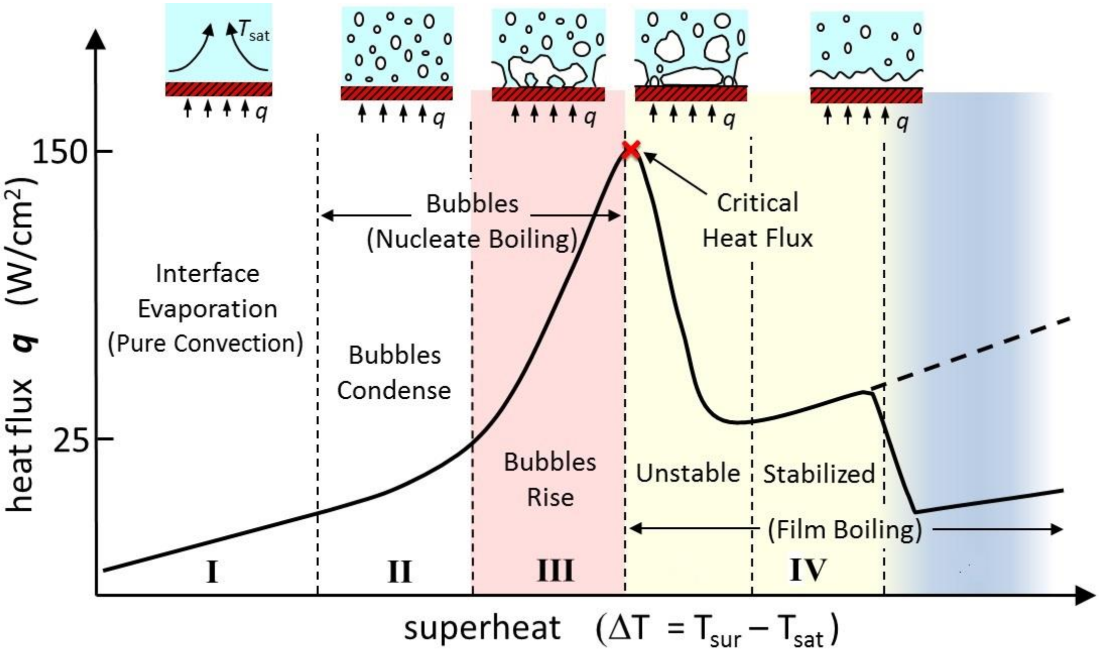

Fig. 1.8 The representative boiling curve of heat flux vs wall superheat.

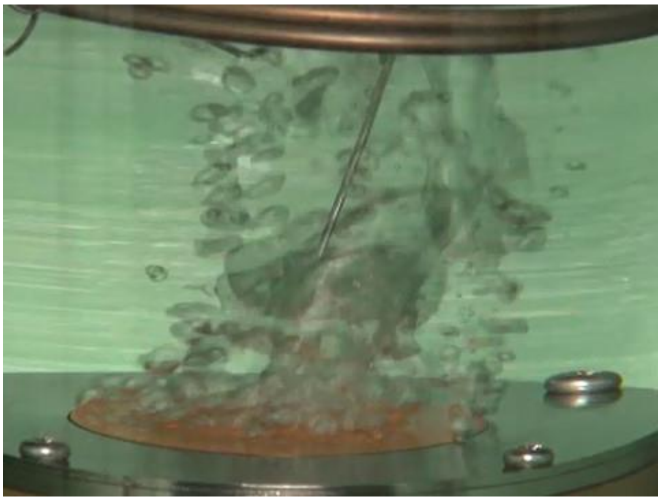

Fig. 1.9 Nucleate boiling, copper/water, $\Delta T_{sat} = 15$ K, $q = 250$ kW/m^{2}K.

The critical heat flux on the peak point marks the upper limit of nucleate boiling where the interaction of the liquid and vapor streams causes a restriction of the liquid supply to the heating surface. The transition boiling region is characterized by the existence of an unstable vapor blanket over the heating surface. Intermittent wetting of the surface is believed to occur. The film boiling is a phenomenon with a stable vapor film covers the entire heating surface as shown in Fig. 1.10. Heat transfer is accomplished by conduction and convection through the vapor film as the increasing surface temperature.

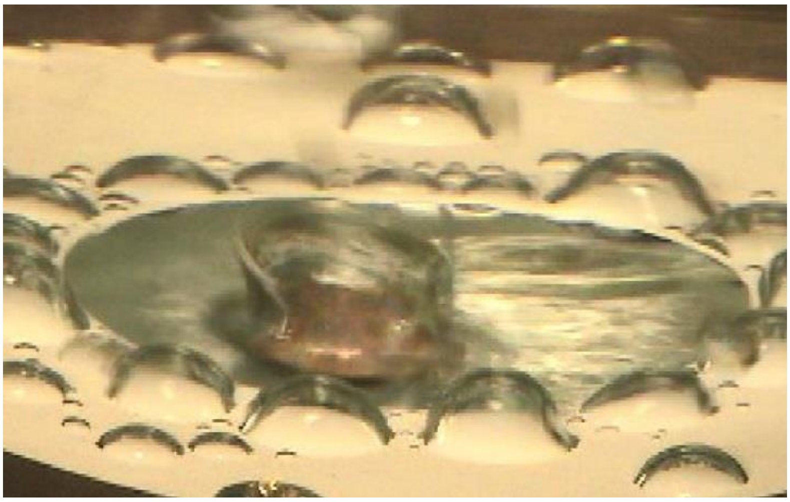

Fig. 1.10 Film boiling, PTFE/water, ΔT_{sat} = 59 K, q = 25 kW/m^{2}K [65].

Aiming at the thermal management of the electronic devices, boiling heat transfer seems to be an advanced way to meet the requirement of heat dissipation. Due to the high heat transfer coefficient and heat flux in the process of the nucleate boiling, we focus on utilizing and enhance the function of this process. The boiling performance of water at low pressures decreases significantly compared to that of water at the atmospheric pressure. Research on the boiling of liquids at sub-atmospheric pressures has mainly focused on the effects of reduced pressures on the bubble nucleation process, critical heat flux, incipient superheat and surface temperature.

Hence, how to reduce the negative effects of reduced pressures on the bubble nucleation process needs to be considered. At sub-atmospheric pressures, both the bubble departure time and radius increase substantially [66], and result in a decreased heat transfer coefficient [67]. Research on the boiling at sub-atmospheric pressures has shown both the departure time and the departure radius increase obviously.

One of the early works on boiling at sub-atmospheric pressures was by Van Stralen [68], who studied boiling within a pressure range of 13.3 – 101.3 kPa. A reduction in heat transfer during boiling at sub-atmospheric pressures was found. He observed that decrease in pressure delayed the onset of nucleate boiling, led to increase in the bubble sizes, while reducing the maximum heat flux attained. He also experimentally investigated the growth rate of vapor bubbles in water using a nickel-plated copper-heating surface for a pressure range of 2 – 26.7 kPa. They observed that the bubble departure time and departure radius increased substantially with decrease in operating pressure [69]. McGillis et al. investigated the boiling of water in a thermosyphon configuration at sub-atmospheric pressures using a plain surface by expended area [70]. They observed that lower pressure generated larger nucleation bubbles, which disturbed growth of active nucleation sites, resulting in larger wall superheats. However, advanced surface improved the heat transfer with lower wall superheat and increased the critical heat flux. An experimental investigation was carried out to understand the effect of operating pressure. It was shown that the maximum heat removal and the total heat resistance of heat pipes increase generally with the increasing of the system pressure [71]. Niro et al. showed, by combining the Clausius-Clapeyron equation with the Laplace equation, the superheat necessary for bubble nucleation would decrease with increasing pressure. The average departure diameter decreases with increasing pressure. This reduction is due to the additional activation of smaller cavities at higher pressures, and smaller cavities give smaller bubbles. But for a given cavity, Slooten observed only a small reduction of the departure diameter at increasing pressure [72].

1.3.2 Working fluids

The most significant factor of thermosyphon performance is the thermal resistance, which is directly representative of heat transfer performance [73]. For years many researchers studied the factors affecting on the performance of thermosyphon [74 – 81]. One way to improve the thermal performance of thermosyphon is through changing the working fluid [82, 83]. The choice of the fluid is indeed of a great importance and it is not so difficult to choose an appropriate fluid for the appropriate heat pipe technology for a specific application. The fluid properties must show a good trade-off between high latent heat of vaporisation, surface tension and thermal conductivity and a low viscosity for the whole range of operating temperatures. A given operating temperature corresponds to a given operating pressure that the heat pipe must be able to withstand. Other criteria, like toxicity for the humans and the environment must also be taken into account. As an example, water can be an appropriate working fluid for an operating temperature range from 50 °C to 150 °C, but problems of low pressure and high pressure can occur out of this range. Moreover, freezing can also be a problem for heat pipes with certain kinds of capillary structures. Studies on new fluids are thus necessary [84].

It is well known that mixing fluid with nanoparticles results in deposition of a nanoparticle layer on the surface and then changes both the surface wettability and roughness. According to the experimental results proposed by Liu et al. that carbon-nanotube suspensions can evidently strengthen the heat transfer coefficient, which has more than doubled compared with water under the low operating pressure [83]. Kamyar et al. added $TiSiO_4$ nanopaticles to water and applied those to a closed thermosyphon [81]. At the heat load of 40 W and 0.05% volume concentration, the thermal resistance had a remarkable reduction of 65%. However, some experimental studies indicated negative results of nanofluids on heat transfer. Xue et al. and Bang et al. mentioned that nanoparticles caused decreases in heat transfer coefficient, which was attributed to the reduced number of active nucleation sites and poor thermal conduction [85, 86]. The nanofluids have an increase in critical heat flux and a higher thermal conductivity with the comparison of conventional solid-liquid suspensions [87].

In the past few decades, nanofluids have been used as working fluids in thermosyphons due to its superior thermophysical properties. Noie et al. studied the thermal performance of thermosyphon using Al_2O_3/water as working fluid [88]. It was found that the efficiency of the thermosyphon was enhanced up by 14.7% when compared to pure water as the working fluid. Huminic et al. studied the heat transfer characteristics of two-phase closed thermosyphon with iron oxide-nanofluids as working media at different inclinations, operating temperatures and nanoparticle concentrations [89]. It was evident that the nano-particles have a significant effect on the enhancement of heat transfer characteristics of thermosyphon. Buschmann et al. studied the thermal performance of thermosyphon using de-ionized water, water based titanium dioxide and gold nanofluids with different concentrations [90]. It was observed that a maximum reduction of thermal resistance of 24% was achieved when nanofluids were replaced with de-ionized water. Liu et al. found that both the solid-liquid contact angle and the surface tension would decrease with increasing the nanoparticle mass concentration [91]. Solomon et al. observed that the heat transfer performance was enhanced/deteriorated due to the deposition of nanoparticles. As we know, the thin porous coating on the wall plays a crucial role in the heat transfer enhancement [92].

1.3.3 Surface with enhanced structure

In recent years, explorations on the effects of surface structure of thermosyphon performance are carried out with new techniques for the enhancement of heat transfer [93]. Surface structure enhancement was found to be one effective way to reduce the incipient superheat of the surface at low pressures, which is understood as the excess wall-superheat necessary to activate the nucleation sites. Using enhanced structure surface at sub-atmospheric pressures is found as one promising and prevailing way to reduce evaporator surface superheat, lower incipience overshoot and increase heat flux. Rough surface also performs a very high heat transfer coefficient caused by the excellent nucleate boiling performance. Gima et al. used the rough plate-finned surface to reduce the evaporator temperature by 18% in comparison with the smooth surface thanks to the larger nucleation site density [94]. Toyoda et al. obtained a 6-fold increase in heat transfer efficiency by depositing a porous structure on the surface [95]. The total thermal resistance was reduced by half. But the results are limited and almost exclusively focused on finned, porous and grooved surfaces [96, 97]. A. Pal et al. designed a thermosyphon with an enhanced structure for the electronic device cooling [98]. Very high heat fluxes were achieved using the enhanced structure evaporator surface (as shown in Fig. 1.11) at sub-atmospheric pressures.

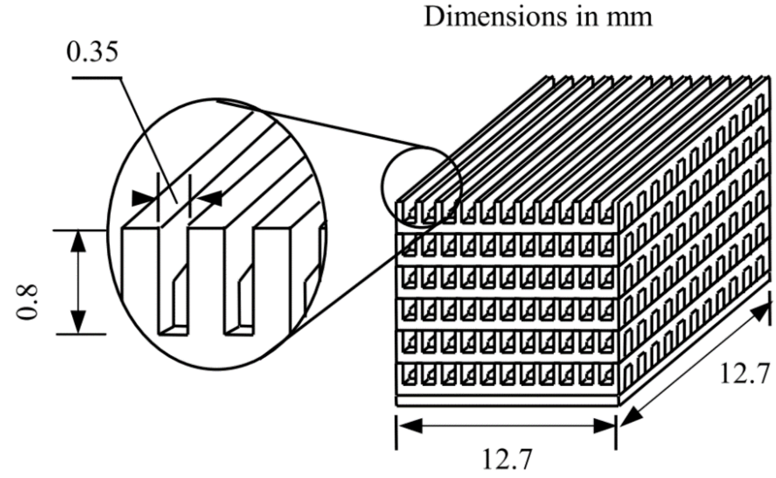

Fig. 1.11 Enhanced structure with stacked multiple layers [98].

1.3.4 Surface wettability

Among the relevant surface characteristics, surface wettability plays a crucial role in heat transfer performance. The wettability of a solid surface, the contact angle is defined as the angle between the solid surface and the vapor-liquid interface. For surfaces with contact angles (CA) less than 90° (Fig. 1.12), the surface is considered hydrophilic (Fig. 1.13), whereas for those with CA > 90° (Fig. 1.14), the surface is hydrophobic (Fig. 1.15). Hydrophilic surfaces can significantly increase the CHF values and delay transition to the film boiling mode by facilitating liquid supply to spread the heated area, but it also incidentally reduces the onset of nucleate boiling [99].

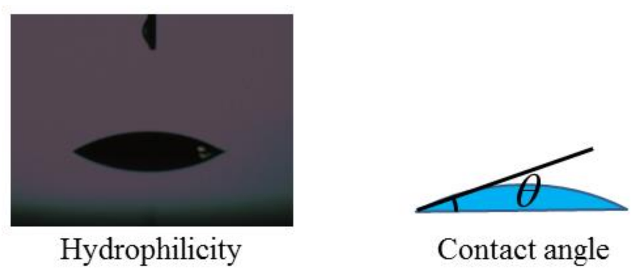

Fig. 1.12 The contact angle of liquid with hydrophilic surface.

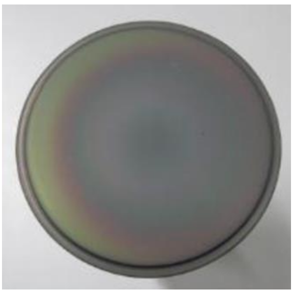

Fig. 1.13 Superhydrophilic TiO_2 surface [100].

On the other hand, hydrophobicity promotes bubble generation and can result in a considerable enhancement of the HTC, which comes at the cost of lowering the CHF as hydrophobic surfaces are prone to the formation of an insulating vapor film [100].

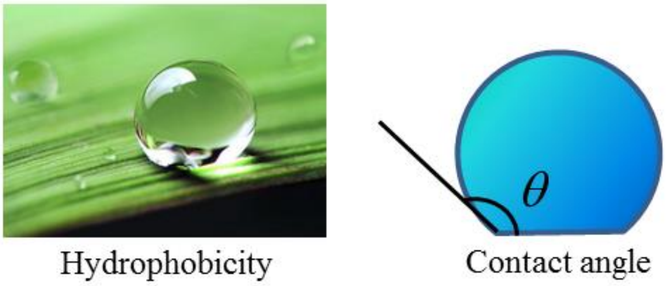

Fig. 1.14 The contact angle of liquid with hydrophobic surface.

Fig. 1.15 Superhydrophobic PTFE coating surface [65].

Thus, it requires carefully designed trade-offs between hydrophilicity and hydrophobicity. Takata et al. investigated the impact of the surface wettability, as one of the dominant parameters, on boiling performance [65, 100]. By using a super-water repellent (SWR) patterned surface (Fig. 1.16), the nucleate boiling heat transfer was enhanced by seven times. Hydrophilic surfaces also lead to a higher critical heat flux and boiling heat transfer, which is caused by lowering the bubble waiting period and increasing the bubble departure frequency [101].

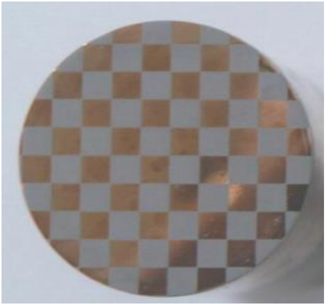

Fig. 1.16 Enhanced mixed-wettability surface (Ni-PTFE coated on copper surface).

1.4 Development of heat pipe models

During the past several years, heat pipe models have been indeed developed to predict operational characteristics. Both analytical and numerical models are proposed. The aim of the present study is not only to precisely indicate a series of equations on the base of published literature, but also to give a brief overview of the developing models today.

Two main numerical studies of heat pipes are presented. The progress in CFD modelling carried out the development of 3D thermal and hydrodynamic models [102], for another, analytical models are proposed [103]. The former one displayed a better integration of the heat pipes in a more complex system, whereas the other one gave simple and accurate engineering tools for the design of the heat pipes themselves. Many interesting studies aim to determine the wick properties by means of detailed thermal and hydrodynamic models at the pore scale [104]. Above mentioned researches are very comprehensive and each of them induces a full understanding of the phenomena involved in each type of conventional heat pipes.

Many modelling works are denoted to predict accurately the behavior of loop heat pipes. Siedel et al. presented a comprehensive review of the steady-state modelling works [105]. They highlighted the large number of models available and noted that most of them are numerical. The same authors illustrated a complete analytical model, requiring a short computational time compared to numerical ones [106]. These models have been validated with a series experimental data. A good agreement has been achieved between the model and experiments. It is noted that the vapor zone at the contact between the porous medium and the heat source is also a topic of discussion. Mottet et al. developed a capillary evaporator using a mixed-pore network model. They used a mesoscale approach with a pore network model [107]. On the base of a mesoscale approach, the capillary effects were modelled. The 3D simulations showed the regime resulting in the best heat transfer performance is a liquid-vapor zone within the wick.

At the scale of the system, transient models of LHPs have been demonstrated. For instance, Kaled et al. proposed a model classically on the base of the energy, mass, and momentum balances for the evaporator-reservoir, the condenser and the transport lines [108]. They found that the fluid motion participates in the pseudo-periodic behavior of the system. In addition, Nishikawara et al. proposed a transient model that precisely predicted the experimental data, despite the presence of an overshoot temperature when the heat load changed, which was not observed experimentally [109].

A great part of the modelling works published in the past few years are focused on pulsating heat pipes. On one side, the increasing number of experimental databases contributed to the development of empirical correlations [110]. On the other side, some 3D CFD models were exhibited and phenomenological models were implemented [111]. They showed a good ability to reproduce the chaotic behaviour of PHPs. As a consequence, these models still have to be optimized in order to consider all physical phenomena, especially at the scale of the thin liquid film and the triple contact line. Detailed models already exist to understand these phenomena, but their experimental validation remains challenging.

1.5 Thesis objective

In the present study, inspired by the enhanced heat transfer due to the mixed-wettability characteristics [65], we fabricate a two-phase loop thermosyphon. Distilled water is used as the working fluid, on account of its superior thermal properties at sub-atmospheric pressures and the decreased saturation temperature to satisfy the safety operating temperature of CPU (T_{safe} < 85 °C). In addition, the experiments are performed to investigate the heat transfer characteristics of this advanced loop thermosyphon. Furthermore, the effects of the pattern size, heat input, filling ratio, and condenser temperature are also investigated and discussed. The detailed heat transfer analysis provides a deeper understanding of the efficiency of high heat transfer on an enhanced mixed-wettability surface at sub-atmospheric pressures for CPU cooling applications. The scopes of the present work are as follows:

(1) The apparatus of a loop thermosyphon with enhanced surface is designed for cooling CPU. A large number of experiments are carried out to study the heat transfer performance. For the patterned surfaces, the nucleate boiling performance is enhanced with the decreasing of the spot diameter.

(2) Multiple mixed-wettability surfaces are studied and performed to compare with a common surface. The thermal resistances and heat transfer coefficient are calculated and discussed.

(3) The influence factors of the heat transfer performance are analyzed, including the pattern size, heat input, filling ratio, system pressure, heat loss, and condenser temperature.

(4) A theoretical model for the condenser heat transfer coefficient is carried out to evaluate the result.

1.6 Thesis outline

The following is a brief description of the contents of each chapter.

Chapter 1 presents the scientific background and overview about the development of the cooling system for electronic devices. Variety of heat pipes and thermosyphons are also presented such as conventional heat pipes, loop heat pipes, pulsating heat pipes, conventional cylindrical thermosyphons, and loop thermosyphons. Then the influence factors are also discussed.

Chapter 2 presents the details of the apparatus and mixed-wettability surface of a loop thermosyphon. The temperature measurements of the thermocouples and heat transfer model are introduced. The experimental procedure and operating principle are described carefully. The calculating equations of the heat flux, thermal resistance, heat transfer coefficient, condensation heat transfer rate, and heat loss are clarified. The uncertainties of the experimental parameter measurements are analysed.

Chapter 3 presents the experimental study on HNTs coated mixed-wettability surface. Firstly, the manufacture process of the mixed wettability surface of HNTs coating is introduced. Experimental data are examined, and the influences of various factors such as filling ratio, condenser temperature, and heat input are discussed. The comparison of the bubble behaviours on various evaporator surfaces is performed. Heat loss and the coating material durability are also considered and discussed.

Chapter 4 presents experimental results of a super water repellent, FDPA coated surface (diameter 1 – 2 mm, pitch 3 mm), including the thermal resistance, effect of filling ratios and heat input. The experimental results of thermal resistance in chapter 4 is to confirm the excellent boiling performance of a mixed-wettability surface, which is more advanced than the surface with a single feature (hydrophilic or hydrophobic).

Chapter 5 presents the experimental results of non-electroplating, and compared with the results of machined structured surface. Non-electroplating Ni-PTFE (polytetrafluoroethylene) patterned surface performs the best results, and all the mixed-wettability surfaces are compared with each other in the same diameter and pitch. The development status of thermosyphons in recent years is also summarised and exhibited.

Chapter 6 presents the overall conclusion of this thesis.

Chapter 2 Experimental apparatus and measurement procedure

In this chapter, the apparatus of a loop thermosyphon and experimental measurement procedure are described. The purpose of this chapter is to introduce the operating principle of this two-pipe thermosyphon and the calculation method of results. Heat loss during the experiments and uncertainty of the experimental data are discussed in detail.

2.1 Experimental apparatus

2.1.1 Schematics of a loop thermosyphon

A schematic of the experimental setup is shown in Fig. 2.1. The setup used in the experiments consists of an evaporator and a condenser, and two connecting pipes of a 10-mm internal diameter. One is for vapor flow to the condenser, and the other is for liquid flow to the evaporator, which is 13 mm lower than vapor pipe in heights. It is different from a conventional thermosyphon, the two smooth-walled pipes are used to separate liquid and vapor pathways to avoid both thermal and viscous interactions between countercurrents of vapor and liquid. Both pipes are insulated in order to reduce heat loss. To activate this loop thermosyphon, the condenser is placed 10 mm higher than the evaporator, which helps the condensed liquid flow from the condenser to the evaporator continuously by gravity.

2.1.2 Apparatus of a loop thermosyphon

The evaporator is a rectangular chamber with thermal insulation property of 33 mm in height, 96 mm in length, and 90 mm in width. The heating block is made of copper to perform the excellent thermal conductivity properties in Fig. 2.2. The copper support for the boiling chamber around the heating block has the good anti-corrosion ability to water. The snake-tube heat exchanger provides condensing power. The press-fitted O-ring is used at the bottom of the boiling chamber for good sealing as shown in Fig. 2.3. Heating power is provided by three cartridge heaters.

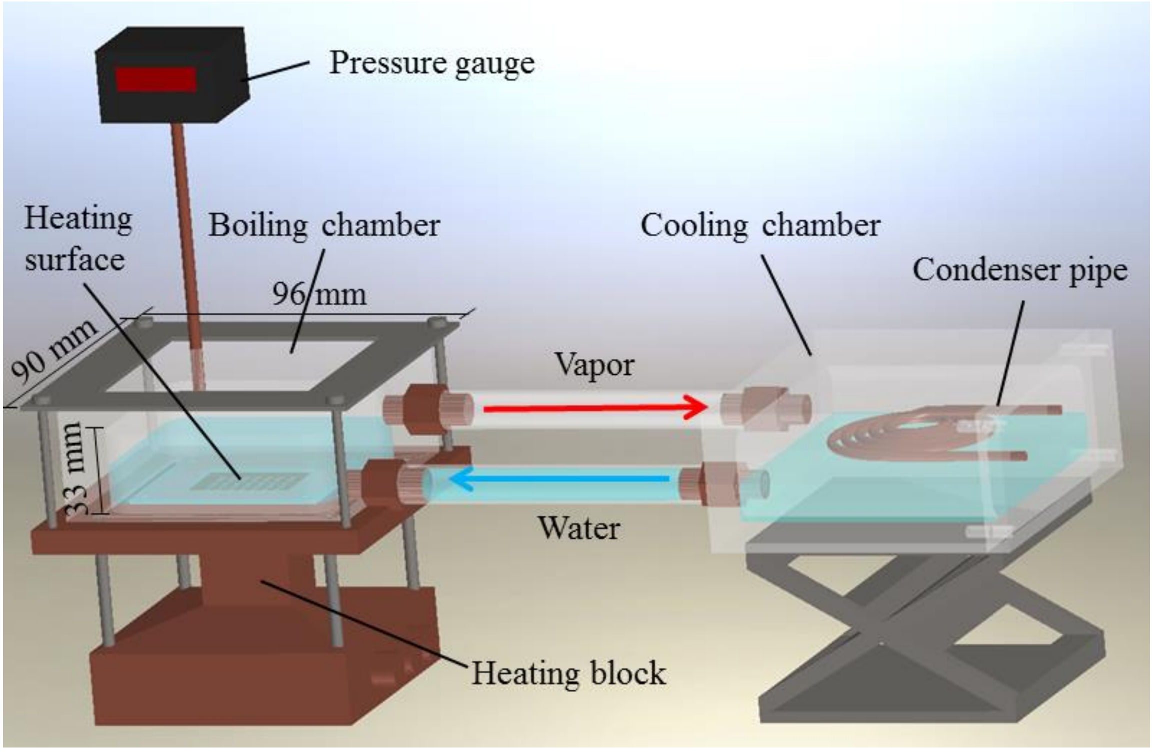

Fig. 2.1 Schematics of a two-phase loop thermosyphon.

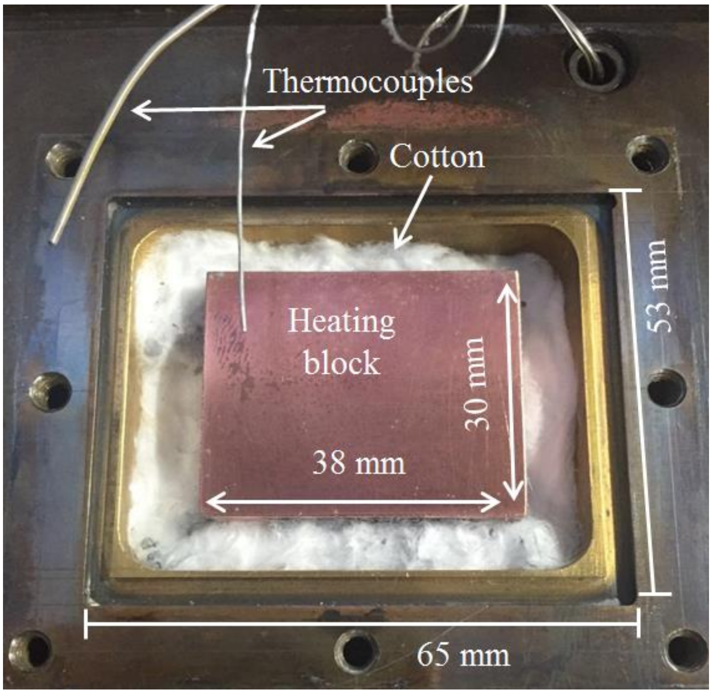

Fig. 2.2 The heating block insulated with cotton.

A high temperature resistant and thermal conductive paste (JunPus nano diamond thermal grease DX1) is used between the top of the heating block and the bottom of evaporator surface to reduce contact thermal resistance, as shown in Fig. 2.3. The thermal conductivity of this grease is 16 W/(m·k). Then the evaporator surface can be fixed on the upper end of the heating block, which has been covered with a homogeneous thermal grease, as seen in Fig. 2.4. The power supply used in the experiment is pointed out from Fig. 2.5, which can be controled to provide the specified output-power.

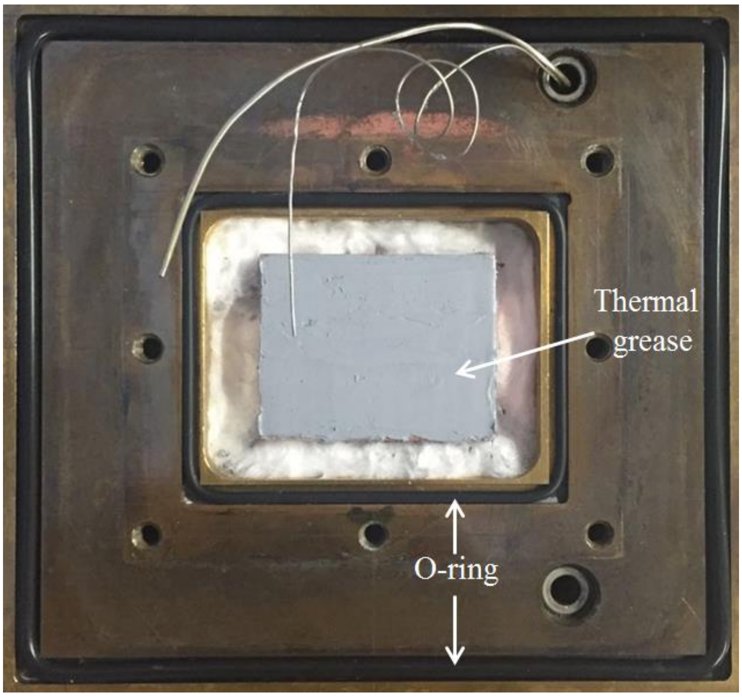

Fig. 2.3 The press-fitted O-ring and thermal conductive grease.

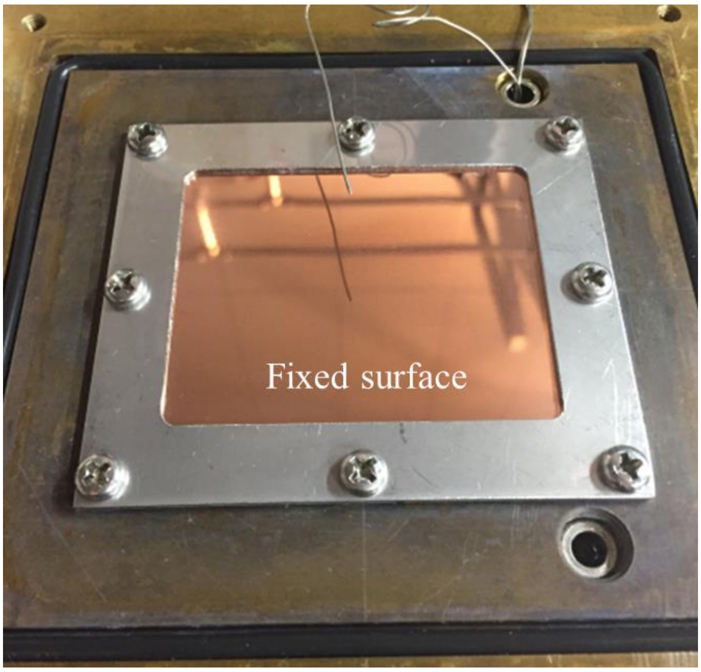

Fig. 2.4 The fixed surface on the upper end of the heating block.

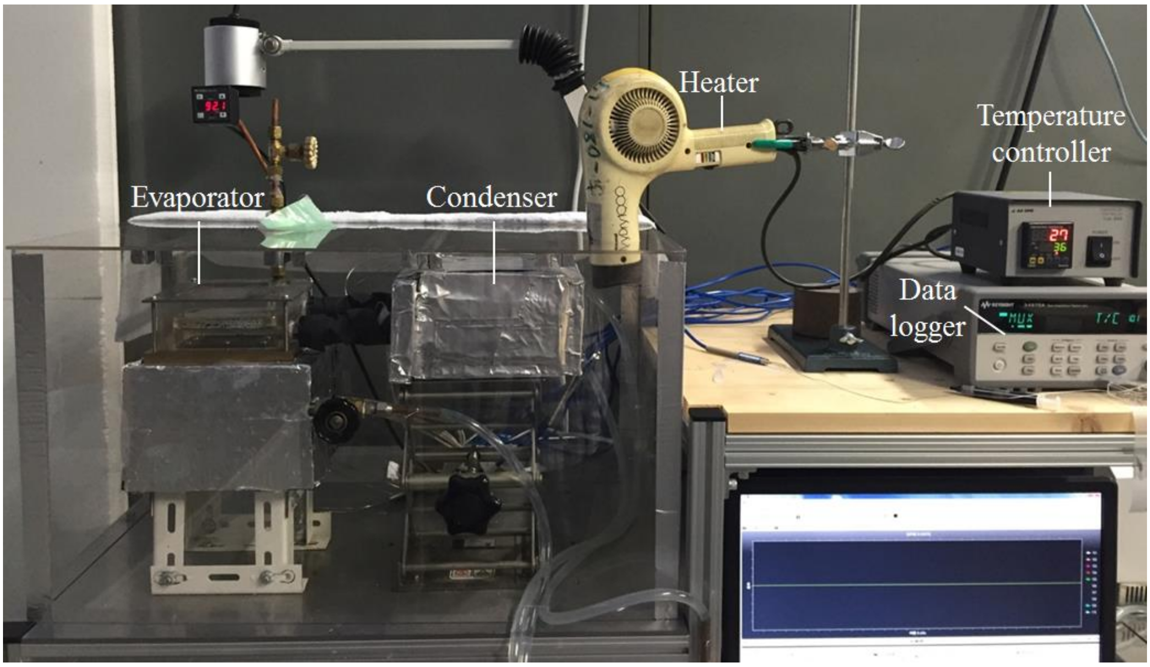

Fig. 2.5 The experimental apparatus of two-phase loop thermosyphon.

The photo of integrated setup is exhibited in Fig. 2.5. The insulation box is used to keep the thermosyphon apparatus operating at the constant environment. The air blower is set to maintain the temperature of the surrounding in the insulation box to simulate the environment temperature in the data center. Both of the heating block and the condenser chamber are totally covered with cellular insulant to reduce heat loss during the experiment and ensure the accuracy of the temperature measurements.

2.1.3 Mixed-wettability evaporator surfaces

This study focuses on the effect of mixed-wettability surfaces on loop thermosyphon boiling performance at sub-atmospheric pressures [65]. Schematic of the patterned surfaces used in the present study are shown in Fig. 2.6. The heating center area is 30×38 mm^2 and the thickness of the surface is 1.5 mm. They are made from polished copper (CA ≈ 80°) and sometimes coated with the material with hydrophilicity, whose CA < 10° [99]. After that, the hydrophilic surface is coated with hydrophobic spots (CA ≈ 150°, material with hydrophobicity) [100]. The spots diameter ranges from 0.5 mm to 4 mm and these spots are distributed in a rectangular array with a pitch ranging from 1.5 mm to 6 mm.

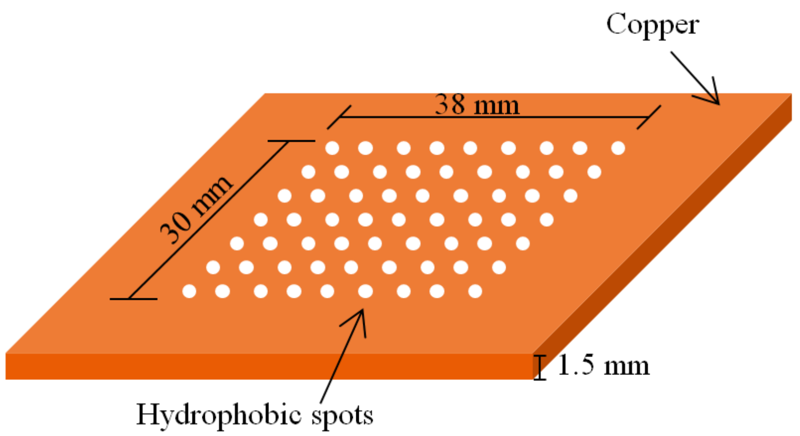

Fig. 2.6 Schematic of a mixed-wettability evaporator surface.

2.2 Experimental procedure

2.2.1 Leakage check

Leakage check is carried out to ensure that the setup maintains a consistent performance over a long period of time. Initially at 10 kPa, the pressure of the closed system is found to increase by only 0.2 kPa after a 24-hour period, which is considered an acceptable amount of leakage. After charging and degassing, the system valve is closed and air initially dissolved in the test liquid can be removed by vacuum degassing for 2 hours prior to the measurement. Each experiment lasts 4 – 5 hours.

2.2.2 Operating principle

The operating principle is as follows: the working fluid is heated by the heater below the surface, and starts to boil on the evaporator surface. Then the vapor of the working fluid moves along the horizontal pipe driven by the pressure difference between the hot region and the cold region of the thermosyphon. In the condenser chamber, the vapor flowing from the evaporation section is condensed into the liquid, and the heat is dissipated into the circulating cooling water in the annular tube. Finally, the liquid from the condenser returns to the evaporator by gravity forming a circulation system. The thermosyphon works by repeating this cycle. The whole experimental system is developed to monitor and control the various process parameters through a data acquisition system.

2.3 Experimental measurement

The heat input Q_{in} is measured by thermocouples in the heat transfer block over 50 consecutive data (sampling rate at 3 points per second). During the experiments, all the sides of heating block assembly are insulated to assure one-dimensional heat flow to the boiling evaporator surface. All measurements have been conducted in a steady state, which is judged by monitoring the outputs of the thermocouples. Various values of the heat load ranging from 10 to 260 W are tested.

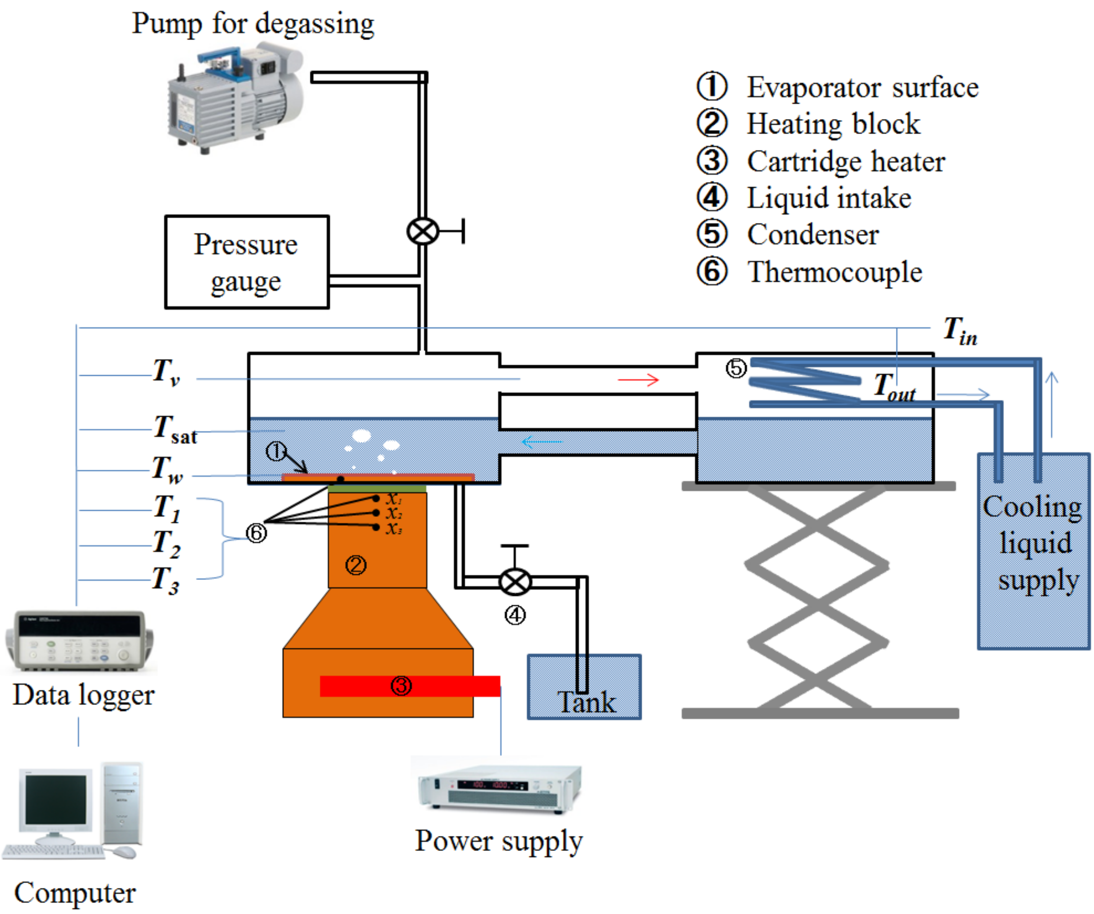

Fig. 2.7 Schematic view of experimental system and thermocouple positions.

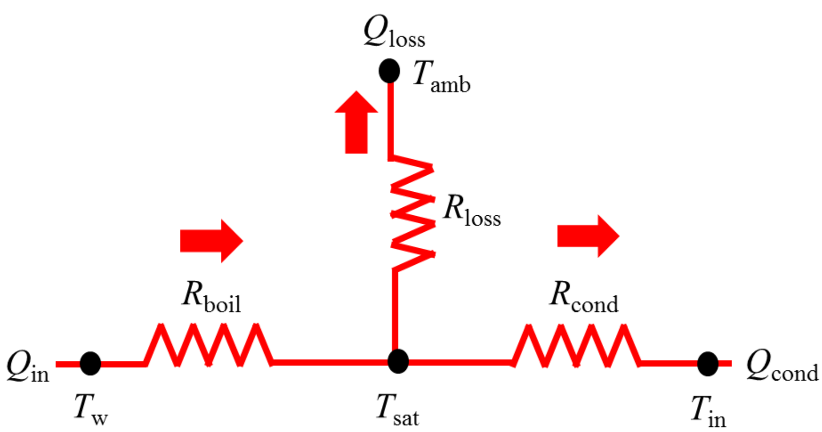

Fig. 2.8 Heat transfer model of the whole process during the experiment.

2.4 Data calculation analysis

Fig. 2.7 and Fig. 2.8 describe the temperature measurement of the whole system and heat transfer model. The heat flux is evaluated as the ratio of the thermocouple temperature difference in the heating block to the distance between the two points:

$$q = \lambda \frac{T_1 - T_3}{x_1 - x_3} \tag{2.1}$$

Here T_1 and T_3 are the temperatures of two thermocouples inserted in the heating block, x_1 and x_3 are the distances to the upper end of the heating block. λ is the thermal conductivity of the copper. The heat input Q_{in} is the heat flux q multiplied by the effective area of the heating surface:

$$Q_{in} = qA \tag{2.2}$$

The thermal resistance is evaluated as the ratio of temperature difference to the heat input Q_{in}. The boiling thermal resistance is defined as the difference between T_w and T_{sat} divided by the heat input Q_{in} [7]:

$$R_{boil} = \frac{T_w - T_{sat}}{Q_{in}} \tag{2.3}$$

Here T_w is the wall temperature at the center of the evaporator surface measured by the thermocouple inserted in the hole inside, T_{sat} is the saturation temperature measured using the thermocouple immersed in the liquid. The condensation thermal resistance is defined as the difference between T_v and T_{in} divided by the condensation heat transfer rate Q_{cond}:

$$R_{cond} = \frac{T_v - T_{in}}{Q_{cond}} \tag{2.4}$$

The condensation heat transfer rate Q_{cond} is calculated by the temperature increase of the cooling water in the tube as follows:

$$Q_{cond} = mc_p\left(T_{out} - T_{in}\right) \tag{2.5}$$

Here m is the mass flow rate, c_p is liquid specific heat, T_{out} is the temperature of the cooling water at the outlet. Here T_{in} is the temperature of the cooling water in the condenser. The total thermal resistance is the sum of the boiling thermal resistance R_{boil} and the condensation thermal resistance R_{cond}. As described above, they can be expressed as:

$$R_{total} = R_{boil} + R_{cond} \tag{2.6}$$

The flow rate of circulating water in the condenser part is set at 0.014 kg/s. The evaporation heat transfer coefficient, as one of the crucial performance parameters of the thermosyphon, is defined by the following equation [92]:

$$h_e = \frac{Q_{in}}{A(T_w - T_{sat})} \tag{2.7}$$

Here A is the evaporator surface area, Q_{in} is the heat input.

2.5 Uncertainty of the experimental data

The uncertainties of the experimental parameter measurements are analysed. The thermocouple uncertainty is 0.2 K. The uncertainty for the distance measurement of two thermocouples is 2%. The thermal conductivity uncertainty is considered negligible. The uncertainty of the wall superheat is 4%. The uncertainty resulting from the evaporator surface area is 0.1%. The uncertainty of the heat flux measurement can be calculated by,

$$\frac{\Delta q}{q} = \sqrt{\left(\frac{\Delta k}{k}\right)^2 + \left(\frac{\Delta(\Delta T)}{\Delta T}\right)^2 + \left(\frac{\Delta x}{x}\right)^2} \tag{2.8}$$

which gives 4.2%.

For HTC and the thermal resistance, the measurement uncertainties,

$$\frac{\Delta h}{h} = \sqrt{\left(\frac{\Delta q}{q}\right)^2 + \left(\frac{\Delta(T_w - T_{sat})}{(T_w - T_{sat})}\right)^2} \tag{2.9}$$

$$\frac{\Delta R}{R} = \sqrt{\left(\frac{\Delta q}{q}\right)^2 + \left(\frac{\Delta(\Delta T)}{\Delta T}\right)^2 + \left(\frac{\Delta A}{A}\right)^2} \tag{2.10}$$

are calculated to be 4.5% and 5.8%, respectively.

Chapter 3 Experimental study on HNTs coated surface

In this chapter, the analysis of the experimental results of HNTs coated evaporator surface is described. Different conditions, including heat input, filling ratios, and condenser temperatures are carried out to examine the influence factors of this thermosyphon.

3.1 Patterned surface

Firstly, the surfaces used in the experiments are made from polished copper (CA ≈ 80°) and then coated with HNTs (Halloysite Nanotubes, $Al_2Si_2O_5(OH)_4{\cdot}nH_2O$) circular spots (CA ≈ 145°) [113]. The spots diameter ranges from 1 mm to 4 mm and these spots are distributed in a rectangular array with a pitch ranging from 3 mm to 6 mm, as shown in Table 3.1.

Table 3.1 Hydrophobic spot parameters on evaporator surfaces of Type A, B, C, and D.

Case	Spot diameter, d (mm)	Pitch, p (mm)
Type A	NA	NA
Type B	1	3
Type C	2	3
Type D	4	6

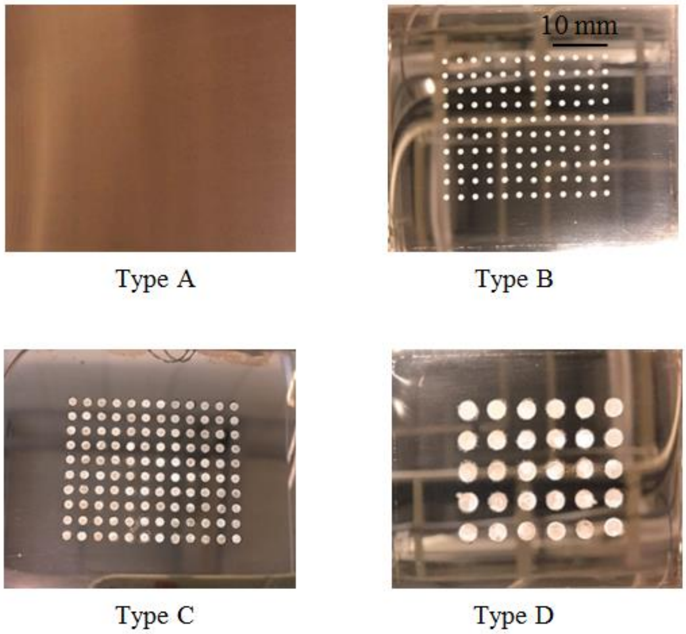

Fig. 3.1 Copper mirror surface (Type A) and mixed-wettability surfaces (with hydrophobic spots coated on copper mirror surfaces), Type B, Type C, and Type D.

3.2 Comparison of experimental results

3.2.1 Experimental results

Table 3.2 Superheat of onset nucleate boiling on surfaces Type A, B, C, and D.

Case	Superheat of ONB, ΔT (K)	q (kW/m^2)
Type A	20.2	128.5
Type B	3.2	30.2
Type C	3.1	29.3
Type D	2.1	21.5

Fig. 3.2 – Fig. 3.5 show the comparison of the experimental results of Type A, B, C, and D surfaces, at heat inputs from Q_{in} = 10 W to Q_{in} = 260 W. Fig. 3.2 presents the variation of the boiling thermal resistance as a function of heat flow rate. From the results of an analysis, as shown in Fig. 3.2, it follows that the boiling thermal resistances

of Type B – Type D surfaces are much lower than that of Type A. R_{boil} decreases accordingly with the increasing heating power due to the rising pressure in the system and more active nucleation sites. At higher pressure, decreasing surface tension, bubble departure diameter and increasing bubble frequency are achieved, which contribute to increasingly higher heat transfer coefficient [69]. The results of the Type A surface (copper mirror) is in agreement with those of Kutateladze correlation (Fig. 3.2), which is shown as follows:

$$\frac{hl_a}{k_l} = 7.0\times10^{-4}\cdot P_{rl}^{\ 0.35}\cdot\left(\frac{ql_a}{\rho_v L_{lv}\nu_l}\right)^{0.7}\left(\frac{Pl_a}{\sigma}\right)^{0.7} \tag{3.1}$$

where l_a is Laplace coefficient, P_{rl} is Prandtl number, L_{lv} is the latent heat, ν_l is dynamic viscosity, ρ_l is the liquid density, σ is surface tension, k_l is the liquid thermal conductivity, h is the heat transfer coefficient, and P is the system pressure. In consideration of both the boiling and condensation thermal resistances, the total thermal resistances are shown in Fig. 3.3, which confirms that the thermal performance of this thermosyphon can be enhanced evidently by using the patterned surfaces.

Fig. 3.4 represents the variation of the surface temperature as a function of heat flow rate. The temperatures of Type B – Type D (hydrophobic spot coated surfaces) rise approximately linearly with the increasing heat input, which are much lower than that of Type A, resulting in a maximum reduction of 17 K, due to the excellent nucleate boiling performance. Fig. 3.5 represents the variation of the heat transfer coefficient as a function of the heat flux. The boiling heat transfer coefficient is dependent on the number of nucleation sites and size. Type B surface coated with 1 mm diameter spots reduces the departure diameter of the bubbles and increases the frequency of bubble departure, achieving the lowest thermal resistance. This can be explained as follows: when the large bubbles leave the wall, they are replaced by plenty of cold liquid that requires longer waiting time to be superheated, therefore, resulting in larger bubble, and longer waiting time [114].

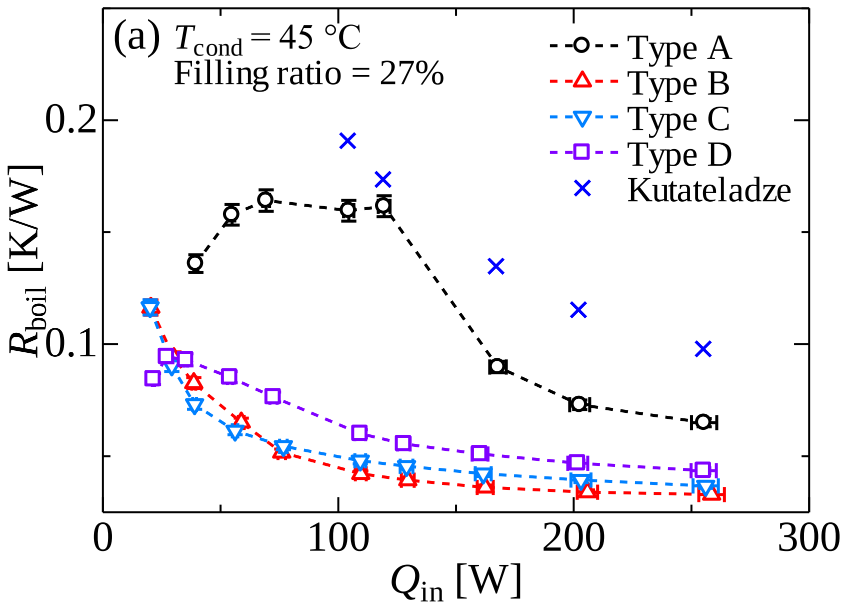

Fig. 3.2 Comparison of experimental results of Type A – Type D. (a) The boiling thermal resistance R_{boil} vs. the heat input Q_{in}.

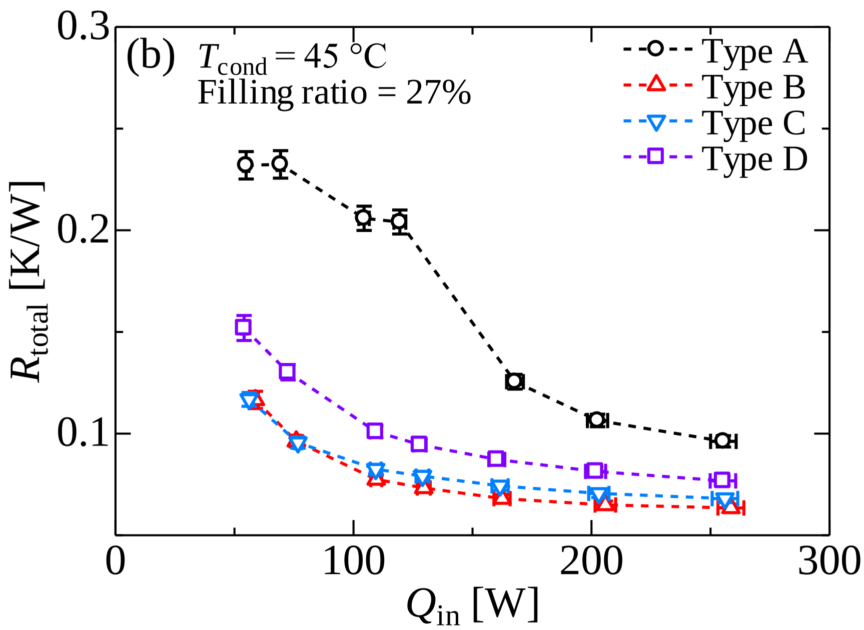

Fig. 3.3 Comparison of experimental results of Type A – Type D. (b) the total thermal resistance R_{total} vs. the heat input Q_{in}.

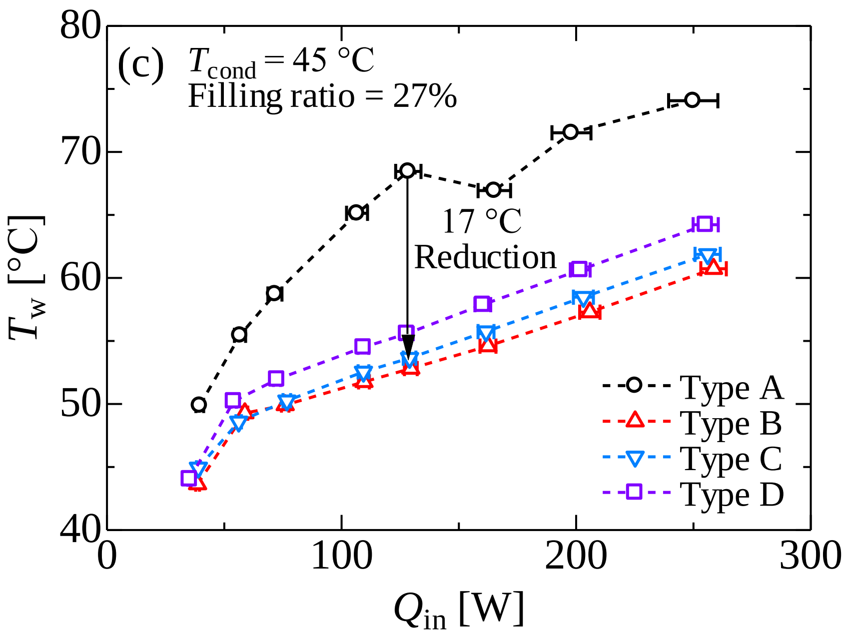

Fig. 3.4 Comparison of experimental results of Type A – Type D. (c) the evaporator surface temperature T_w vs. the heat input Q_{in}.

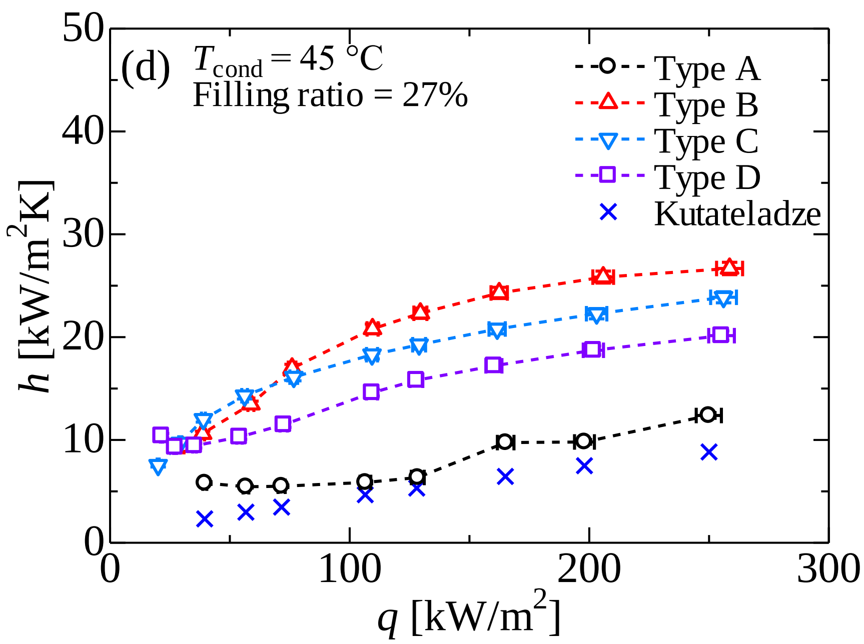

Fig. 3.5 Comparison of experimental results of Type A – Type D. (d) the heat transfer coefficient of the evaporator h vs. the heat flux at the evaporator surface q.

3.2.2 Bubble behaviors

As mentioned above, we are focusing on realizing an enhanced boiling surface, which induces onset of nucleate boiling (ONB) at extremely low superheating. During a large number of experiments, it was found that it is easier for bubbles to be generated and grow on hydrophobic spot coated surface than that of the copper mirror surface. For the surfaces (Type B – Type D), ONB is only 2.5 K – 3 K at a very low heat flux of q = 25 kW/m^2, whereas it is 20 K for copper mirror surface (Type A) at the corresponding q = 120 kW/m^2.

The observations of the contrasting bubble behaviors are shown in Fig. 3.6 and Fig. 3.7 including Type A – Type D surfaces from moderate (130 W) to high (220 W) heating powers. At the early stage of operation, the pressure is low and amount of vapor inside the loop thermosyphon is relatively small. Apparently, the boiling at higher heat fluxes and pressures show more violent bubbles. With further increases in the heat input, the boiling process gradually enhances. We can also see clearly from Fig. 3.6 that the bubble diameters (Type D > Type C > Type B) depend on the diameters of hydrophobic spots (Type D > Type C > Type B). The hydrophobic spots are perfectly covered with bubbles at wall superheats from 5.8 K – 8.1 K, whereas it is 22 K for uncoated surface (Type A) at about q = 120 kW/m^2. In the case of the uncoated surface (Type A) shown in Fig. 3.6, an incipient overshoot caused by the big and intermittent boiling is observed as the surface temperature drops suddenly after boiling starts, while it is suppressed on the hydrophobic spot coated surfaces. This intermittent process may result in large, undesirable temperature oscillations at the heated surface.

Type A

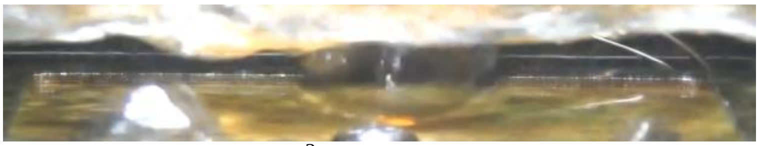

q = 119.5 kW/m^2, ΔT_{sat}=22.0 K, T_w=69.6 °C

Type B

q= 129.5 kW/m^2, ΔT_{sat}=5.8 K, T_w=52.8 °C

Type C

q = 128.9 kW/m^2, ΔT_{sat}=6.7 K, T_w=53.6 °C

Type D

q = 127.8 kW/m^2, ΔT_{sat}=8.1 K, T_w=55.6 °C

Fig. 3.6 Bubble behaviors on surfaces Type A – Type D at low heat fluxes. The operating pressure is 10 kPa, the heat input is 130 W, and FR = 27%.

It is obvious that R_{boil} and R_{total} decrease with decreasing spot diameter. As compared with the mirror surface (Type A), the boiling thermal resistance is on average reduced by 62% for Type B (with the lowest value of 0.03 K/W at the corresponding heat input beyond Q_{in} = 150 W approximately).

Type A

q = 202.5 kW/m^2, ΔT_{sat}=16.8 K, T_w=66.5 °C

Type B

q = 205.8 kW/m^2, ΔT_{sat}=7.9 K, T_w=57.2 °C

Type C

q = 203.1 kW/m^2, ΔT_{sat}=9.1 K, T_w=58.5 °C

Type D

q = 201.7 kW/m^2, ΔT_{sat}=10.8 K, T_w=60.6°C

Fig. 3.7 Bubble behaviors on surfaces of Type A – Type D at high heat fluxes. The operating pressure is 12.5 kPa, the heat input is 220 W, and FR = 27%.

3.3 Effect of filling ratios

3.3.1 Height of liquid level

The performance of the loop thermosyphon is also influenced by the charging level of the working fluid. The filling ratio (ratio of the working fluid volume to the total thermosyphon loop volume) is one of the key factors. In the present investigation, the above effect has been studied for four filling ratios (FR), 15%, 20%, 27%, and 32%, respectively.

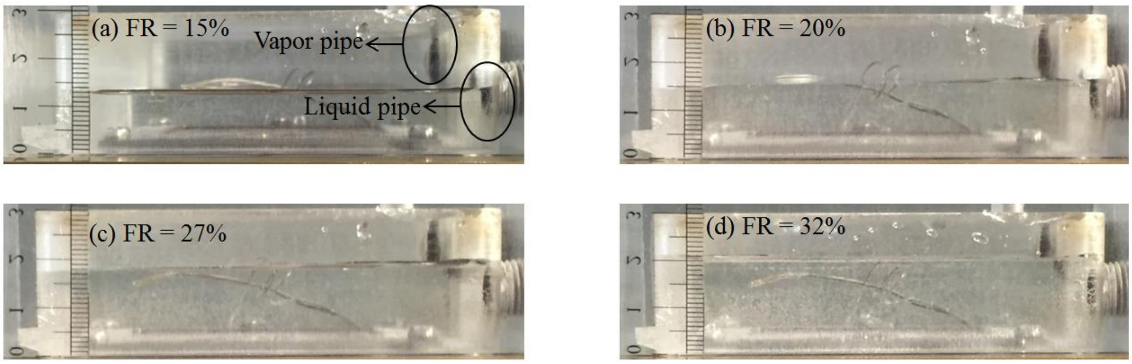

Fig. 3.8 The liquid levels of (a) FR = 15%, (b) FR = 20%, (c) FR = 27%, and (d) FR = 32%. Heating power of 30 W – 260 W.

The liquid levels are shown in Fig. 3.8. We can see that they correspond to liquid levels of 13 mm, 15 mm, 18 mm, and 19.5 mm. These filling ratios were chosen in order to avoid the surface dry-out condition and vapor pipe blockage. The heat transfer surface used was Type B. The four groups of experiments performed under the same surface structure and condenser temperature. As the heat input increases to 260 W, the evaporator with FR = 15% still remains partially wet, but the liquid height is a little lower than the top of the liquid pipe, as seen from the above Fig. 3.8 (a). It has the effect of countercurrent between the vapor and the liquid in the liquid pipe. For the case of higher charging levels above FR = 32%, partial flooding of the vapor tube could occur, reduce the driving force and weaken the vapor-liquid circulation more or less.

3.3.2 Experimental results

Figs. 3.9 and 3.10 present the the boiling thermal resistance and total thermal resistance at different filling ratios. According to that, with an increased filling ratio, the boiling thermal resistances decrease apparently, but the condensation resistances increase, both at low and high heat fluxes. We can see clearly the minimum thermal resistance is 0.04 K/W at FR = 15%, whereas the minimum boiling thermal resistance of 0.03 K/W is achieved with FR = 27%, reduced by approximately 25% compared to that of with FR = 15%.

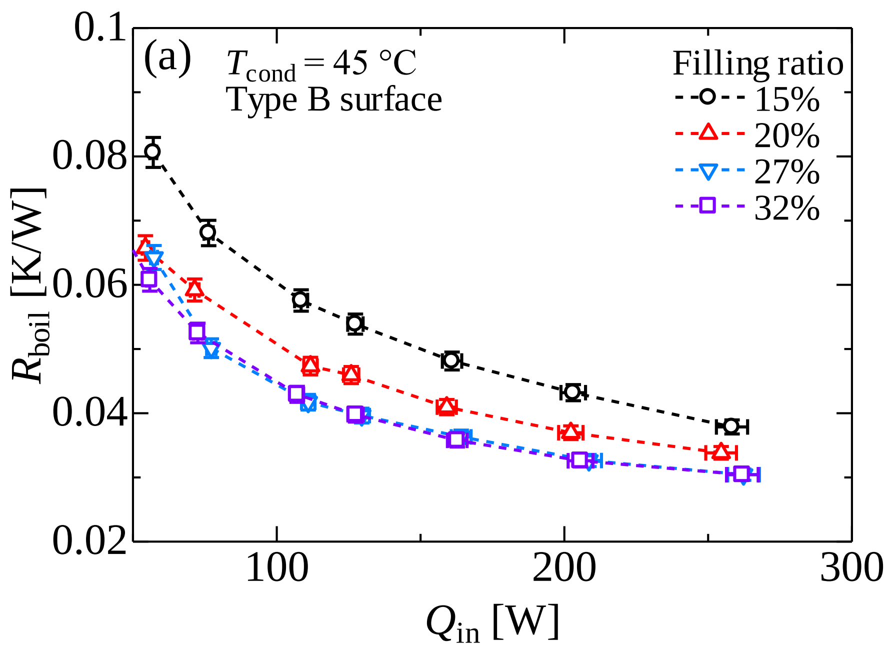

Fig. 3.9 Comparison of experimental results at different filling ratios. (a) The boiling thermal resistance R_{boil} vs. the heat input Q_{in}.

Fig. 3.11 represents the variation of the total thermal resistance as a function of heat flow rate. In light of the experimental results, the optimum system performance occurs when FR = 27%. The boiling thermal resistance varies from 0.07 K/W at Qin = 50 W to 0.03 K/W at Qin = 260 W. FR = 27% corresponds to the minimum of the evaporator operating temperature, heat transfer coefficient, and total thermal resistance, which are illustrated clearly in Fig. 3.12, and 3.13, the higher filling ratio, the higher heat transfer coefficient.

However, with an increase in the filling ratio, the effect of this factor weakens, and practically disappears from FR = 27% to FR = 32%. As seen from the comparison of thermal resistance, there is no remarkable difference between FR = 27% and FR = 32%. Because in the case of FR = 32%, there is a certain quantity of liquid occupying the vapor pipe, the difference in the liquid level in the boiling chamber is not obvious, less than 1.5 mm. When more working fluid is charged into the evaporator, the system pressure increases because the space for the vapor becomes smaller. Fig. 3.14 represents the variation of the system pressure as a function of heat flow rate. A higher system pressure leads to a higher saturation temperature of working fluid and hence reduces the superheat necessary for boiling under a given heat flux. For the case of FR = 15%, low system pressure gives high bubbles growth rates, large bubble volumes at detachment, and long waiting time between bubbles, leading to deterioration of the boiling performance [114]. Another reasonable explanation is that as the filling ratio increases, the resistance decreases due to the increase in liquid supply to the evaporator and high efficiency of vapor-liquid circulation [92]. On the other hand, for the condenser section, a larger system pressure (large filling ratio) enhances the temperature difference between vapor and tube wall of the condenser. Therefore, the efficiency of heat exchange becomes lower, which results in worse performance of the condenser.

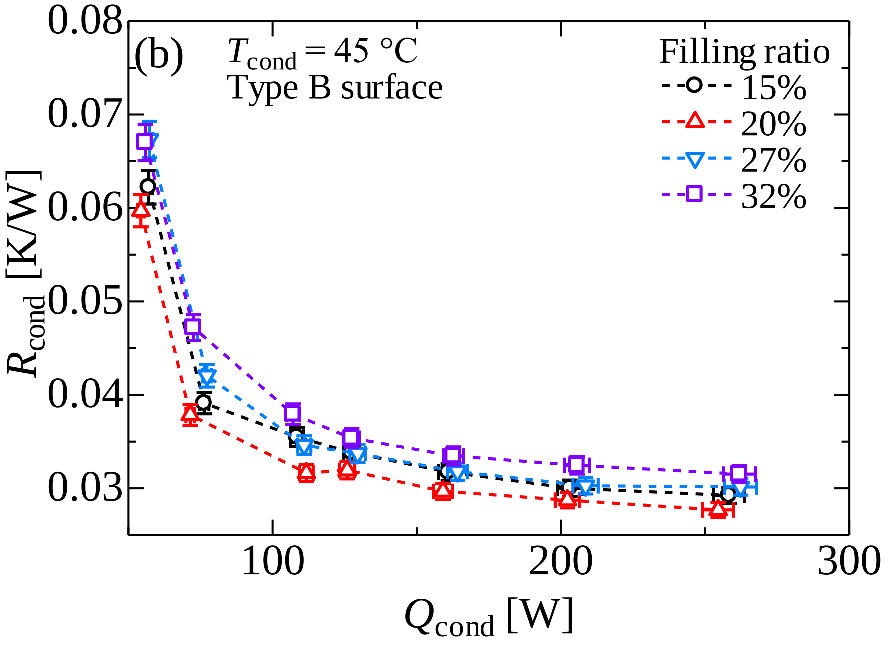

Fig. 3.10 Comparison of experimental results at different filling ratios. (b) the condensation thermal resistance R_{cond} vs. the condensation heat transfer rate Q_{cond}.

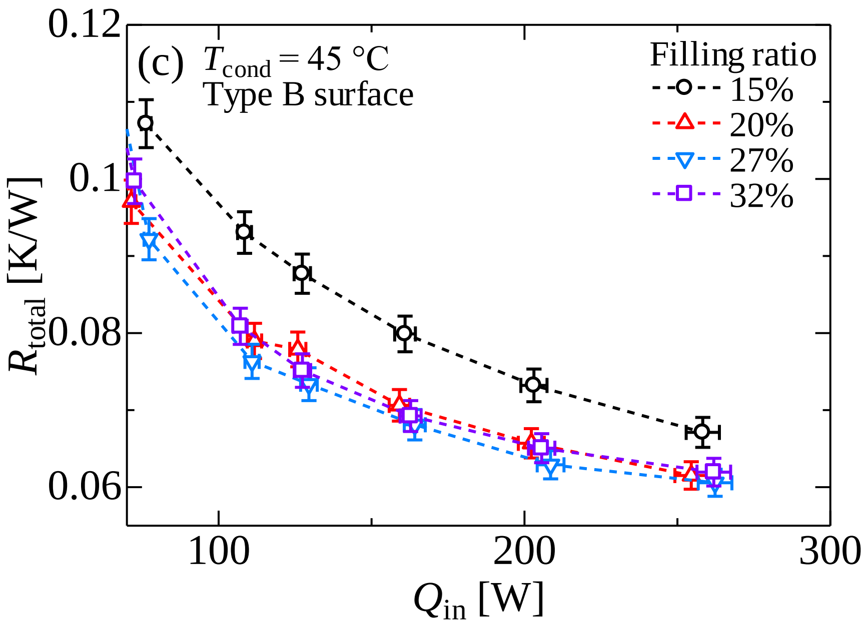

Fig. 3.11 Comparison of experimental results at different filling ratios. (c) the total thermal resistance R_{total} vs. the heat input Q_{in}.

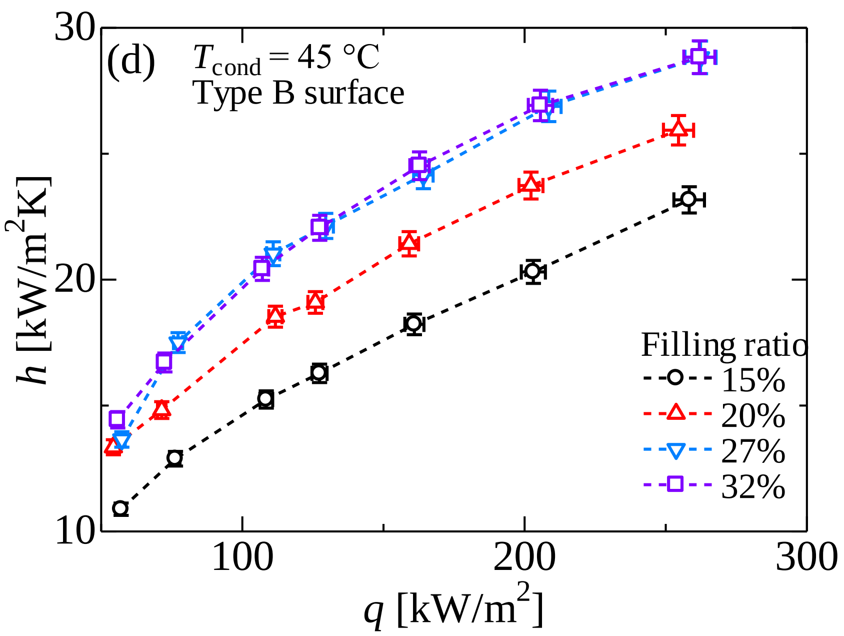

Fig. 3.12 Comparison of experimental results at different filling ratios. (d) the heat transfer coefficient of the evaporator h vs. the heat flux at the evaporator surface q.

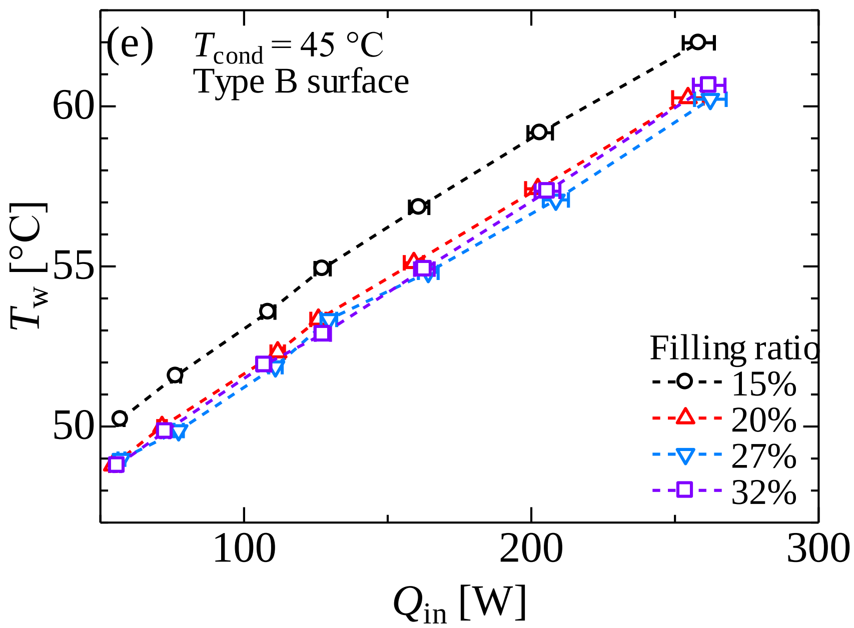

Fig. 3.13 Comparison of experimental results at different filling ratios. (e) the evaporator surface temperature T_w vs. the heat input Q_{in}.

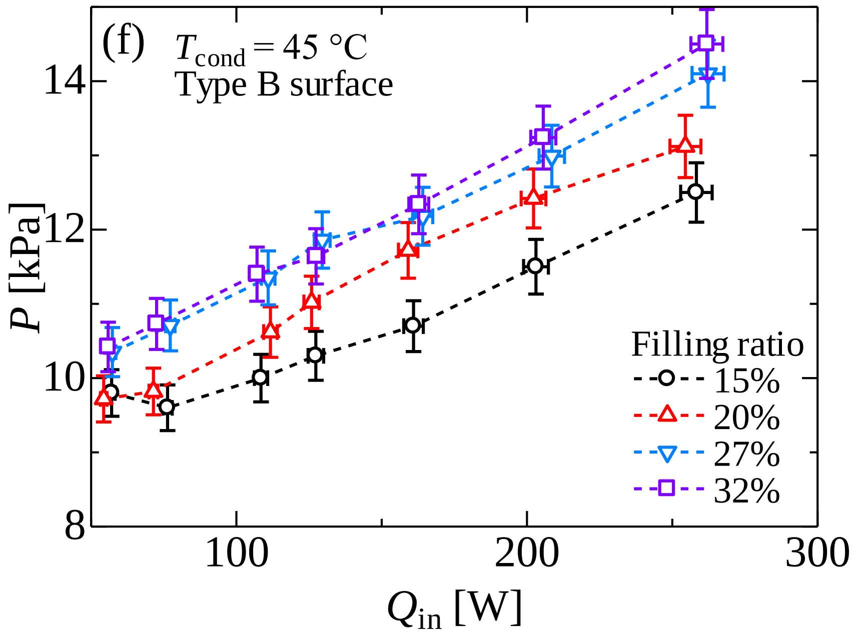

Fig. 3.14 Comparison of experimental results at different filling ratios. (f) the system pressure P vs. the heat input Q_{in}.

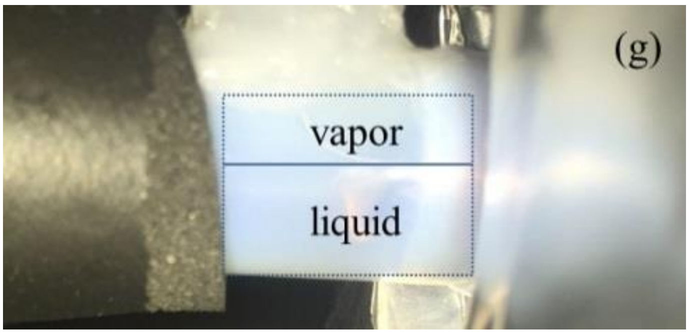

Fig. 3.15 Image of the vapor tube at FR = 32% which exhibits partial flooding.

For the case of higher charging levels above FR = 32%, partial flooding of the vapor tube could occur, reduce the driving force and weaken the vapor-liquid circulation more or less, as seen in Figs.3.15.

3.4 Effect of condenser temperature

3.4.1 Experimental results

The effect of the condenser temperature are investigated with Type B surface for the filling ratio of FR = 27% under the two conditions of T_{in} = 35 °C and T_{in} = 45 °C, respectively. Fig. 3.16, Fig. 3.17, and Fig. 3.18 show the changes in the thermal resistances with varying condenser temperatures in the range of heat loads from 50 W to 260 W. It is clear that heat transfer performance is enhanced effectively by increasing the condenser temperature. For the boiling thermal resistance, the values in the case of T_{in} = 45 °C are obviously lower than that of T_{in} = 35 °C by 20% to 30% owing to the more stable nucleation sites and better boiling performance shown in Fig. 3.16 and Fig. 3.17.

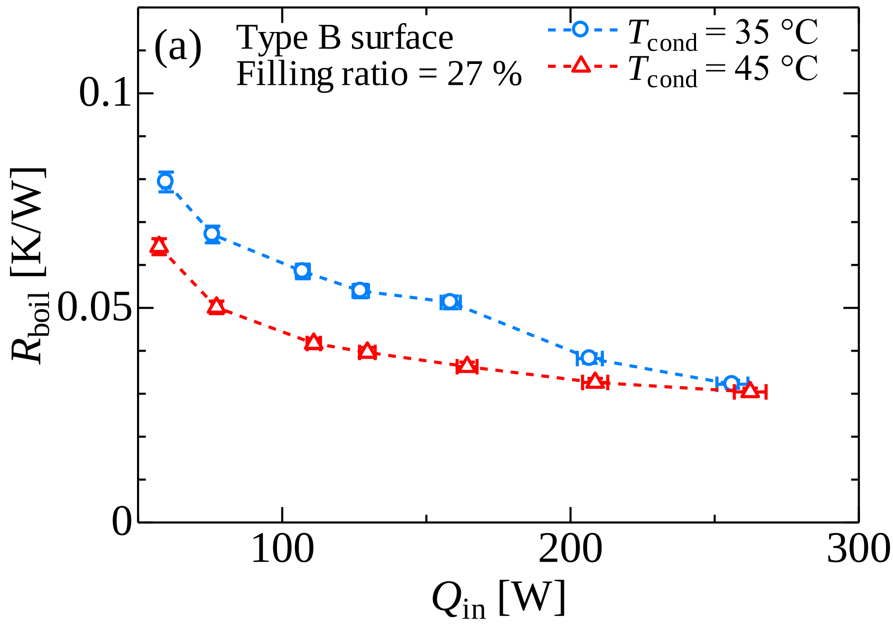

Fig. 3.16 Comparison of experimental results at different condenser temperatures. (a) The boiling thermal resistance R_{boil} vs. the heat input Q_{in}.

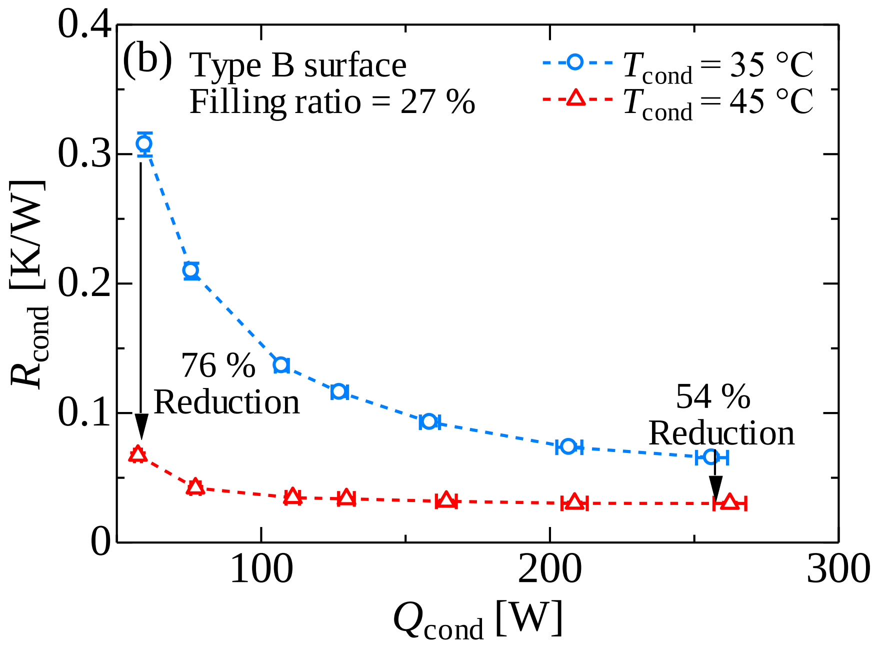

Fig. 3.17 Comparison of experimental results at different condenser temperatures. (b) the condensation thermal resistance R_{cond} vs. the condensation heat transfer rate Q_{cond}.

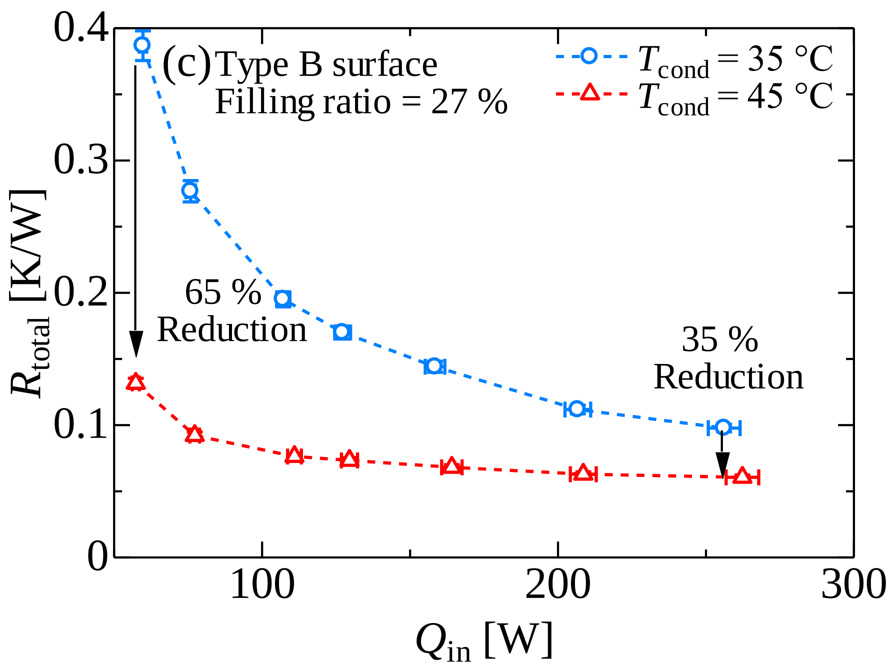

Fig. 3.18 Comparison of experimental results at different condenser temperatures. (c) the total thermal resistance R_{total} vs. the heat input Q_{in}.

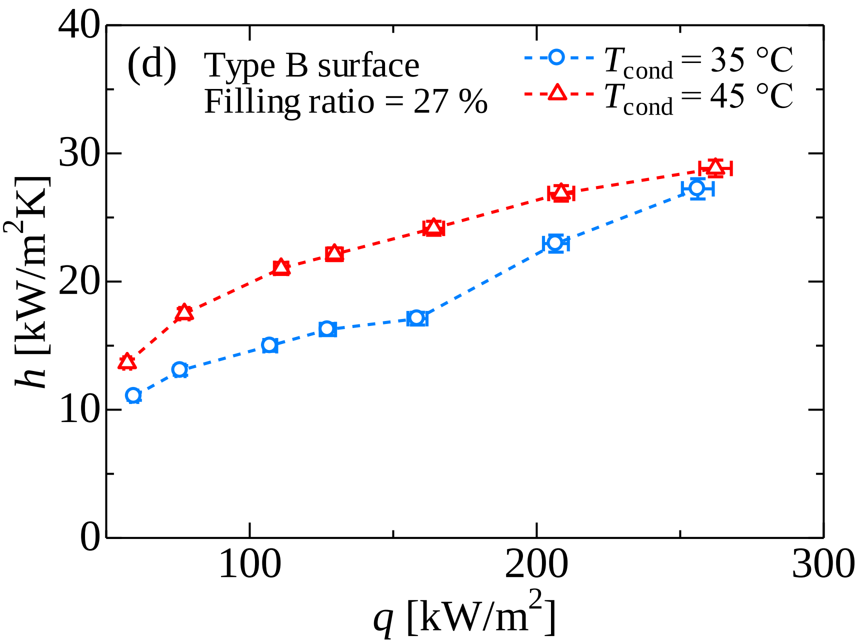

Fig. 3.19 Comparison of experimental results at different condenser temperatures. (d) the heat transfer coefficient of the evaporator h vs. the heat flux at the evaporator surface q.

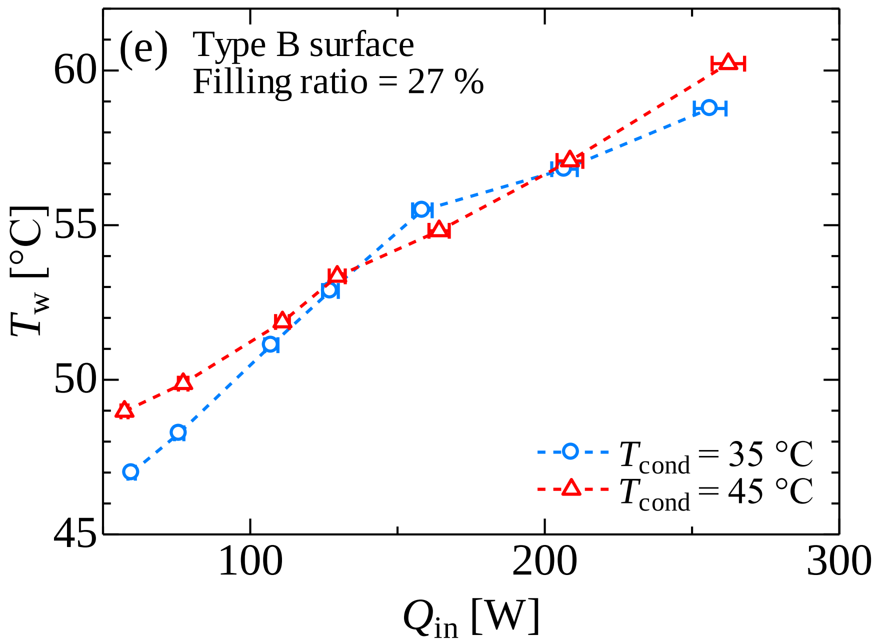

Fig. 3.20 Comparison of experimental results at different condenser temperatures. (e) the evaporator surface temperature T_w vs. the heat input Q_{in}.

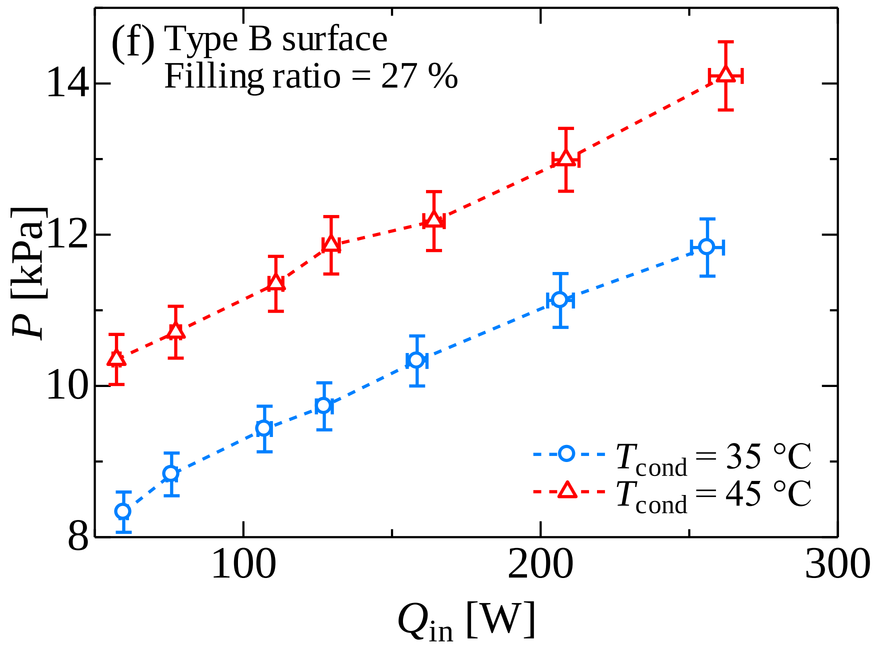

Fig. 3.21 Comparison of experimental results at different condenser temperatures. (f) the system pressure P vs. the heat input Q_{in}.

There are still inactive spots on the surface at q = 107.1 kW/m^2 in the case T_{in} = 35 °C, as shown in Fig. 3.16. For T_{in} = 35 °C, the saturation pressure is lower than the case for T_{in} = 45 °C. Due to the delay of ONB at lower pressure, it is difficult for the bubble nucleation to occur at T_{in} = 35 °C, resulting therefore in the higher superheat [72]. When T_{in} = 45 °C shown in Fig. 3.17, it is reduced by around 54% to 76% for the condenser thermal resistance due to the smaller temperature difference between the evaporator and condenser. In contrast, the larger temperature difference reduces the heat transfer efficiency.

These results make it clear the total thermal resistance of this loop thermosyphon decreases considerably at more suitable condenser cooling T_{in} = 45 °C in the entire range of heat loads, with the maximum reduction over 0.2 K/W at low heat flux. With the increase of heating power and system pressure, the similar quantities of active nucleation sites under these two conditions result in smaller gap, as seen in Fig. 3.18

and Fig. 3.19. When the condenser temperature increases from T_{in} = 35 °C to T_{in} = 45 °C as shown in Fig. 3.19, the heat transfer coefficient is improved significantly by around 40%, from 15 kW/m^{2}K to 21 kW/m^{2}K, at the corresponding heat flux q = 100 kW/m^2. The saturation temperature (pressure) will decrease with decreasing condenser temperature. The evaporator surface temperatures in both cases coincide with each other throughout the whole experimental process from Fig. 3.20. That means we observe the similar heat dissipation performance even when using the less intensive condenser. The result shows cooling water at T_{in} = 45 °C in the condenser is more suitable for the present system due to the lower boiling and condensation thermal resistances.

In the case of T_{in} = 35 °C, the system pressure and saturation temperatures are lower than those at T_{in} = 45 °C, as shown in Fig. 3.21, and both the departure time and the departure radius of the bubbles increase substantially with decreasing pressure [69].

3.4.2 Bubble behaviors

(a)

q = 107.1 kW/m^2, ΔT_{sat}=7.1 K, T_w=51.1 °C

(b)

q = 110.9 kW/m^2, ΔT_{sat}=5.2 K, T_w=51.9 °C

(c)

q = 206.7 kW/m^2, ΔT_{sat}=9.0 K, T_w=56.8 °C

(d)

q = 205.8 kW/m^2, ΔT_{sat}=7.9 K, T_w=57.2 °C

Fig. 3.22 Comparison of bubble behaviors at the conditions of (a) T_{in} = 35 °C, and Q_{in} = 110 W, (b) T_{in} = 45 °C, and Q_{in} = 110 W, (c) T_{in} = 35 °C, and Q_{in} = 220 W, and (d) T_{in} = 45 °C, and Q_{in} = 220 W. The surface is Type B, and FR = 27%.

It is found that the condenser temperature is related to the bulk (saturation) temperature as well as the system pressure. Thus, since the heat transfer performance is dependent on the system pressure, the higher system pressure (T_{in} = 45 °C), leads higher density of active nucleation sites and larger heat transfer coefficient [115]. This will dramatically decrease the wall superheat and enhance the heat transfer as seen in Fig.

3.22 (b) and (d). We have also tested the pool boiling experiments at sub-atmospheric pressures and the results (which will be published elsewhere) show the same trend.

3.5 Heat loss test

For measuring the effect of the heat loss to the ambient on the loop thermosyphon operation, several measurements and calculations are studied. Heat loss is calculated from the difference of the heat transfer rates between the evaporator and condenser. Three series of experiments are performed to test the heat transfer performance in the recent environment. The amount of input heat Q_{in} and the condensation heat transfer rate Q_{cond} are different due to the heat loss of the thermosyphon [112]. Therefore the heat loss of loop thermosyphon Q_{loss} is defined by the following equation:

$$Q_{loss} = Q_{in} - Q_{cond} \tag{3.1}$$

When the heat input is lower than 100 W, Q_{loss} is occupied averagely about 50% of the total heat input due to the smaller temperature gap between the evaporator and the condenser. There is almost no absorption heat in the condenser part. While it is over 100 W, Q_{loss} is less than 30%, as seen in Fig. 3.23. The temperature difference between the boiling and condenser part is about 5 K at the corresponding heat input of 260 W. Heat loss caused by the natural convection of the heating block and boiling chamber to the ambient take up over 80% of the total heat loss, as shown in Fig. 3.24.

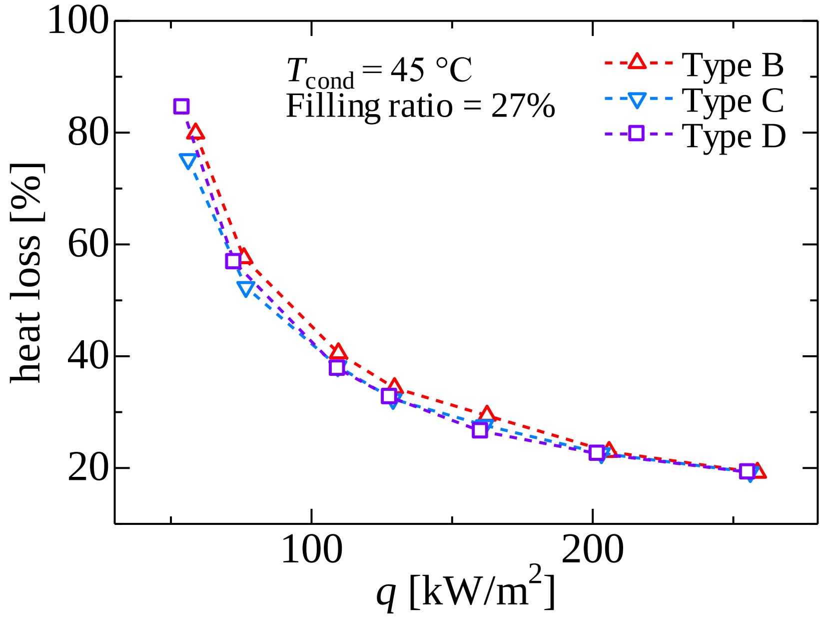

Fig. 3.23 Heat loss of the loop thermosyphon on operating condition. The tested evaporator surfaces are Type B, C, and D, heat flux from 50 to 260 kW/m^2.

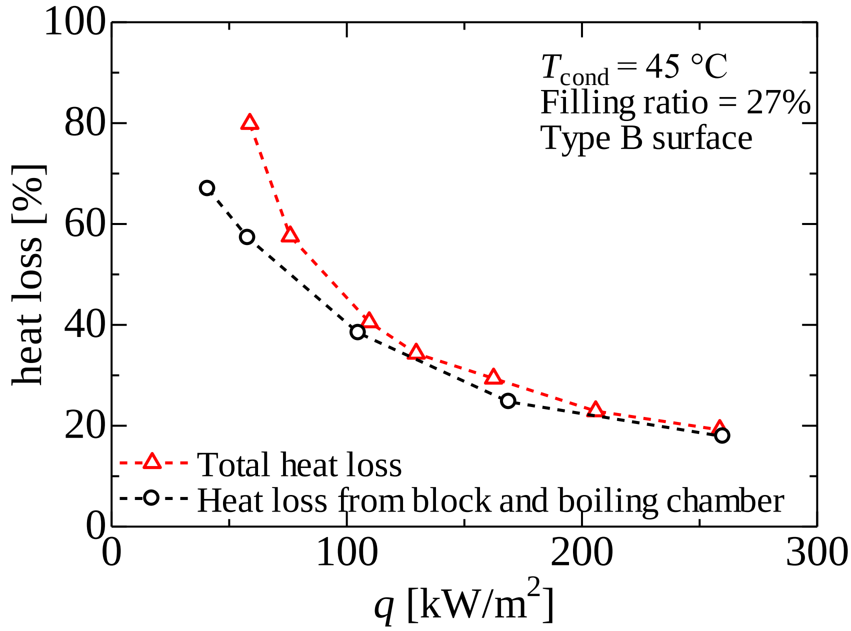

Fig. 3.24 The proportion of the heat loss from the boiling chamber and heating block The durability test of the hydrophobic spots coating.

3.6 Durability test of hydrophobic spots

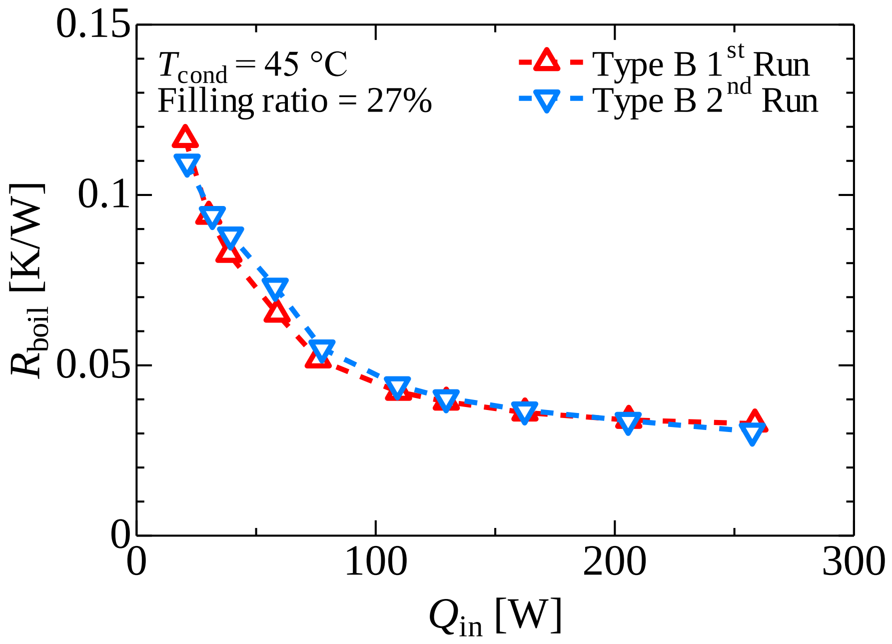

Fig. 3.25 Durability test of the coating on the surface. The boiling thermal resistance R_{boil} vs. the heat input Q_{in}.

The durability is always a problem. From Fig. 3.25, there is not a distinct difference between the 1st run and 2nd run using the same coating surface. This confirms that the coating spots are not damaged in the 1st run. It will not affect the experimental results. This paper focuses only on elucidating the effect of surface wettability design of the evaporator on overall heat-pipe thermal performance. For practical application, of course more durable hydrophobic coating material is needed, which will be studied at the future work.

3.7 Comparison between experimental results and models

According to Li's correlation [116], the relation of the wall superheat and the heat flux can be expressed as follows:

$$\frac{c_{pl}\Delta T_{sat}}{h_{lv}} = 0.013 C_s^{-0.33}\left[\frac{q_w}{h_{lv}\mu}\sqrt{\frac{\sigma}{g(\rho_l-\rho_v)}}\right]^{0.33} \mathrm{Pr}_l\, l \tag{3.2}$$

$(1° \leq \theta \leq 90°,\ 0.212 \leq C_s \leq 1.206)$

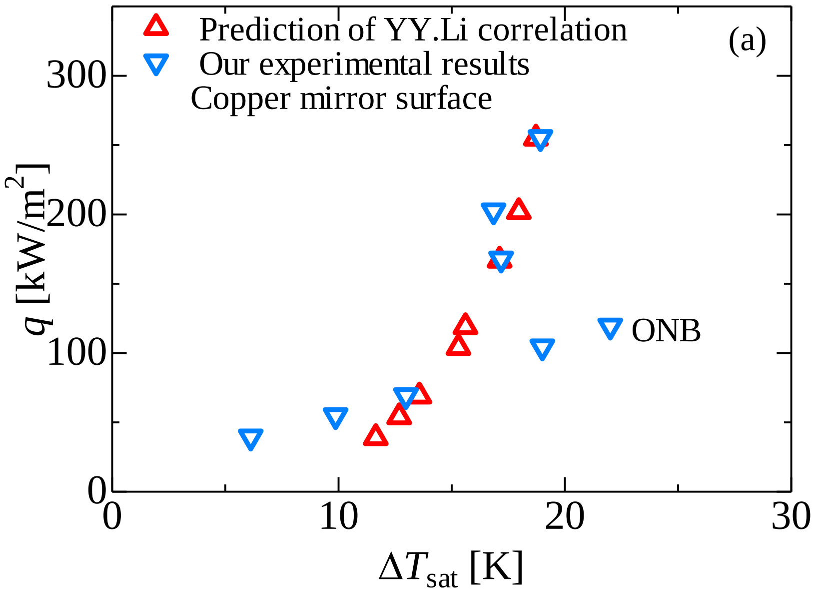

Fig. 3.26 Comparison of the predicted value by Li's correlation and our experimental results. (a) copper mirror surface.

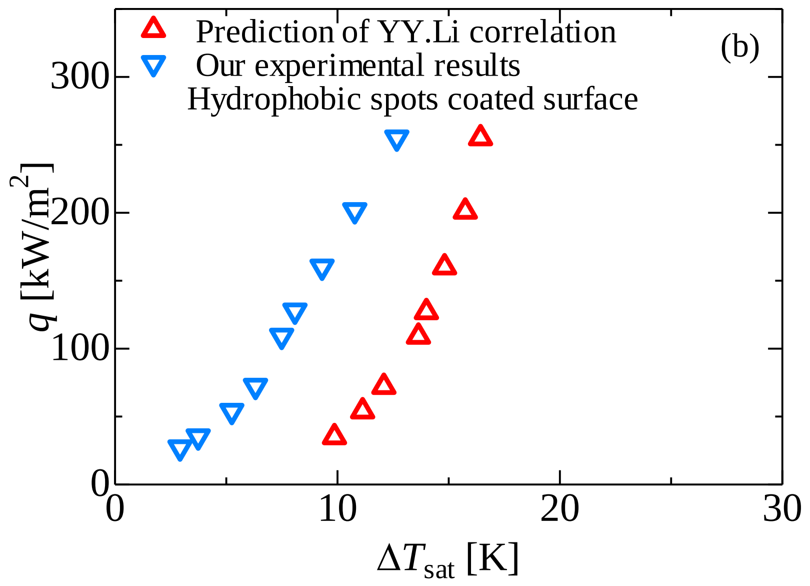

Fig. 3.27 Comparison of the predicted value by Li's correlation and our experimental results. (b) hydrophobic spots coated surface.

Firstly, a comparison between Li's correlation and our experimental result on copper mirror surface has been performed. As you can see from Fig. 3.26, without regard to the onset of nucleate boiling, the predicted values of Li's correlation and our experimental results coincide within ± 10%. For the hydrophobic spot-coated surface, the predicted values and the experimental data coincide within ± 40% in Fig. 3.27. The big error is caused by the limited range of parameters θ and C_s. The parameters for hydrophobic spot-coated surface are out of range (θ = 145° and C_s = 1.72). Therefore, Li's correlation unfortunately cannot represent the boiling performance of the present biphilic surface.

3.8 Conclusions

The experimental study of a two-phase loop thermosyphon for cooling CPU from a mixed-wettability evaporator surface has been carried out. The pattern of coating on the surface comprises hydrophobic spots with three different sizes. A parametric analysis of the heat transfer performance under various heat inputs, filling ratios, and condensation temperatures has been performed. The conclusions are as follows,

(1) Mixed-wettability surfaces show much better boiling heat transfer performance due to the steady and continuous bubble behavior compared with the copper mirror surface. The maximal reduction of the surface temperature is 17 K.

(2) For the patterned surfaces, the nucleate boiling performance is enhanced as the spot diameter decreases.

(3) Two condenser conditions (35 °C and 45 °C) are studied. The total thermal resistance at the condenser temperature of T_{in} = 45 °C is reduced by 35% to 65% compared with that of 35 °C.

(4) An increasing filling ratio enhances the saturation pressure and temperature of the system significantly, and results in excellent nucleate boiling.

(5) The optimum system performance occurs when the Type-B surface is applied under the conditions of Q_{in} =150 W – 260 W and FR = 27%. Boiling thermal resistance is as low as 0.03 K/W with a corresponding total thermal resistance of 0.057 K/W.

Chapter 4 Experimental study on FDPA coated surface

In this chapter, the nano-textured surface is tested. FDPA (1H,1H,2H,2H-perfluorodecylphosphonic acid) coated evaporator surface is studied to compare with different size of patterned spots. The results will be used for the comparison with other structured surfaces in Chapter 5.

4.1 Patterned surface

Photos of the patterned mixed-wettability surfaces used in this study are shown in Fig. 4.1. They are made from polished copper (CA ≈ 80°) and then coated with TiO_2 layer, using sputtering method. When TiO_2 surface is exposed to a UV light for more than 12 hours, its contact angle for water is close to 10°, which can provide a very high critical heat flux [99]. After that, a perfluorinated compound (PFC), FDPA is coated on a TiO_2 surface, which have large contact angles, more than 150°. The spots diameter ranges from 1 mm to 2 mm and these spots are distributed in a rectangular array with a pitch 3mm, and also the full cover pattern in the center, as shown in Table 4.1.

Table 4.1 Hydrophobic spot parameters on TiO_2 surfaces of Type-a, b, c, and d.

Case	Spot diameter, d (mm)	Pitch, p (mm)
Type a	NA	NA
Type b	1	3
Type c	2	3
Type d	Full cover	Full cover

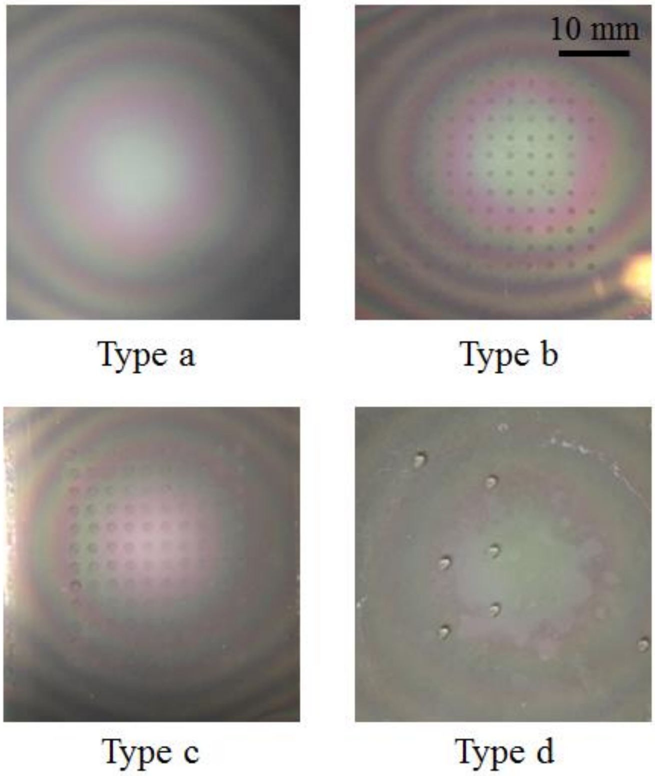

Fig. 4.1 TiO_2 surface Type-a and mixed-wettability surfaces (with hydrophobic spots coated on TiO_2 surfaces) Type-b, Type-c, and Type-d (full cover).

The contact angles with TiO_2 surface and FDPA coated surface are shown in Fig. 4.2. The contact angle with TiO_2 surface is lower than 20° without UV light, which is more than 150° of FDPA coated surface and with excellent bubble nucleation performance.

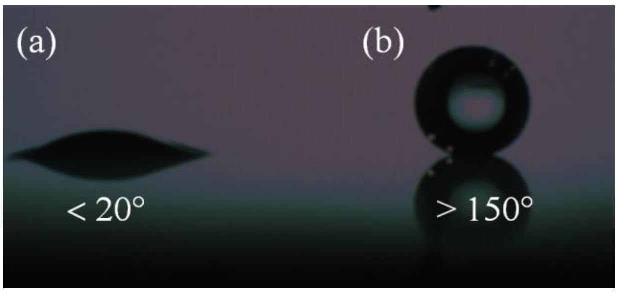

Fig. 4.2 Contact angles of (a) TiO_2 surface, (b) hydrophobic spots coated surface.

4.2 Comparison of experimental results

4.2.1 Experimental results

Fig. 4.3 – Fig. 4.6 show the comparison of the experimental results of Type-a, b, c, and d surfaces, as the heating power rising from Q_{in} = 30 W to Q_{in} = 260 W. The saturation temperature changes from 45 – 53 °C. The superheats of the surfaces at ONB are presented in Table 4.2. From the results of an analysis, as shown in Fig. 4.3, it indicates that the boiling thermal resistances of Type-b – Type-d surfaces are much smaller than that of Type-a, which is TiO_2 coating surface. R_{boil} decreases accordingly with the increasing heating power due to the rising pressure in the system and more active nucleation sites. The mixed-wettability surfaces Type-c – Type-d induce onset of nucleate boiling (ONB) at extremely low superheating, near 3 K at a very low heat flux of q = 30 kW/m^2, whereas it is 18 K for TiO_2 surface (Type-a) at the corresponding q = 120 kW/m^2. Owing to the small coating area on Type-b surface, ONB is about 6 K at q = 50 kW/m^2. Due to the material properties, FDPA coating is harder than HNTs coating, and the durability and bubble nucleation performance also are not as well as that of HNTs coated surfaces.

Table 4.2 Superheat of onset nucleate boiling on surfaces Type-a, b, c, and d.

Case	Superheat of ONB, ΔT (K)	q (kW/m^2)
Type a	21.7	125.3
Type b	6.3	41.2
Type c	3.28	31.1
Type d	3.0	30.5

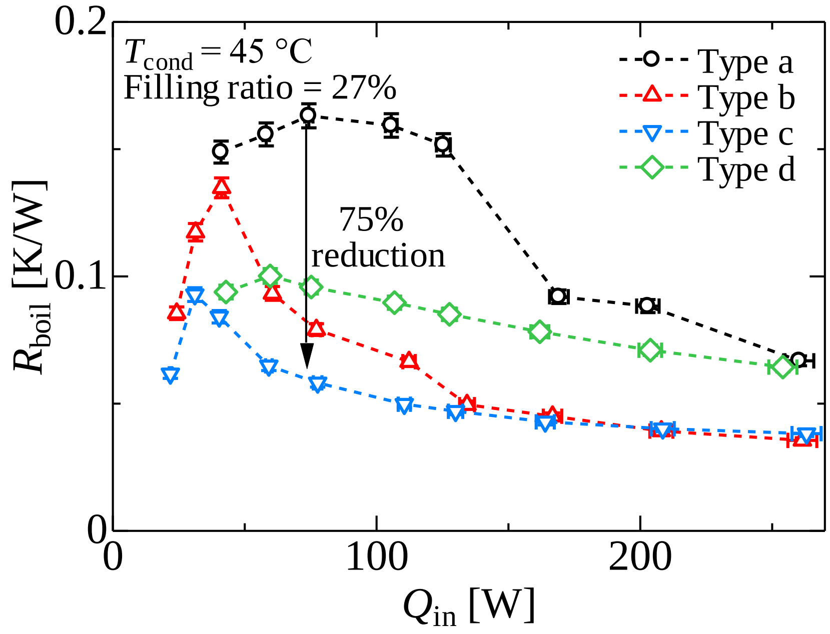

Fig. 4.3 Comparison of experimental results of Type-a – Type-d. The boiling thermal resistance R_{boil} vs. the heat input Q_{in}.

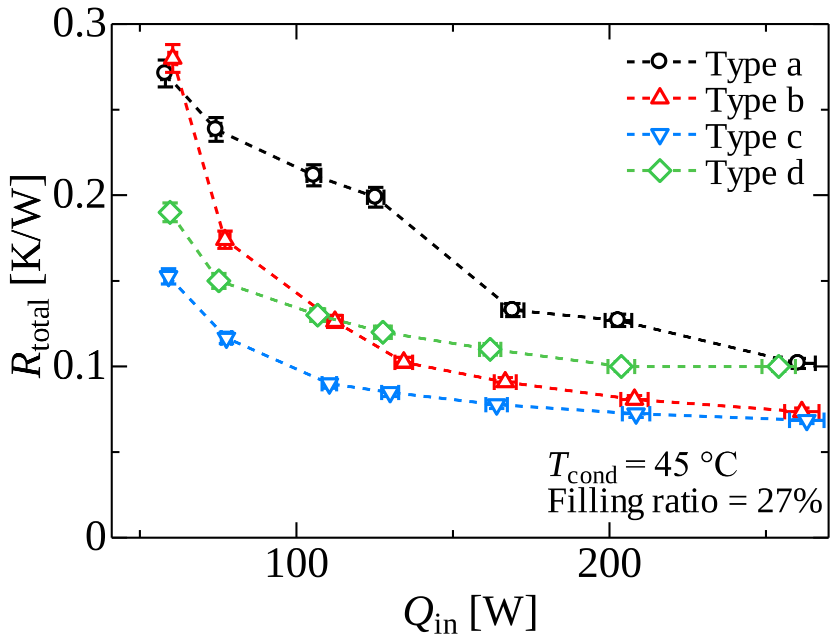

Fig. 4.4 Comparison of experimental results of Type-a – Type-d. The total thermal resistance R_{total} vs. the heat input Q_{in}.

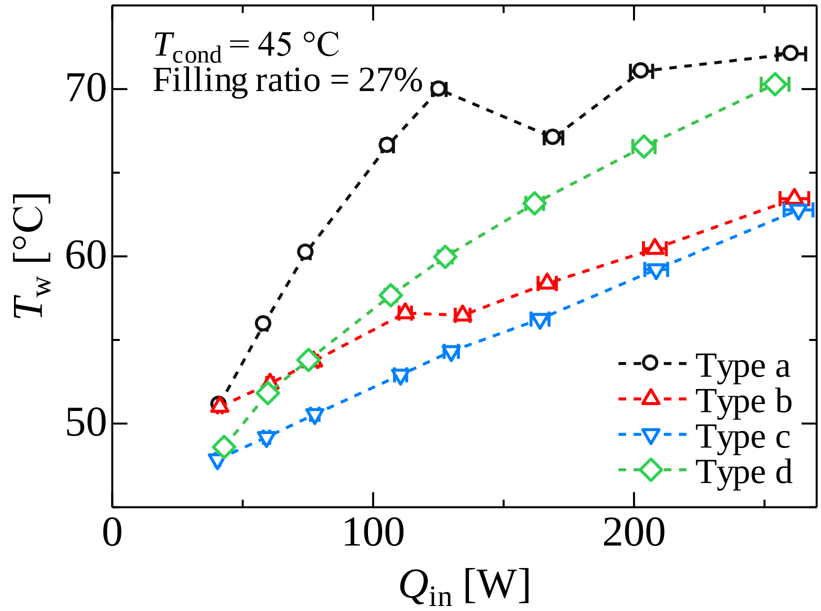

Fig. 4.5 Comparison of experimental results of Type-a – Type-d. The evaporator surface temperature T_w vs. the heat input Q_{in}.

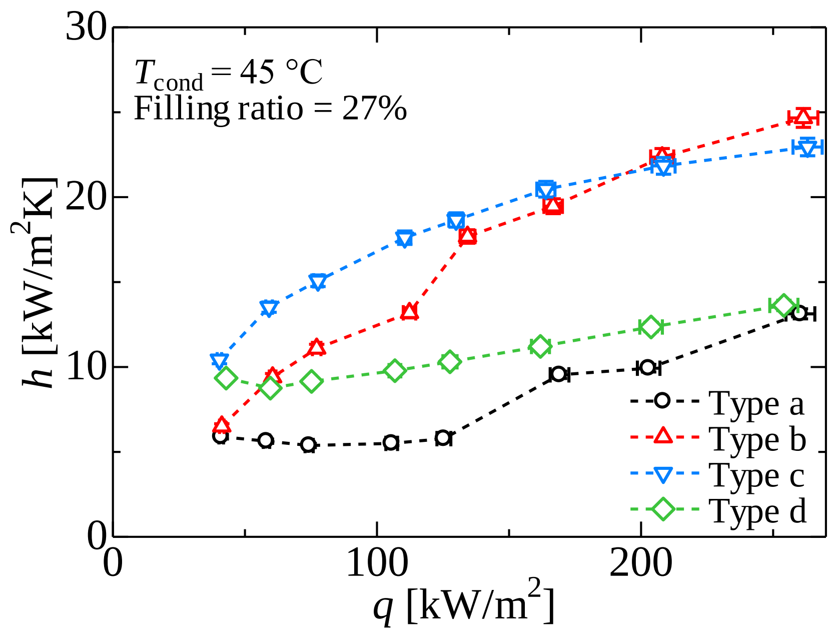

Fig. 4.6 Comparison of experimental results of Type-a – Type-d. The heat transfer coefficient of the evaporator h vs. the heat flux at the evaporator surface q.

As seen in Fig. 4.3 and Fig. 4.4, Type-c surface, which has diameter 2 mm, pitch 3 mm patternned spots, gives the lowest boiling and total thermal resistances. The results maybe a little bit difference from that of chapter 3, HNTs patternned surface. The best result is achieved from the surface with diameter1 mm, pitch 3 mm spots. In this chapter, the coating process is totally different. The mask covered surface is immersed in the solution with FDPA particles. For the smaller diameter mask, the solution maybe can not touch the surface sufficiently and affect the coating performance.

4.2.2 Bubble behavoirs

In consideration of both the boiling and total thermal resistance are shown in Fig. 4.3 and Fig. 4.4, which confirms that the thermal performance of this thermosyphon can be strengthened evidently by using patterned surfaces. As compared to the plain surface (Type-a), the boiling thermal resistance is an average reduced 75% for Type-c. The observations of the compared bubble behaviors are shown in Fig. 4.7, including Type-a – Type-d surfaces at the moderate heat fluxes 130 kW/m^2. Same as HNTs coating surfaces, the boiling with higher heat fluxes and pressures show more violently bubbles. It is easier for the bubble to be generated and grown on hydrophobic spot coated surface than that of the plain surface, which may results in large undesirable temperature oscillations at the heated surface. For the full-cover surface, Type-d achieves the higher thermal resistance and surface temperature compared with Type-b and Type-c. As shown in Fig. 4.7, the center part of the heat transfer surface is covered with a vapor blanket. The bubbles coalescence and then transition to film boiling with large superheat, which provides the poor heat transfer performance [100].

Type-a

q = 125.3 kW/m^2, ΔT_{sat}=21.7 K, T_w=69.9 °C

Type-b

q= 134.3 kW/m^2, ΔT_{sat}=7.6 K, T_w=56.5 °C

Type-c

q = 129.9 kW/m^2, ΔT_{sat}=6.9 K, T_w=54.3 °C

Type-d

q = 127.6 kW/m^2, ΔT_{sat}=12.4 K, T_w=59.9 °C

Fig. 4.7 Bubble behaviors on surfaces Type-a – Type-d at heat flux of 130 kW/m^2. The operating pressure is 10 kPa, and FR = 27%.

4.3 Effect of filling ratio

The filling ratio is a very important factor to influence the heat transfer performace of the loop thermosyphon [117, 118]. We have studied the effect of filling ratio in chapter 3. In this chapter, we consider the filling ratio tests with FDPA coated surface once again to prove the results we get. The above effect has been studied for three filling ratios, FR = 22%, FR = 27%, and FR = 33%, respectively. There are no dry-out and flooded phenomenon during the experiemtal operation.

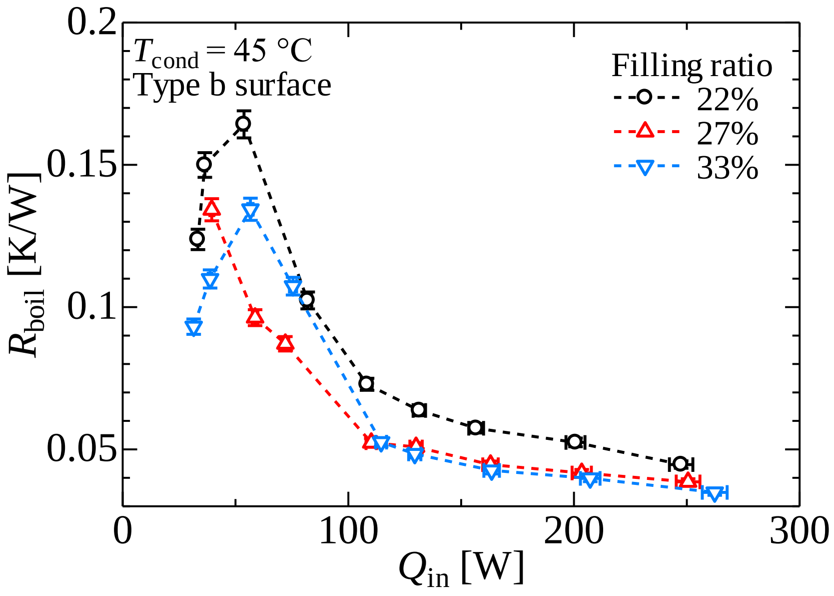

Fig. 4.8 Comparison of experimental results at different filling ratios. The boiling thermal resistance R_{boil} vs. the heat input Q_{in}.

According to Fig. 4.8, with an increased filling ratio, the boiling thermal resistances decrease apparently when the heat input achieves 100 W. It is reduced by more than 20% compared to that of with FR = 22%. Lower filling ratio results in worse thermal performance, this conclusion is agree with that of chapter 3. For the condensation thermal resistance, as shown in Fig. 4.9, with the increasing of filling ratio, R_{cond} increases gradually. Taken together, the total thermal resistances are shown in Fig. 4.10. It is found that the lowest thermal resistance comes from FR = 27%, which is always excellent during the whole experimental operating process.

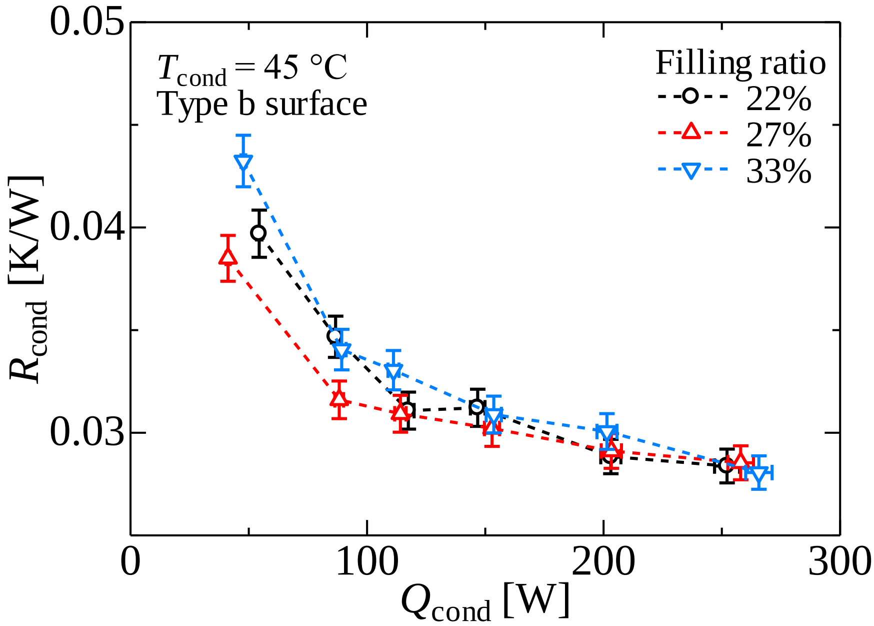

Fig. 4.9 Comparison of experimental results at different filling ratios. The condensation thermal resistance R_{cond} vs. the condensation heat transfer rate Q_{cond}.

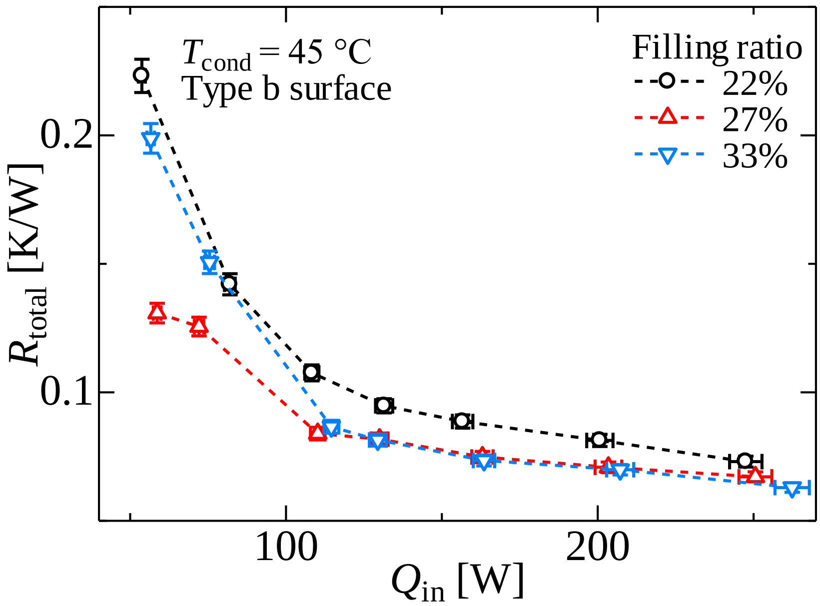

Fig. 4.10 Comparison of experimental results at different filling ratios. The total thermal resistance R_{total} vs. the heat input Q_{in}.

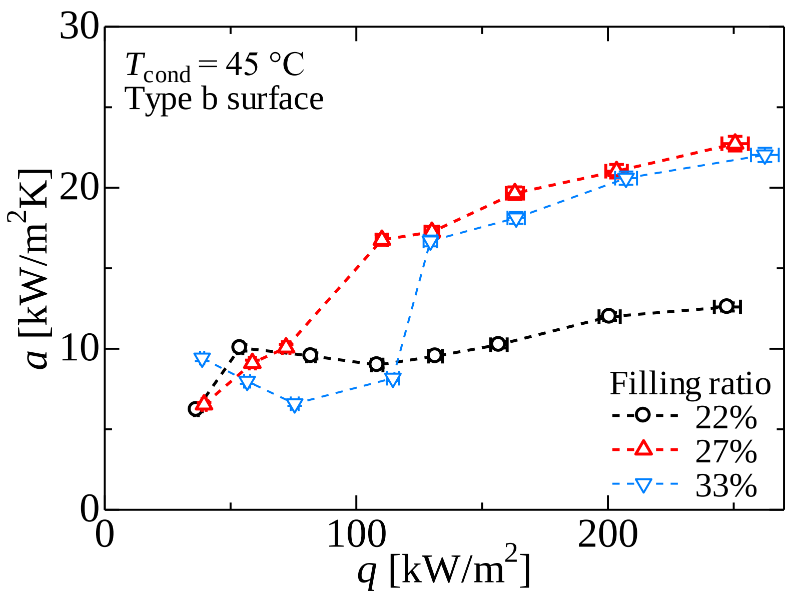

Fig. 4.11 Comparison of experimental results at different filling ratios. The heat transfer coefficient of the evaporator *h* vs. the heat flux at the evaporator surface *q*.

In light of the experimental results of heat transfer coefficient in Fig. 4.11, the optimum system performance occurs while FR = 27%. The heat transfer coefficient of FR = 27% and FR = 33% are twice larger than that of FR = 22%. This conclusion can be attributed to the system pressure and liquid supply efficiency. The system pressure measurement are shown in Fig. 4.12. If plenty of working fluid is charged into the boiling chamber, the system pressure increases because the space for the vapor becomes smaller. Low system pressure gives the high bubbles growth rates, the large bubble volumes at detachment, the long waiting time between bubbles, and the deterioration of the boiling performance [114]. Another reason is that higher filling ratio strengthens the liquid supply ability, and then accelerates the circulation of the vapor and liquid flowing.

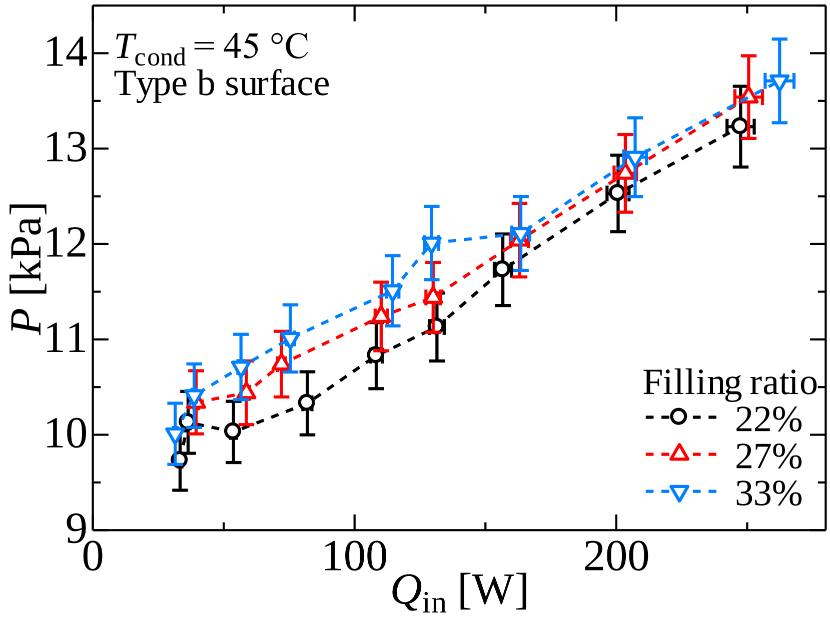

Fig. 4.12 Comparison of experimental results at different filling ratios. The system pressure P vs. the heat input Q_{in}.

Chapter 5 Experimental study on Ni-PTFE coated surface

In this chapter, the new experimental tests of non-electroplating Ni-PTFE (polytetrafluoroethylene) coated surfaces are presented, and the influences of operating parameters on the patterned spots size and heat input are discussed. Best results of three kinds of hydrophobic spot coated surfaces are compared with the machined surface.

5.1 Patterned surface

To optimize the performance of a loop thermosyphon, this work focuses on providing a detailed understanding of heat transfer enhancement of a mixed-wettability surface at sub-atmospheric pressures with water as the working fluid. We found that the heat transfer coefficient of patterned surfaces was enhanced by 3 times compared to that of an uncoated copper surface, with an evaporator surface temperature reduction of 10 K – 17 K corresponding to the heat flux changes from 30 kW/m^2 to 260 kW/m^2.

The evaporator surfaces coated with a pattern of hydrophobic circle spots (non-electroplating, 0.5 – 2 mm in diameter and 1.5 – 3 mm in pitch) achieve very high heat transfer coefficient and lower the incipience temperature overshoot using water as the working fluid. Sub-atmospheric boiling on the hydrophobic spot-coated surface shows a much better heat transfer performance.

The production processes of non-electroplating mixed-wettability surface, as shown in Fig. 5.1:

(a) Mirror finishing and cleaning with acetoneand, alkaline degreasing for 20 min.
(b) Patterning with photolithography and baking at 110 °C for 5 min.
(c) Covered by the mask and exposed under the UV light for 2 min 40 seconds.
(d) Immersed in the imaging liquid for 6 min.
(e) Base Ni plating for 20 min at 85 °C, main PTFE plating for 40 min at 85 °C.
(f) Removing of the photoresist-mask at 50 – 70 °C for 20 min.

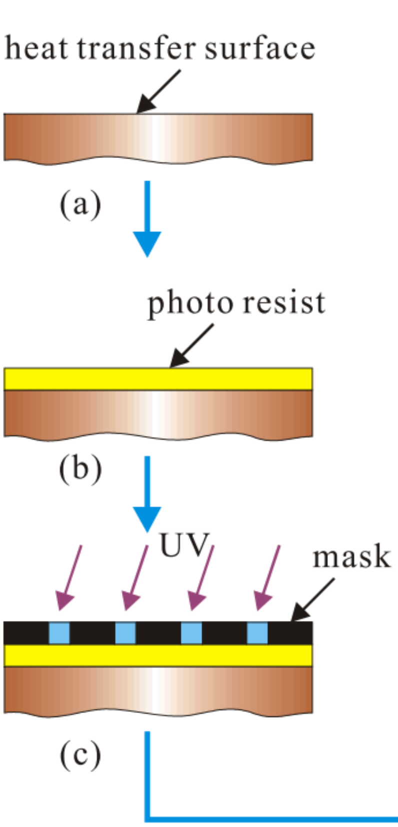

Fig. 5.1 Process of Ni-PTFE coating by photolithography [1].

Table 5.1 Hydrophobic spot parameters on copper mirror surfaces of Type Ⅰ, Ⅱ, Ⅲ, Ⅳ, Ⅴ, and Ⅵ.

Case	Spot diameter, d (mm)	Pitch, p (mm)
Type Ⅰ	NA	NA
Type Ⅱ	0.5	3
Type Ⅲ	1	1.5
Type Ⅳ	1	3
Type Ⅴ	2	3
Type Ⅵ	Full cover	Full cover

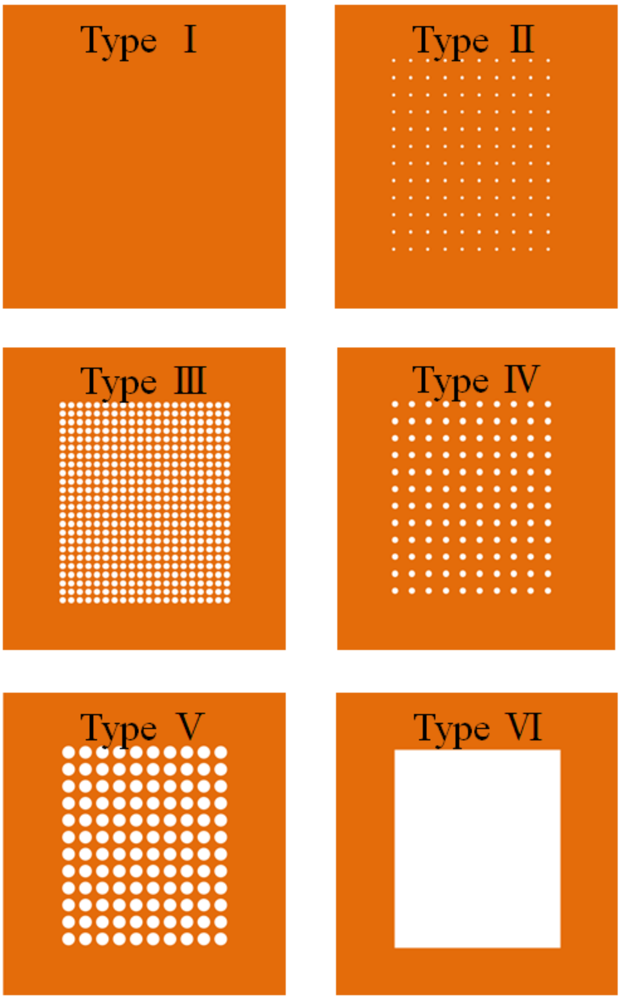

Fig. 5.2 Non-electroplating mixed-wettability surfaces of Type Ⅱ, Ⅲ, Ⅳ, Ⅴ, Ⅵ, and copper mirror Type Ⅰ.

The surfaces we used in loop thermosyphon experiments are shown in Fig. 5.2 Table 5.1 shows the pattern parameters of them, different diameters and pitches of coated spots. Particularly in the case of Type Ⅵ surface, it is full covered with hydrophobic material on the heating area. Type Ⅰ surface is mirror surface without any coating. The photograph of the Ni-PTFE spots patterned surface is presented in Fig. 5.3.

Fig. 5.3 Photograph of the Ni-PTFE spots patterned surface, Type Ⅴ.

5.2 Experimental results of Ni-PTFE coated surface

5.2.1 Experimental results

We have used the non-electro plating with Ni-PTFE particles and its contact angle to water is over 150°. As seen from Fig. 5.4, there is the comparison of the experimental results of Type Ⅰ to Ⅵ surfaces, at heat inputs from 30 to 260 W. The boiling thermal resistance of patternned surface is reduced by more than 60% averagely compared to that of mirror surface. The comparison among spots coated surfaces of Type Ⅱ – Type Ⅴ because of the large density of spots. For the case of Type Ⅱ surface with spots diameter 0.5 mm, it is very difficult to start the nucleate boiling at such small coating area of the spot. There are still inactive spots on the surface when heat input is 130 W. So the boiling thermal resistance is much larger than that of other spots coated surface at low heat flux. Due to the larger diameter spots, the larger bubbles are generated from Type Ⅴ surface, which affect the frequency of bubble departure and HTC. On the base of Fig. 5.5 and Fig. 5.7, we can see Type Ⅲ still indicates the highest HTC and the lowest total thermal resistance due to the large density of the nucleation sites. The surface temperature is lowered by 15 K between Type Ⅲ and Type Ⅰ surface seen in Fig. 5.6. From the results of an analysis, it is found that the boiling thermal resistances of Type Ⅱ – Type Ⅵ surfaces are much lower than that of Type Ⅰ resulting from the outstanding bubble nucleation as shown in Fig. 5.8. Type Ⅲ surface gives the lowest boiling thermal resistance. A large amount of coated spots provide more opportunities for the bubble nucleation, as shown in Fig. 5.8.

Table 5.2 Superheat of onset nucleate boiling on surfaces Type Ⅱ, Ⅲ, Ⅳ, Ⅴ, Ⅵ, and copper mirror Type Ⅰ.

Case	Superheat of ONB, ΔT (K)	q (kW/m^2)
Type Ⅰ	20.2	128.5
Type Ⅱ	2.94	37.0
Type Ⅲ	2.1	38.6
Type Ⅳ	2.6	33.2
Type Ⅴ	2.7	38.4
Type Ⅵ	2.5	36.5

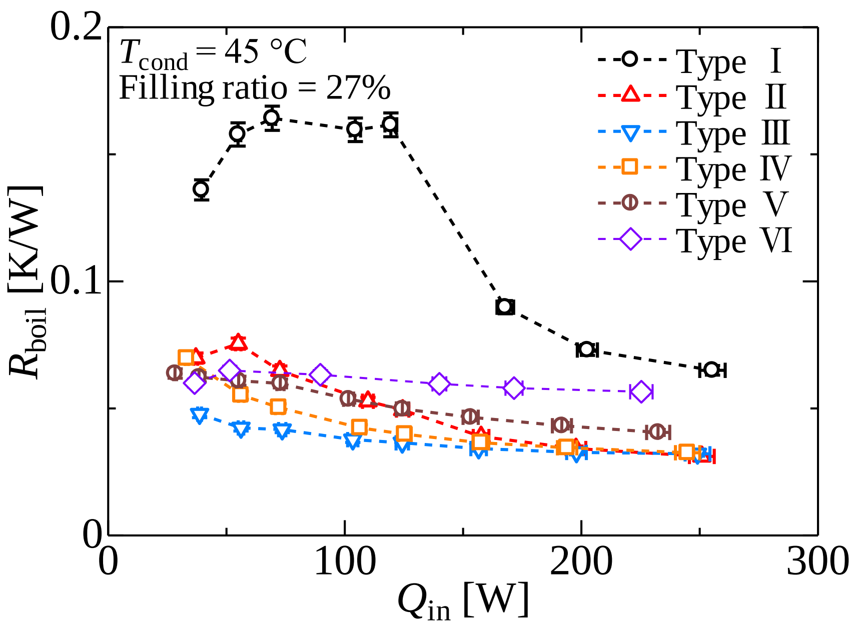

Fig. 5.4 Comparison of experimental results of Type Ⅰ – Type Ⅵ. The boiling thermal resistance R_{boil} vs. the heat input Q_{in}.

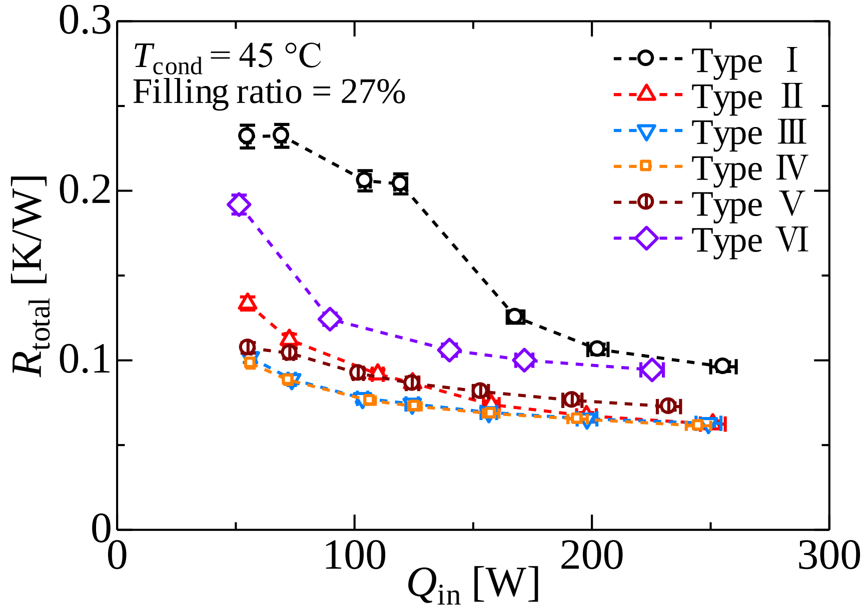

Fig. 5.5 Comparison of experimental results of Type Ⅰ – Type Ⅵ. The total thermal resistance R_{total} vs. the heat input Q_{in}.

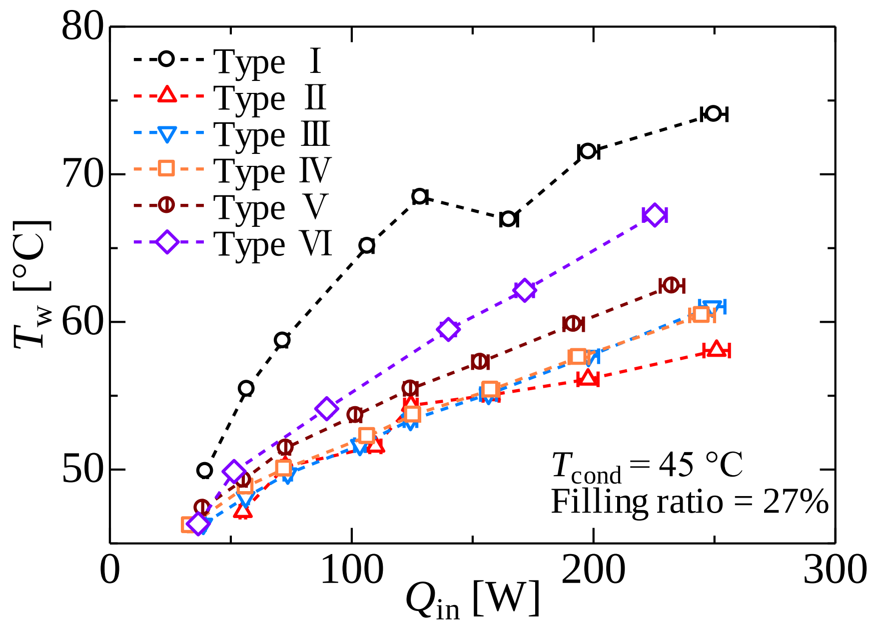

Fig. 5.6 Comparison of experimental results of Type Ⅰ – Type Ⅵ. The evaporator surface temperature T_w vs. the heat input Q_{in}.

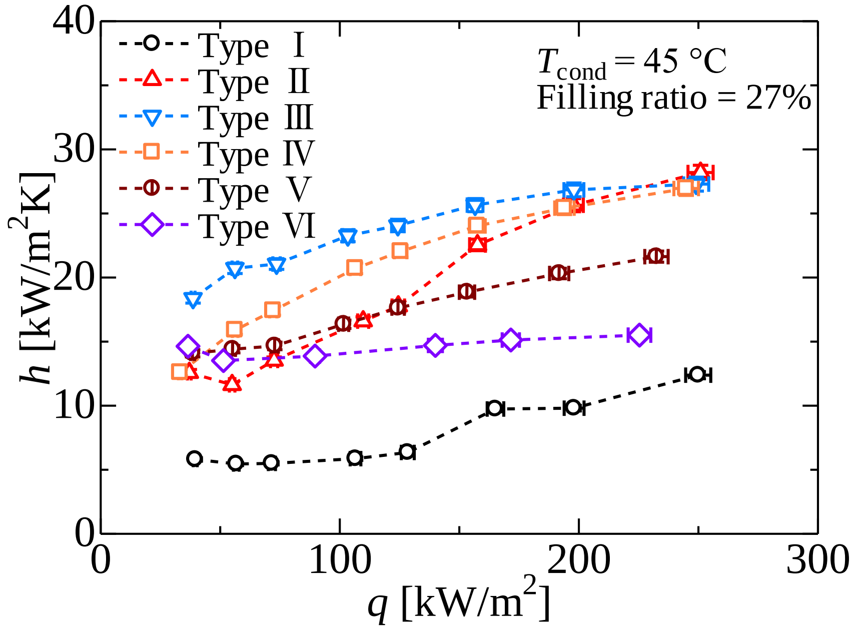

Fig. 5.7 Comparison of experimental results of Type Ⅰ – Type Ⅵ. The heat transfer coefficient of the evaporator h vs. the heat flux at the evaporator surface q.

5.2.2 Bubble behaviors

Ⅰ

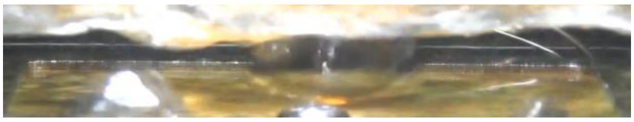

q = 119.5 kW/m^2, ΔT_{sat}=22.0 K, T_w=69.6 °C

Ⅱ

q = 124.5 kW/m^2, ΔT_{sat}=7.0 K, T_w=55.1 °C

Ⅲ

q = 124.3 kW/m^2, ΔT_{sat}=5.2 K, T_w=53.3 °C

Ⅳ

q = 125.4.8 kW/m^2, ΔT_{sat}=5.7 K, T_w=53.7 °C

Ⅴ

q = 124.4 kW/m^2, ΔT_{sat}=7.1 K, T_w=55.5 °C

Ⅵ

q = 139.9 kW/m^2, ΔT_{sat}=9.5 K, T_w=59.5 °C

Fig. 5.8 Bubble behaviors on surfaces Type Ⅰ – Type Ⅵ at heat flux of 130 kW/m^2. The operating pressure is 10 kPa, and FR = 27%.

The observations of the comparison bubble behaviors at 130 W heating powers are shown in Fig. 5.8. In the case of the uncoated surface Type Ⅰ, an incipient overshoot caused by the big and intermittent bubble is observed as the surface temperature drops suddenly after boiling starts, while it is suppressed on the hydrophobic spot coated surfaces. For the case of Type Ⅵ surface, due to the full covered hydrophobic materials, the whole surface is covered by the vapor film, and it results in the larger superheat. These bubbles do not depart from the surface, instead, forming a vapor film. A stable vapor film is observed, which influences the heat transfer efficiency of the surface.

5.3 Development status of thermosyphons

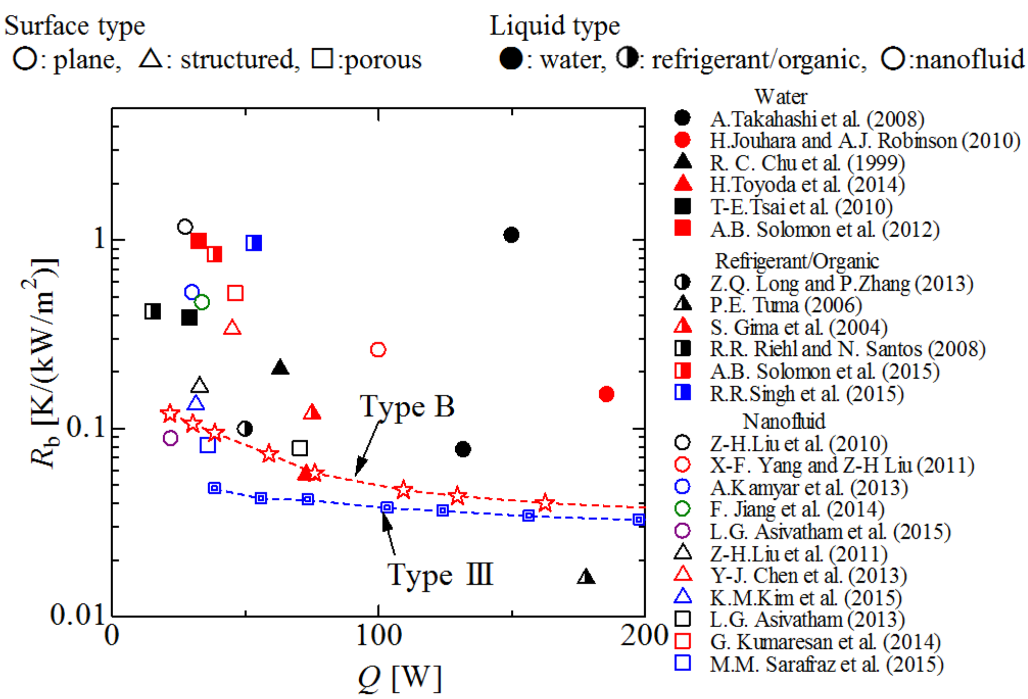

Fig. 5.9 Comparison of the boiling thermal resistances of different working fluids and surface designs [119 – 124].

The status of development of thermosyphons and heat pipes in recent years is shown in Fig. 5.9. As can be seen in the figure, compared with the results of the other researchers, we obtain one of the best resluts that match the highest thermal performance across all heat loads. By changing the diameter and pitch of the coated spots, we enhance the heat transfer coefficient by more than 10% compared with previous results we got.

We acknowledge that refrigerants are more appropriate for application where freezing could be a matter of concern. In this study, we only focus on the heat transfer aspect of heat pipe evaporator design. Refrigerants always give the lower boiling thermal resistance compared with other fluids such as water. From Fig. 5.9, we want to show that the boiling performance of mixed-wettability surface is much better than that of structured surface. For the working fluids, until now we only use water. In the future, we will try the other working fluids such as refrigerants.

5.4 Comparison of mixed-wettability surfaces

Photographs of the patterned surfaces used to compare with each other are shown in Fig. 5.10. They are Type B (HNTs coated), Type b (FDPA coated), and Type Ⅳ (Ni-PTFE) surfaces. All the surfaces are coated with hydrophobic spots of diameter 1 mm, pitch 3 mm. Type B and Type Ⅳ are copper mirror substrate, where is TiO_2 substrate for Type b surface. The contact angles of the hydrophobic spots range 145° – 150°. The experimental processes and conditions are same. Filling ratio is 27%, and condenser temperature is 45 °C.

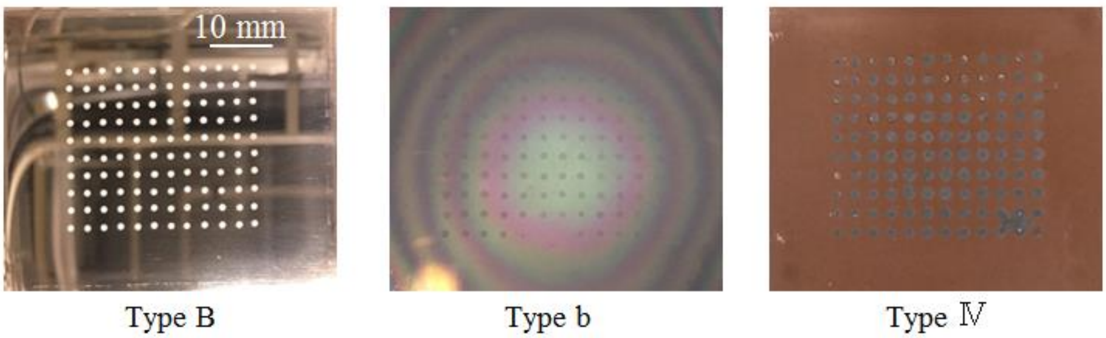

Fig. 5.10 Photographs of mixed-wettability surfaces, Type B, Type b, and Type Ⅳ. Diameter 1 mm, pitch 3 mm.

Fig. 5.11 shows that the boiling thermal resistance results of Type B, Type b, and Type Ⅳ surfaces at heating power from 30 W to 260 W. They decrease with the increasing of heater power due to the rising saturation temperature. As the heat flux increases, the number of nucleation site on the surface increases. For Type B and Type

Ⅳ surfaces, onset of nucleate boiling happen while the superheat is only 3 K, where is 6 K for Type b surface. From heat flux of 30 kW/m^2 to 70 kW/m^2, the boiling thermal resistance of Type Ⅳ surface is a little lower than that of Type B surface. This maybe because that there is existed gas in the structure of the surface after degasing process, inducing the nucleate boiling earlier.

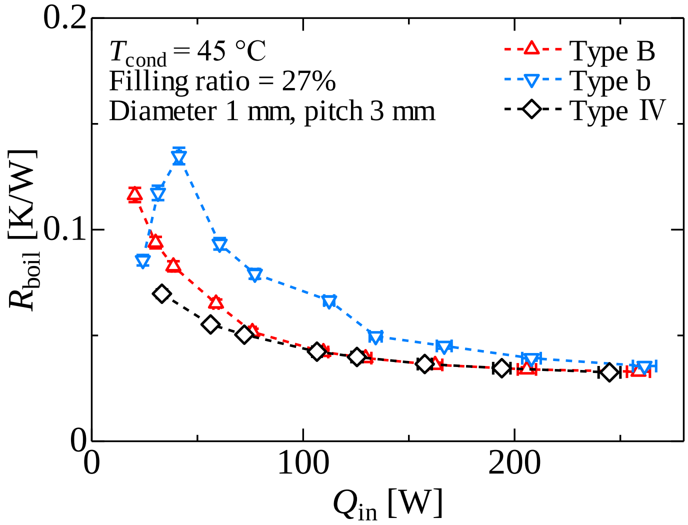

Fig. 5.11 Comparison of experimental results of Type B, Type b, and Type Ⅳ. The boiling thermal resistance R_{boil} vs. the heat input Q_{in}.

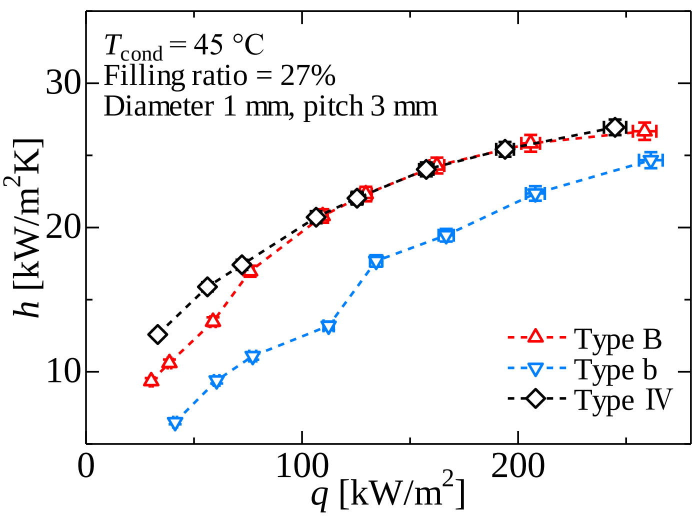

Fig. 5.12 Comparison of experimental results of Type B, Type b, and Type Ⅳ. The heat transfer coefficient of the evaporator h vs. the heat flux at the evaporator surface q.

The average heat transfer coefficient of Type b surface is less than half that of Type B and Type Ⅳ due to the stable durability of spots, as seen in Fig. 5.12. Although from the figures we can see the result of Type Ⅳ surface is better than that of others. But on the base of durability, onset of nucleate boiling, and coating process, we provide Type B (HNTs coated) surface is the best choice to be the evaporator surface of the loop thermosyphon.

5.5 Comparison with machined surface

5.5.1 Machined surface

In this part, we report a rather comprehensive comparison of the heat transfer performance of several structured and coated surfaces, which give the superior nucleated boiling phenomenon. Firstly, machined surface commercially used is introduced, as seen in Fig. 5.13. The three dimensions of this surface are 38 mm × 30 mm × 4 mm (triangle pores of 1 mm in depth). This kind of surface is easily produced by making oblique cuts with sharp rotating cutting tools from two directions. It has many saw-toothed fins. For this machined surface, it is easy to get onset of nucleate boiling at low heat flux owing to the trapped gas inside the cavities, which cannot be degased sufficiently before the experiment, as shown in Fig. 5.14.

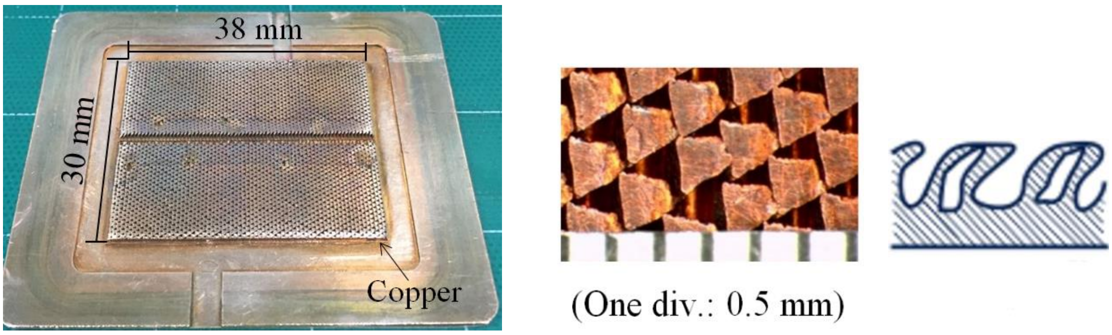

Fig. 5.13 Machined evaporator surface (38 mm × 30 mm × 4 mm).

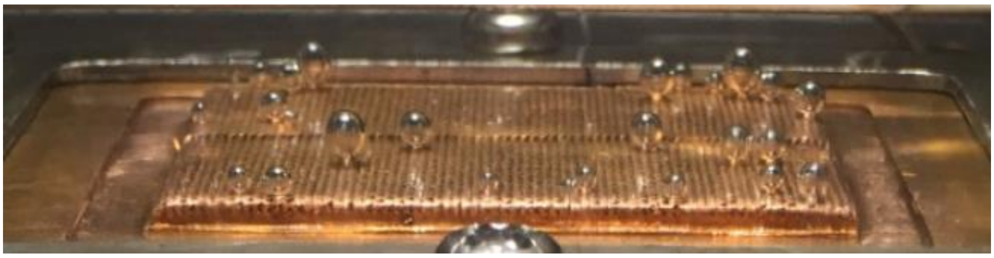

Fig. 5.14 Trapped gas in the machined surface after degassing.

5.5.2 Experimental results

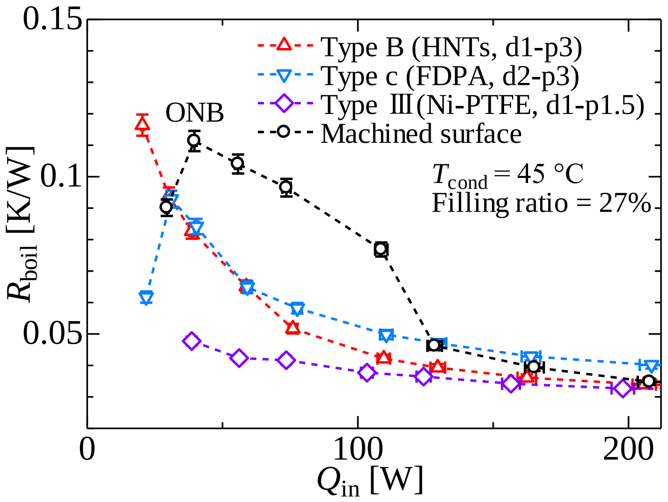

Fig. 5.15 Comparison of experimental results of Type B, Type c, Type Ⅲ, and machined surfaces. The boiling thermal resistance R_{boil} vs. the heat input Q_{in}.

From Fig. 5.15, the boiling thermal resistances of four surfaces are calculated and compared. The boiling and total thermal resistance decrease with the increasing of heater power due to the high pressure in the system and excellent boiling performance. As mentioned before, we are focusing on realizing an advanced boiling surface provides onset of nucleate boiling at extremely low superheating. During a large number of experiments, it is observed that the bubble is always much easier generated from hydrophobic spots coated surface than that of machined surface. When the heat flux is from 50 kW/m^2 to 130 kW/m^2, the boiling and total thermal resistances for patternned surfaces are much lower than the machined surface, reducd by 30% averagely. The heat transfer performance gets better for the machined surface due to the higher pressure and large surface area when the heat flux is from 130 kW/m^2.

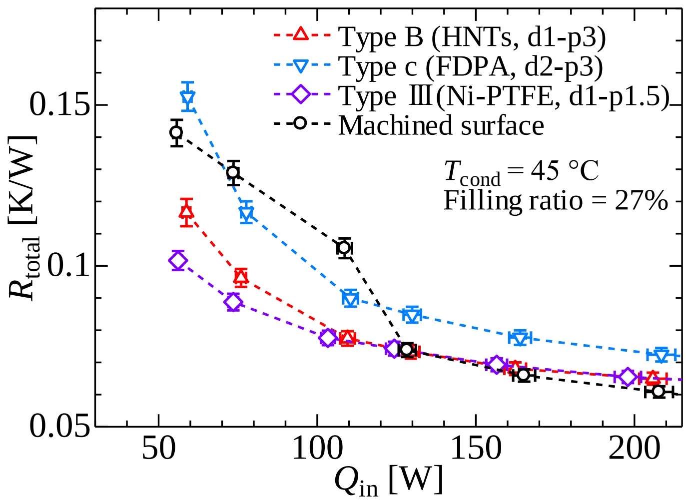

Fig. 5.16 Comparison of experimental results of Type B, Type c, Type Ⅲ, and machined surfaces. The total thermal resistance R_{total} vs. the heat input Q_{in}.

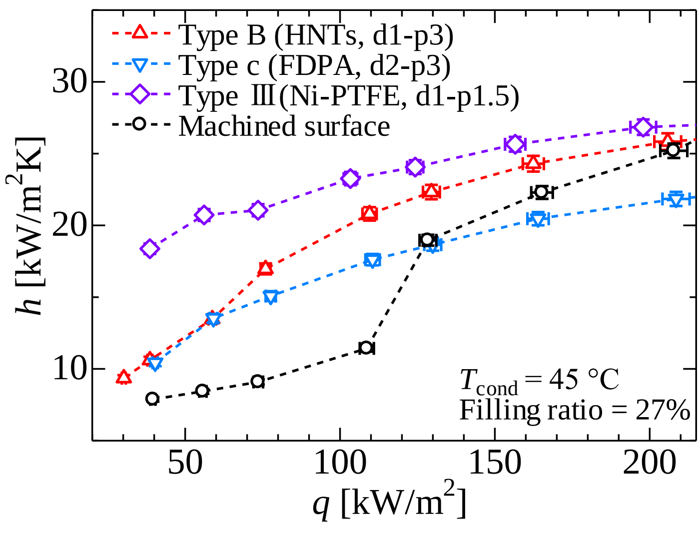

Fig. 5.17 Comparison of experimental results of surfaces Type B, Type c, Type Ⅲ, and machined. The heat transfer coefficient of the evaporator h vs. the heat flux at the evaporator surface q.

5.5.3 Bubble behaviors

The density of nucleation sites and size decide the heat transfer coefficient of the surface. Surfaces Type Ⅲ and Type B perform the excellent nucleate boiling performance resulting from more active sites on the surfaces, as seen in Fig. 5.18 and Fig. 5.19. For the hydrophobic spots coated surfaces in my experiments, superheating is only 4 – 6 K at a low heat flux of q = 110 kW/m^2, whereas it is 9.5 K for machined surface at the same heat flux. As seen in Fig. 5.16, the bubble behaviors of the surfaces at the heat flux 200 kW/m^2 are totally different. There are only 5 – 6 nucleation sits on the edge of the machined surface, and the nucleation sites are not fixed all the time.

Type-B

q = 109.5 kW/m^2, ΔT_{sat}=5.3 K, T_w=51.8 °C

Type-c

q= 110.5 kW/m^2, ΔT_{sat}=6.3 K, T_w=52.9 °C

Type-Ⅲ

q = 103.4 kW/m^2, ΔT_{sat}=4.4 K, T_w=51.7 °C

Machined surface

q = 108.7 kW/m^2, ΔT_{sat}=9.5 K, T_w=56.1 °C

Fig. 5.18 Bubble behaviors on surfaces Type-B, Type-c, Type-Ⅲ, and machined surface at heat flux of 110 kW/m^2. The operating pressure is 10 kPa, and FR = 27%.

Type-B

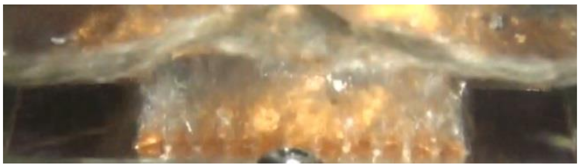

q = 205.8 kW/m^2, ΔT_{sat}=7.9 K, T_w=57.3 °C

Type-c

q= 208.5 kW/m^2, ΔT_{sat}=9.5 K, T_w=59.2 °C

Type-Ⅲ

q = 197.9 kW/m^2, ΔT_{sat}=7.4 K, T_w=57.7 °C

Machined surface

q = 207.8 kW/m^2, ΔT_{sat}=8.3 K, T_w=57.5 °C

Fig. 5.19 Bubble behaviors on surfaces Type-B, Type-c, Type-Ⅲ, and machined surface at heat flux of 200 kW/m^2. The operating pressure is 12 kPa, and FR = 27%.

Chapter 6 Conclusions and future work

6.1 Conclusions

The primary objective of thesis is to investigate the heat transfer performance of a two-phase loop thermosyphon with an enhanced mixed-wettability evaporator surface at sub-atmospheric pressures. For central-processing-unit (CPU) cooling applications, a lowering of the saturation temperature (pressure) is essential when water is used as the working fluid. Compared with copper mirror surfaces, up to over 100% enhancement of high heat transfer coefficient was observed using surfaces with spotted wettability patterns. Various measurements and experiments are performed to confirm the excellent heat transfer efficiency of the mixed-wettability surface.

In Chapter 1, the background and overview about heat pipe cooling systems such as conventional heat pipe, loop heat pipe, pulsating heat pipe, conventional thermosyphon, and loop thermosyphon are presented based on literature reviews. The previous study is also reviewed and the current results of this thesis are pointed out for understanding the development situation of heat pipes. Furthermore, the influence factors of heat pipes are analysed, including the working fluids, structured surface, pressure, and wettability of the surface. The theoretical models for predicting the heat transfer performance of heat pipes are carried out through reviewing the literatures.

In Chapter 2, the detailed description of the apparatus and evaporator surface of the loop thermosyphon are presented. Experimental procedure and operating principle in this two-phase loop thermosyphon are clarified. Hydrophobic material is used to be patterned on the copper mirror surface, forming a mixed-wettability surface. The temperature measurements of every part and the thermocouple positions are shown in the schematic figure. In addition, the detailed analysis of the data calculation method is discussed.

In Chapter 3, extensive experimental results are presented to confirm the advanced heat transfer coefficient of mixed-wettability evaporator surface. HNTs solution is used as the hydrophobic material. The pattern of coating on the surface comprises hydrophobic spots with three different sizes. A parametric analysis of the heat transfer performance under various heat inputs, filling ratios, and condensation temperatures has been performed. Heat loss and durability of the coating material are also indicated. The experimental result is in agreement with Li's model. The following findings are also obtained.

(1) Mixed-wettability surfaces show much better boiling heat transfer performance due to the steady and continuous bubble behavior compared with the copper mirror surface. The maximal reduction of the surface temperature is 17 K.

(2) For the patterned surfaces, the nucleate boiling performance is enhanced as the spot diameter decreases.

(3) Two condenser conditions (35 °C and 45 °C) are studied. The total thermal resistance at the condenser temperature of T_{in} = 45 °C is reduced by 35% to 65% compared with that of 35 °C.

(4) An increasing filling ratio enlarges the saturation pressure and temperature of the system significantly, and results in excellent nucleate boiling.

(5) The optimum system performance occurs when the Type-B surface is applied under the conditions of Q_{in} =150 W – 260 W and FR = 27%. Boiling thermal resistance is as low as 0.03 K/W with a corresponding total thermal resistance of 0.057 K/W.

(6) For the durability test, there is not a distinct difference between the 1st run and 2nd run using the same coating surface.

(7) At low heat flux, Q_{loss} is occupied averagely more than 50%, where it is less than 30% at high heat flux.

In Chapter 4, measurement and calculation results of the FDPA coated mixed-wettability surfaces are presented. TiO_2 surface with small contact angle can provide a very high critical heat flux. Three patterns of surfaces are presented, diameter 1 mm and 2 mm with pitch 3 mm, and full cover pattern, for comparing with plain surface. The main findings are as follows:

(1) Hydrophobic spots patterned surfaces reduce the boiling and total thermal resistance more than 60% averagely compared with that of a plain surface.

(2) Durability and stability of FDPA material are not as well as HNTs due to more inactive spots during the experiments and worse bubble nucleation performance.

(3) Filling ratio test is carried out. The optimal filling ratio on FDPA coated surface is very agreement with that of HNTs coating test. The optimal filling ratio is 27%.

In Chapter 5, the evaporator surfaces coated with a pattern of hydrophobic circle spots (Ni-PTFE) through non-electroplating is proposed (0.5 – 2 mm in diameter and 1.5 – 3 mm in pitch). The detailed coating process is indicated. By comparing among six different patterned surfaces, the heat transfer coeffiicient of patternned surface is enhanced by more than 200% averagely compared to that of mirro surface. The contrasting bubble behaviors are shown in this chapter clearly. Comparison between our best results and machined surface is presented. The obtained results are as follows:

(1) Based on the results of boiling thermal resistance, total thermal resistance, and heat transfer coefficient, hydrophobic spots patterned surfaces are proved a promising way for heat transfer enhancement.

(2) A large density of spots coated on a given surface area provides more opportunities for the bubble nucleation sites, especially at low heat flux.

(3) Small diameter spots (< 1 mm) on the surface cannot get nucleate boiling at low heat flux (saturation pressure) easily, but getting better at higher heat flux.

(4) Hydrophobic spots coated surface is considered as an advanced boiling surface, which provides onset of nucleate boiling at extremely low superheating, about 2 K.

(5) Results of comparison among the mixed-wettability surfaces coated by three different materials are discussed. All the spots are diameter 1, pitch 3 mm. Although the boiling thermal resistance of Ni-PTFE coated surface is lower than the other two surfaces. On the base of durability and onset of nucleate boiling performance, HNTs coated surface is recommended to be the first candidate to be used on the thermosyphon.

(6) Compared with machined surface, our mixed-wettability surface improves the heat transfer coefficient by 100% averagely, from 30 W to 200 W, and avoids the temperature oscillation at onset of nucleate boiling.

As an overall conclusion, this study presents an experimental investigation of the heat transfer performance of a closed two-phase thermosyphon with an enhanced evaporator surface. Coated with a pattern of hydrophobic spots surface is shown to increase heat transfer coefficient and lower the incipience temperature overshoot. One of the best results on heat transfer efficiency is achieved using water as the working fluid. The present study contributes to provide a design aspect for the cooling system of electronic devices.

6.2 Future work

Until now, the advanced mixed-wettability surface has been carried out as the evaporator surface of this loop thermosyphon, and one of the best results has been achieved. In the future, hydrophobic spots coated on structured surface, for instance, finned surface will be tried due to the large heat transfer area, which is very advantageous for providing more nucleation sites on a given surface. We also understand the importance of CHF in assessing the practical use of heat pipes. The CHF measurement of the present loop thermosyphon will be done in the near future. In the present study, the experimental maximal heat flux is much lower than CHF. Rather, we are focusing on lowering the threshold of boiling on the evaporator, thus ensuring reliable activation of the loop thermosyphon below the safe operating temperature of CPU (< 80 °C).

For the condenser part, in the present apparatus, the time for starting the circulation of the thermosyphon is a little bit longer compared with that of other researches because of the large amount of existed liquid in the condenser. To improve this issue, offset fin structured condenser will be applied instead of cooling tube. It not only speeds up the transient response, but also simulates the air cooling application in the data center, as shown in Fig. 6.1. It has cost advantage and simple production process. This finned structure must be very practical and very promising to reduce the total thermal resistance of the system.

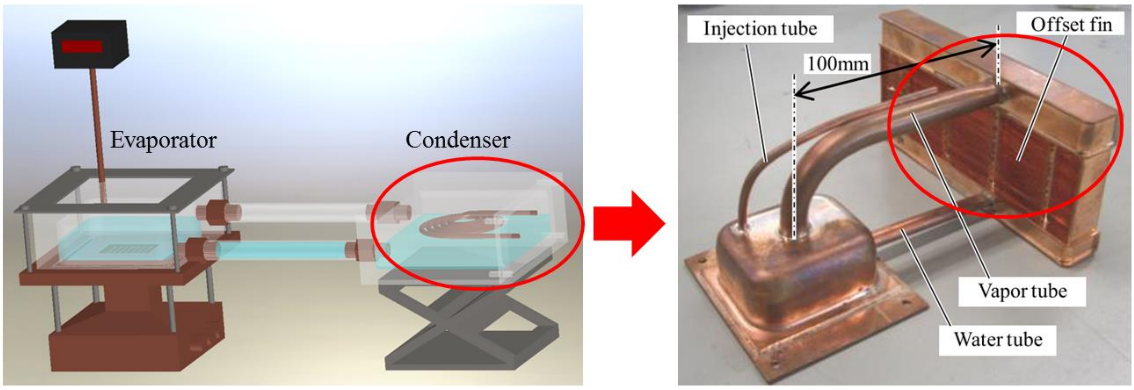

Fig. 6.1 Condenser of cooling tube and offset fin structure.

References

[1] S.H. Noie, "Heat transfer characteristics of a two-phase closed thermosyphon," *Appl. Therm.Eng.*, vol. 25, pp. 495–506, 2005.

[2] P.E. Tuma, "Evaporator/boiler design for thermosyphons utilizing segregated hydrofluoroether working fluids, " *Prooceedings of the 22th IEEE SEMI-THERM Symposium*, pp. 69–77, 2006.

[3] L.L. Vasiliev, "Heat pipes in modern heat exchangers," *Appl. Therm. Eng*., vol. 25, pp. 1–19, 2005.

[4] R.L. Webb, "Test results on a thermo-syphon concept to high-power cool desktopcomputers and servers," Eighteenth Annu. *IEEE Semicond. Therm. Meas. Manag. Symp. Proc*., pp. 151–158, 2002.

[5] R. Khodabandeh, "Thermal performance of a closed advanced two-phase thermosyphon loop for cooling of radio base stations at different operating conditions," *Appl. Therm. Eng.*, vol. 24, no. 17–18, pp. 2643–2655, 2004.

[6] L. G. Asirvatham, R. Nimmagadda, and S. Wongwises, "Heat transfer performance of screen mesh wick heat pipes using silver-water nanofluid," *Int. J. Heat Mass Transf.*, vol. 60, no. 1, pp. 201–209, 2013.

[7] Y.J. Chen, P.Y. Wang, Z.-H. Liu, and Y.-Y. Li, "Heat transfer characteristics of a new type of copper wire-bonded flat heat pipe using nanofluids," *Int. J. Heat Mass Transf.*, vol. 67, pp. 548–559, 2013.

[8] M. a. Chernysheva, S. I. Yushakova, and Y. F. Maydanik, "Effect of external factors on the operating characteristics of a copper–water loop heat pipe," *Int. J. Heat Mass Transf.*, vol. 81, pp. 297–304, 2015.

[9] T. Jaipurkar, P. Kant, S. Khandekar, B. Bhattacharya, and S. Paralikar, "Thermo-mechanical design and characterization of flexible heat pipes," *Appl. Therm. Eng.*, vol. 1, pp. 1–10, 2017.

[10] G. Kumaresan, S. Venkatachalapathy, and L. G. Asirvatham, "Experimental investigation on enhancement in thermal characteristics of sintered wick heat pipe using CuO nanofluids," *Int. J. Heat Mass Transf.*, vol. 72, pp. 507–516, 2014.

[11] J. Li, D. Wang, and G. P. Peterson, "Experimental studies on a high performance compact loop heat pipe with a square flat evaporator," *Appl. Therm. Eng.*, vol. 30, no.

6–7, pp. 741–752, 2010.

[12] A. S. Sundaram, "Thermal Modeling of Thermosyphon Integrated Heat Sink for CPU Cooling," *J. Electron. Cool. Therm. Control*, vol. 1, no. 2, pp. 15–21, 2011.

[13] S. Appliqu and T. Kanpur, "Overview of heat pipe studies during the period 2010-2015," *Interfacial Phenomena and Heat Transfer*. pp. 33–53, 2016.

[14] Y.F. Maydanik, "Loop heat pipes," *Appl. Therm. Eng.*, vol. 25, pp. 635–657, 2005.

[15] Y.F. Maydanik, S. V. Vershinin, M. a. Korukov, and J. M. Ochterbeck, "Miniature loop heat pipes - A promising means for cooling electronics," *IEEE Trans. Components Packag. Technol.*, vol. 28, no. 2, pp. 290–296, 2005.

[16] K. N. Shukla, "Heat Pipe for Aerospace Applications-An Overview," *J. Electron. Cool. Therm. Control*, vol. 5, no. March, pp. 1–14, 2015.

[17] V. G. Pastukhov and Y. F. Maydanik, "Low-noise cooling system for PC on the base of loop heat pipes," *Appl. Therm. Eng.*, vol. 27, no. 5–6, pp. 894–901, 2007.

[18] B. Verma, V. L. Yadav, and K. K. Srivastava, "Experimental Studies on Thermal Performance of a Pulsating Heat Pipe with Methanol/DI Water," *Scientific Research.*, pp. 27–34, 2013.

[19] H. Yang, S. Khandekar, and M. Groll, "Operational limit of closed loop pulsating heat pipes," *Appl. Therm. Eng.*, vol. 28, no. 1, pp. 49–59, 2008.

[20] L. M. Poplaski, S. P. Benn, and A. Faghri, "Thermal performance of heat pipes using nanofluids," *Int. J. Heat Mass Transf.*, vol. 107, pp. 358–371, 2017.

[21] J. R. Hartenstine, R. W. B. Iii, and J. R. Montgomery, "Loop thermosyphon design for cooling of large area, High Heat Flux Sources," *Proc. IPACK2007*, pp. 1–8, 2007.

[22] M. A. Chan, C. R. Yap, and K. C. Ng, "Modeling and testing of an advanced compact two-phase cooler for electronics cooling," *Int. J. Heat Mass Transf.*, vol. 52, no. 15–16, pp. 3456–3463, 2009.

[23] M. M. Sarafraz, F. Hormozi, and S. M. Peyghambarzadeh, "Role of nanofluid fouling on thermal performance of a thermosyphon: Are nanofluids reliable working fluid?," *Appl. Therm. Eng.*, vol. 82, pp. 212–224, 2015.

[24] Y. F. Maydanik, M. a. Chernysheva, and V. G. Pastukhov, "Review: Loop heat pipes with flat evaporators," *Appl. Therm. Eng.*, vol. 67, no. 1–2, pp. 294–307, 2014.

[25] V. G. Pastukhov and Y. F. Maydanik, "Active coolers based on copper-water LHPs for desktop PC," *Appl. Therm. Eng.*, vol. 29, no. 14–15, pp. 3140–3143, 2009.

[26] J. Li, D. Wang, and G. P. Bud Peterson, “A compact loop heat pipe with flat square evaporator for high power chip,” *IEEE Transactions on Components and Packaging Technologies*, vol. 1, no. 4. 2011.

[27] R. R. Riehl and N. dos Santos, “Loop heat pipe performance enhancement using primary wick with circumferential grooves,” *Appl. Therm. Eng.*, vol. 28, no. 14–15, pp. 1745–1755, 2008.

[28] D. Butler, J. Ku, and T. D. Swanson, “Loop heat pipes and capillary pumped loops-an applications perspective,” *AIP Conf. Proc.*, vol. 608, pp. 49–56, 2002.

[29] Z. Xiong, C. Ye, M. Wang, and H. Gu, “Experimental study on the sub-atmospheric loop heat pipe passive cooling system for spent fuel pool,” *Prog. Nucl. Energy*, vol. 79, pp. 40–47, 2015.

[30] J. Li and L. Lv, “Performance investigation of a compact loop heat pipe with parallel condensers,” *Exp. Therm. Fluid Sci.*, vol. 62, pp. 40–51, 2015.

[31] B. S. Taft, A. D. Williams, and B. L. Drolen, “Review of pulsating heat pipe working fluid selection,” *J. Thermophys. Heat Transf.*, vol. 26, no. 4, pp. 651–656, 2012.

[32] Y. Zhang and A. Faghri, “Advances and unsolved issues in pulsating heat pipes,” *Heat Transf. Eng.*, vol. 29, no. 1, pp. 20–44, 2008.

[33] M. B. Shafii, A. Faghri, and Y. Zhang, “Thermal modeling of unlooped and looped pulsating heat pipes,” *J. Heat Transfer*, vol. 123, no. 6, p. 1159, 2001.

[34] V. Tsoi, S. W. Chang, K. F. Chiang, and C. C. Huang, “Thermal performance of plate-type loop thermosyphon at sub-atmospheric pressures,” *Appl. Therm. Eng.*, vol. 31, no. 14/15, pp. 2556–2567, 2011.

[35] S. W. Chang and C. Y. Lin, “Thermal performance improvement with scale imprints over boiling surface of two-phase loop thermosyphon at sub-atmospheric conditions,” *Int. J. Heat Mass Transf.*, vol. 56, no. 1–2, pp. 294–308, 2013.

[36] M. Karthikeyan, S. Vaidyanathan, and B. Sivaraman, “Heat transfer analysis of two phase closed thermosyphon using aqueous solution of n-butanol,” *International Journal of Engineering and Technology*, vol. 3, no. 6, pp. 661–667, 2013.

[37] H. Shabgard, B. Xiao, A. Faghri, R. Gupta, W. Weissman, “Thermal characteristics of a closed thermosyphon under various filling conditions,” *Int. J. Heat Mass Transf*. vol. 70, pp. 91–102, 2014.

[38] R. C. Chu, R. E. Simons, and G. M. Chrysler, “Experimental investigation of an

enhanced thermosyphon heat loop for cooling of a high performance electronics module," *IEEE Semi-Therm Symp.*, pp. 1–9, 1999.

[39] C. a. Pappas, P. M. De Cecchis, D. a. Jordan, and P. M. Norris, "The effect of fill volume on heat transfer from air-cooled thermosyphons," *J. Heat Transfer*, vol. 135, no. 4, pp. 044–504, 2013.

[40] T.E. Tsai, H.H. Wu, C.C. Chang, S.L. Chen, "Two-phase closed thermosyphon vapor-chamber system for electronic cooling," *Heat Mass Transf*. vol. 37, pp. 484–489, 2010.

[41] A. Pal, Y. K. Joshi, M. H. Beitelmal, C. D. Patel, and T. M. Wenger, "Design and performance evaluation of a compact thermosyphon," *Components Packag. Technol.*, vol. 25, no. 4, pp. 601–607, 2002.

[42] Y. F. Maydanik, V. I. Dmitrin, and V. G. Pastukhov, "Two-Phase loop thermosyphons," *Proceedings of the VIII Int. Seminar*, vol. 1, pp. 144–154, 2011.

[43] R. Renjith Singh, V. Selladurai, P. K. Ponkarthik, and A. B. Solomon, "Effect of anodization on the heat transfer performance of flat thermosyphon," *Exp. Therm. Fluid Sci.*, vol. 68, pp. 574–581, 2015.

[44] H. Reeot, P. J. Lid, M. Takuma, and M. Groll, "Annular closed two phase thermosyphon with small fill rates," *Heat Recovery System*, vol. 7, no. 4, pp. 319–327, 1987.

[45] H. Farsi, J.-L. Joly, M. Miscevic, V. Platel, and N. Mazet, "An experimental and theoretical investigation of the transient behavior of a two-phase closed thermosyphon," *Appl. Therm. Eng.*, vol. 23, no. 15, pp. 1895–1912, 2003.

[46] L. G. Asirvatham, S. Wongwises, and J. Babu, "Heat Transfer Performance of a Glass Thermosyphon Using Graphene-Acetone Nanofluid," *J. Heat Transfer*, vol. 137, no. 11, pp. 111-502, 2015.

[47] H. Jouhara and A. J. Robinson, "Experimental investigation of small diameter two-phase closed thermosyphons charged with water, FC-84, FC-77 and FC-3283," *Appl. Therm. Eng.*, vol. 30, no. 2–3, pp. 201–211, 2010.

[48] Y. J. Park, H. K. Kang, and C. J. Kim, "Heat transfer characteristics of a two-phase closed thermosyphon to the fill charge ratio," *Int. J. Heat Mass Transf.*, vol. 45, pp. 4655–4661, 2002.

[49] Z. Q. Long and P. Zhang, "Impact of cooling condition and filling ratio on heat transfer limit of cryogenic thermosyphon," *Cryogenics (Guildf).*, vol. 52, no. 1, pp. 66–76, 2012.

[50] X. F. Yang and Z. H. Liu, "Application of Functionalized Nanofluid in Thermosyphon.," *Nanoscale Res. Lett.*, vol. 6, no. 1, pp. 494, 2011.

[51] Z. Q. Long and P. Zhang, "Heat transfer characteristics of thermosyphon with N2-Ar binary mixture working fluid," *Int. J. Heat Mass Transf.*, vol. 63, pp. 204–215, 2013.

[52] A. Samba, H. Louahlia-Gualous, S. Le Masson, and D. Nörterhäuser, "Two-phase thermosyphon loop for cooling outdoor telecommunication equipments," *Appl. Therm. Eng.*, vol. 50, no. 1, pp. 1351–1360, 2013.

[53] Kapitanchuk I.I., "Development of evaporating cooling systems," *Voprosy Radioelectroniki.*, no. 2, pp. 69–74, 1967.

[54] W. Qu, "Hydrodynamics of Two-Phase Loop Thermosyphon," *Front. Heat Pipes*, vol. 1, no. 2, pp. 1–7, 2010.

[55] K. Shung-Wen, T. Meng-Chang, H. Chih-Sheng, and C. Jian-You, "Thermal Performance of a Loop Thermosyphon," *Tamkang J. Sci. Eng.*, vol. 13, no. No. 3, pp. 281–288, 2010.

[56] J. E. Hart, "A new analysis of the closed loop thermosyphon," *Int. J. Heat Mass Transf.*, vol. 27, no. 1, pp. 125–136, 1984.

[57] M. Hirashima, K. Kawabata, and K. Negishi, "Experimental study on a separate type thermosyphon," *Environment*, vol. 9, pp. 479–486, 1994.

[58] H. Bieliński and J. Mikielewicz, "Natural circulation in single and two phase thermosyphon loop with conventional tubes and minichannels," *Heat Transfer - Mathematical Modelling, Numerical Methods and Information Technology 19*, pp. 475–496, 2011.

[59] H. Imura, K. Sasaguchi, H. Kozai, and S. Numata, "Critical heat flux in a closed two-phase thermosyphon," *Int. J. Heat Mass Transf.*, vol. 26, no. 8, pp. 1181–1188, 1983.

[60] H. Louahlia-Gualous, S. Le Masson, and A. Chahed, "An experimental study of evaporation and condensation heat transfer coefficients for looped thermosyphon," *Appl. Therm. Eng.*, vol. 110, pp. 931–940, 2017.

[61] S. Woei, K. Feng, and C. Yuan, "Loop thermosyphon electronic cooling device operated at sub-atmospheric pressure," *10th IHPS*, pp. 158–166, 2011.

[62] J. Li, F. Lin, and G. Niu, "An insert-type two-phase closed loop thermosyphon for split-type solar water heaters," *Appl. Therm. Eng.*, vol. 70, no. 1, pp. 441–450, 2014.

[63] P. Zhang, B. Wang, W. Shi, and X. Li, "Experimental investigation on two-phase

thermosyphon loop with partially liquid-filled downcomer," *Appl. Energy*, vol. 160, pp. 10–17, 2015.

[64] C. C. J. Vincent and J. B. W. Kok, "Investigation of the overall transient performance of the industrial two-phase closed loop thermosyphon," *Int. J. Heat Mass Transf.*, vol. 35, no. 6, pp. 1419–1426, 1992.

[65] Y. Takata, S. Hidaka, M. Kohno, "Enhanced nucleate boiling by superhydrophobic coating with checkered and spoted patterns," *Int. J. Air-Cond. Ref.* vol. 20, 2006.

[66] J. Kim, "Review of nucleate pool boiling bubble heat transfer mechanisms," *Int. J. Multiph. Flow*, vol. 35, no. 12, pp. 1067–1076, 2009.

[67] P. K. Tewari, R. K. Verma, M. P. S. Ramani, D. Division, B. Atomic, A. Chatterjee, and S. P. Mahajan, "Nucleate boiling at atmospheric in a thin film on a horizontal tube and subatmospheric pressures," *Int. J. Heat Mass Transf.*, vol. 32, no. 4, pp. 723–728, 1989.

[68] S.J.D. VAN Stralen, "Heat transfer to boiling binary liquid mixtures subatmospheric pressures at atmospheric," *Chemical Engineering Science*., vol. 5, no. 4, pp. 290–296, 1956.

[69] S. J. D. VAN. Stralen, R. Cole, W. M. Sluyter, M. S. Sohalt, and T. Section, "Bubble Growth Rates in Nucleate," *Int. J. Heat Mass Transf.*, vol. 18, pp. 655–669, 1975.

[70] W. R. McGillis, J. S. Fitch, W. R. Hamburgen, and V. P. Carey, "Pool boiling enhancement techniques for water at low pressure," *WRL Research Report*, p. 33, 1990.

[71] B. D. Marcus, "Theory and design of variable conductance heat pipes," Report No. CR-2018(NASA. Washington, DC), 1972.

[72] A. Niro and G. P. Beretta, "Boiling regimes in a closed two-phase thermosyphon," *Int. J. Heat Mass Transf.*, vol. 33, no. 10, pp. 2099–2110, 1990.

[73] R. Khodabandeh and B. Palm, "Influence of system pressure on the boiling heat transfer coefficient in a closed two-phase thermosyphon loop," *International Journal of Thermal Sciences*, vol. 41, no. 7. pp. 619–624, 2002.

[74] M. Shiraishi, K. Kikuchi, and T. Yamanishi, "Investigation of heat transfer characteristicx of a two-phase closed thermosyphon," *Journal of Heat Recovery Systems*, vol. 1, pp. 287–297, 1981.

[75] S. S. Nam, S. B. Choi, J. H. Kim, and H. Y. Kwak, "Transient Characteristics of a Two-Phase Thermosyphon Loop for Multichip Module," *ETRI J.*, vol. 20, no. 3, pp. 284–299,

1998.

[76] P. Zhang, X. Li, S. Shang, W. Shi, and B. Wang, "Effect of Height Difference on the Performance of Two-phase Thermosyphon Loop Used in Air-conditioning System," *International Refrigeration and Air Conditioning Conference*, pp. 1–10, 2014.

[77] G. L. Morrison and C. M. Sapsford, "Long Term Performance of Thermosyphon Solar Water Heaters," *Test*, vol. 30, no. 4, pp. 341–350, 1983.

[78] T. Sukchana and N. Pratinthong, "A two-phase closed thermosyphon with an adiabatic section using a flexible hose and R-134a filling," *Exp. Therm. Fluid Sci.*, vol. 77, pp. 317–326, 2016.

[79] S. S. Panse and S. G. Kandlikar, "A thermosiphon loop for high heat flux removal using flow boiling of ethanol in OMM with taper," *Int. J. Heat Mass Transf.*, vol. 106, pp. 546–557, 2016.

[80] A. D. Patil and R. B. Yarasu, "Factors Affecting the Thermal Performance of Two Phase Closed Thermosyphon : A Review," *Int. J. Emerg. Technol. Adv. Eng.*, vol. 2, no. 9, pp. 202–206, 2012.

[81] A. Kamyar, K. S. Ong, and R. Saidur, "Effects of nanofluids on heat transfer characteristics of a two-phase closed thermosyphon," *Int. J. Heat Mass Transf.*, vol. 65, pp. 610–618, 2013.

[82] A. Amiri, R. Sadri, M. Shanbedi, G. Ahmadi, B. T. Chew, S. N. Kazi, and M. Dahari, "Performance dependence of thermosyphon on the functionalization approaches: An experimental study on thermo-physical properties of graphene nanoplatelet-based water nanofluids," *Energy Convers. Manag.*, vol. 92, pp. 322–330, 2015.

[83] Z. h. Liu, X. f. Yang, G. s. Wang, and G. liang Guo, "Influence of carbon nanotube suspension on the thermal performance of a miniature thermosyphon," *Int. J. Heat Mass Transf.*, vol. 53, no. 9–10, pp. 1914–1920, 2010.

[84] F. Jiang, W. J. Chen, Z. Liu, J. T. Shi, and X. L. Li, "Heat transfer enhancement in a three-phase closed thermosyphon," *Appl. Therm. Eng.*, vol. 65, no. 1–2, pp. 495–501, 2014.

[85] H. S. Xue, J. R. Fan, Y. C. Hu, R. H. Hong, and K. F. Cen, "The interface effect of carbon nanotube suspension on the thermal performance of a two-phase closed thermosyphon," *J. Appl. Phys.*, vol. 100, no. 10, pp. 1–6, 2006.

[86] I.C. Bang, S. H. Chang, "Boiling heat transfer performance and phenomena of Al_2O_3–water nano-fluids from a plain surface in a pool," *Int. J. Heat Mass Transf.* vol. 48, pp. 2407–2419, 2005.

[87] S. Khandekar, Y. M. Joshi, and B. Mehta, "Thermal performance of closed two-phase thermosyphon using nanofluids," *Int. J. Therm. Sci.*, vol. 47, no. 6, pp. 659–667, 2008.

[88] S. H. Noie, S. Z. Heris, M. Kahani, and S. M. Nowee, "Heat transfer enhancement using Al2O3/water nanofluid in a two-phase closed thermosyphon," *Int. J. Heat Fluid Flow*, vol. 30, no. 4, pp. 700–705, 2009.

[89] G. Huminic and A. Huminic, "Heat transfer characteristics of a two-phase closed thermosyphons using nanofluids," *Exp. Therm. Fluid Sci.*, vol. 35, no. 3, pp. 550–557, 2011.

[90] M. H. Buschmann and U. Franzke, "Improvement of thermosyphon performance by employing nanofluid," *Int. J. Refrig.*, vol. 40, pp. 416–428, 2014.

[91] Z. H. Liu, Y. Y. Li, and R. Bao, "Compositive effect of nanoparticle parameter on thermal performance of cylindrical micro-grooved heat pipe using nanofluids," *Int. J. Therm. Sci.*, vol. 50, no. 4, pp. 558–568, 2011.

[92] A. B. Solomon, R. Roshan, W. Vincent, V. K. Karthikeyan, and L. G. Asirvatham, "Heat transfer performance of an anodized two-phase closed thermosyphon with refrigerant as working fluid," *Int. J. Heat Mass Transf.*, vol. 82, pp. 521–529, 2015.

[93] C. Ramaswamy, Y. Joshi, W. Nakayama, and W. B. Johnson, "High-speed visualization of boiling from an enhanced structure," *Int. J. Heat Mass Transf.*, vol. 45, no. 24, pp. 4761–4771, 2002.

[94] S. Gima, T. Nagata, X. Zhang, and M. Fujii, "Experimental study on CPU cooling system of closed-Loop two-phase thermosyphon," vol. 34, no. 3, pp. 147–159, 2005.

[95] H. Toyoda and Y. Kondo, "Heat transfer performance of loop thermosyphon using enhanced boiling and condensation surfaces," *Transaction on Control and Mechanica Systems*, pp. 432–435, 2013.

[96] M. Zhang, Z. Liu, and G. Ma, "The experimental investigation on thermal performance of a flat two-phase thermosyphon," *Int. J. Therm. Sci.*, vol. 47, no. 9, pp. 1195–1203, 2008.

[97] J. Yeo, S. Yamashita, M. Hayashida, and S. Koyama, "A loop thermosyphon type cooling system for high heat flux," *Journal of Electronics Cooling and Thermal Control*,

vol. 1, pp. 128–137, 2014.

[98] A. Pal and Y. Joshi, "Boiling at sub-atmospheric conditions with enhanced structures," *Therm. Thermomechanical Proc. 10th Intersoc. Conf. Phenom. Electron. Syst. 2006. ITHERM 2006.*, pp. 620–629, 2006.

[99] Y. Takata, S. Hidaka, M. Masuda, T. Ito, "Pool boiling on a superhydrophilic surface," *Int. J. Energy Res*., Vol. 27, pp. 111–119, 2003.

[100] Y. Takata, S. Hidaka, T. Uraguchi, "Boiling feature on a super water-repellent surface," *Heat Transf. Eng*., vol. 27, pp. 25–30, 2006.

[101] K.M. Kim, Y.S. Jeong, I.G. Kim, I.C. Bang, "Comparison of thermal performances of water-filled, SiC nanofluid-filled and SiC nanoparticles-coated heat pipes," *Int. J. Heat Mass Transf.*, vol. 88, pp. 862–871, 2015.

[102] J. C. Wang, "3-D numerical and experimental models for flat and embedded heat pipes applied in high-end VGA card cooling system," *Int. Commun. Heat Mass Transf.*, vol. 39, no. 9, pp. 1360–1366, 2012.

[103] S. Lips and F. Lefèvre, "A general analytical model for the design of conventional heat pipes," *Int. J. Heat Mass Transf.*, vol. 72, pp. 288–298, 2014.

[104] R. Ranjan, A. Patel, S. V. Garimella, and J. Y. Murthy, "Wicking and thermal characteristics of micropillared structures for use in passive heat spreaders," *Int. J. Heat Mass Transf.*, vol. 55, no. 4, pp. 586–596, 2012.

[105] B. Siedel, V. Sartre, and F. Lefèvre, "Literature review: Steady-state modelling of loop heat pipes," *Appl. Therm. Eng.*, vol. 75, pp. 709–723, 2015.

[106] B. Siedel, V. Sartre, and F. Lefèvre, "Complete analytical model of a loop heat pipe with a flat evaporator," *Int. J. Therm. Sci.*, vol. 89, pp. 372–386, 2015.

[107] L. Mottet, T. Coquard, and M. Prat, "Three dimensional liquid and vapor distribution in the wick of capillary evaporators," *Int. J. Heat Mass Transf.*, vol. 83, pp. 636–651, 2015.

[108] Kaled, A., Dutour, S., Platel, V., Lachassagne, L., Ayel, V., "A theoretical analysis of the transient behavior of a CPL for terrestrial application," *16th International Heat Pipe Conference.*Lyon, France, 2012.

[109] M. Nishikawara, H. Nagano, and T. Kaya, "Transient thermo-fluid modeling of loop heat pipes and experimental validation," *J. Thermophys. Heat Transf.*, vol. 27, no. 4, pp. 641–647, 2013.

[110] J. Qu and Q. Wang, "Experimental study on the thermal performance of vertical closed-

loop oscillating heat pipes and correlation modeling," *Appl. Energy*, vol. 112, pp. 1154–1160, 2013.

[111] Z. Lin, S. Wang, R. Shirakashi, and L. Winston Zhang, "Simulation of a miniature oscillating heat pipe in bottom heating mode using CFD with unsteady modeling," *Int. J. Heat Mass Transf.*, vol. 57, no. 2, pp. 642–656, 2013.

[112] A. M. Khudhair, S. A. K. Razack, and S. Al-Hallaj, "A review on phase change energy storage, materials and applications," *Energy Convers. Manag.*, vol. 45, no. 9–10, pp. 1597–1615, 2004.

[113] H. Li, X. Zhu, H. Zhou, S. Zhong, "Functionalization of halloysite nanotubes by enlargement and hydrophobicity for sustained release of analgesic," *Eng. Asp.* vol. 487, pp. 154–161, 2015.

[114] F. Giraud, R. Rulliere, C. Toublanc, M. Clausse, J. Bonjour, "Experimental evidence of a new regime for boiling of water at subatmospheric pressure," *Exp. Therm. Fluid Sci.* vol. 60, pp. 45–53, 2014.

[115] K.N. Rainey, S.M. You, S. Lee, Effect of Pressure, "Subcooling, and Dissolved Gas on Pool Boiling Heat Transfer From Microporous Surfaces in FC-72," *J. Heat Transfer.* vol. 125, pp. 75, 2003.

[116] Y. Y. Li, Y. J. Chen, and Z. H. Liu, "A uniform correlation for predicting pool boiling heat transfer on plane surface with surface characteristics effect," *Int. J. Heat Mass Transf.*, vol. 77, pp. 809–817, 2014.

[117] S. H. Noie, M. R. Sarmasti Emami, and M. Khoshnoodi, "Effect of Inclination Angle and Filling Ratio on Thermal Performance of a Two-Phase Closed Thermosyphon under Normal Operating Conditions," *Heat Transf. Eng.*, vol. 28, pp. 365–371, 2007.

[118] B. Jiao, L. M. Qiu, X. B. Zhang, and Y. Zhang, "Investigation on the effect of filling ratio on the steady-state heat transfer performance of a vertical two-phase closed thermosyphon," *Appl. Therm. Eng.*, vol. 28, no. 11–12, pp. 1417–1426, 2008.

[119] L. G. Asirvatham, S. Wongwises, and J. Babu, "Heat Transfer Performance of a Glass Thermosyphon Using Graphene–Acetone Nanofluid," *J. Heat Transfer*, vol. 137, no. 11, p. 111502, 2015.

[120] A. B. Solomon, K. Ramachandran, and B. C. Pillai, "Thermal performance of a heat pipe with nanoparticles coated wick," *Appl. Therm. Eng.*, vol. 36, no. 1, pp. 106–112, 2012.

[121] F. Jiang, W. J. Chen, Z. Liu, J. T. Shi, and X. L. Li, "Heat transfer enhancement in a three-phase closed thermosyphon," *Appl. Therm. Eng.*, vol. 65, no. 1–2, pp. 495–501, 2014.

[122] R. R. Riehl and N. dos Santos, "Loop heat pipe performance enhancement using primary wick with circumferential grooves," *Appl. Therm. Eng.*, vol. 28, no. 14–15, pp. 1745–1755, 2008.

[123] H. Jouhara and A. J. Robinson, "Experimental investigation of small diameter two-phase closed thermosyphons charged with water, FC-84, FC-77 and FC-3283," *Appl. Therm. Eng.*, vol. 30, no. 2–3, pp. 201–211, 2010.

[124] L. G. Asirvatham, R. Nimmagadda, and S. Wongwises, "Heat transfer performance of screen mesh wick heat pipes using silver-water nanofluid," *Int. J. Heat Mass Transf.*, vol. 60, no. 1, pp. 201–209, 2013.

Acknowledgements

I would like to take this opportunity to express my gratitude to all the people who have ever helped me during my doctoral period. Firstly, my sincere thanks and appreciations go first to my supervisor, ***Professor Takata***, for taking me in his laboratory as a Ph.D. student. It has been a great privilege and joy to study under his guidance and supervision. I also really appreciate to ***Professor Xing Zhang*** for his recommendation and help.

I am also deeply indebted to ***Professor Kohno***, for his instructive advice and useful suggestions on my experiments during the seminar. I express my deep appreciation to ***Ms. Shuto*** for her kind help in my study life.

I express my deep thanks to my dissertation committee members, ***Professor Kohno*** and ***Professor Takahashi*** for their invaluable time and advice.

Especially, I really appreciate to ***Dr. Hidaka*** for designing and improving the apparatus of loop thermosyphon.

I would like to express my gratitude to ***Dr. Biao Shen*** for his help and patience on my experiment and published paper. He spent much time reading through each draft and provided me with inspiring advice. I am indebted to ***Dr. Daniel***, ***Dr. Alex***, ***Dr. Kuroki***, ***Dr. Harish***, ***Dr. Yutaka***, for giving me many good advices on my study.

I wish to express my warm thanks to members of Thermofluid Physics Laboratory. ***Mr. Yamada*** and ***Mr. Furusato*** helped me a lot on my experimental study of thermosyphon.

I would like to thank my family for their support and understanding. Especially to my wife ***Jie Li***, who introduced me to Professor Takata. I am grateful having you always by my side.

Lastly, I gratefully acknowledge to I^2CNER and Hydrogen Energy System for giving me the opportunity to work as a research assistant.

Fukuoka, July 2017

Hongbin He

Appendix

A.1 Filling ratio above 32%

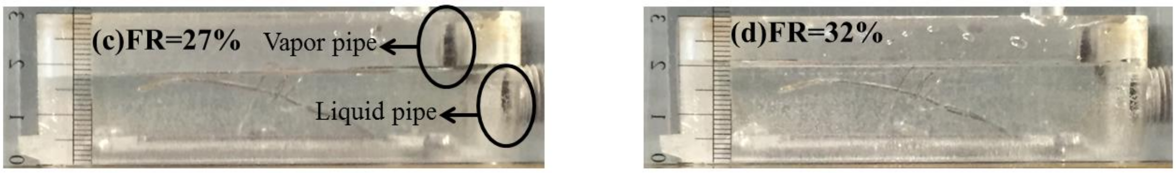

Fig. A.1. The liquid levels of FR = 27% and FR = 32%.

From the figure of liquid level in the filling ratio of FR = 27% and FR = 32%, we can see that they correspond to liquid levels of 18 mm and 19.5 mm in Fig. A.1. The difference of liquid level in the boiling chamber is not obvious (within 1.5 mm). Besides, in the case of FR = 32%, there is a certain quantity of liquid occupying the vapor pipe. With increasing liquid levels, the effect of flooding of the vapor pipe becomes significant. We have performed experiments using a copper surface coated with hydrophobic spots (diameter = 1 mm, pitch = 3 mm). The results show deterioration of heat transfer beyond FR = 32%, as shown in Fig. A.2. The deterioration of the boiling performance is clearly visible due to the space limitation of the boiling chamber and the seriously blocked vapor pipe.

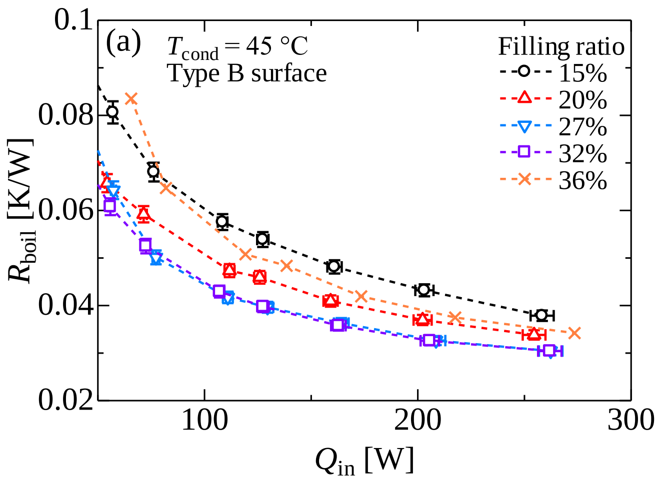

Fig. A.2. Comparison of the boiling thermal resistances, vs. Q_{in} at different filling ratios.

In this experiment, different filling ratios translate to different pressures in the boiling chamber. As we know, there is a correlation between pressure and bubble departure diameter. With the increase of pressure, the bubble departure diameter decreases. However, for filling ratio changes from FR = 15% to FR = 32%, the pressure difference is only 2 kPa, which has a limited effect on the bubble departure diameter.

A.2 Condensation heat transfer coefficient

The heat transfer coefficient in the condenser section is generally predicted by Nusselt's theory for filmwise condensation,

$$R_e = \frac{\rho V D}{\mu} \tag{A.1}$$

Here ρ is the liquid density, V is flow rate, D is the diameter of the tube, μ is dynamic viscosity. Gnielinski correlation is as follows,

$$Nu = \frac{(f/8)(R_{eD} - 1000)P_r}{1 + 12.7(f/8)^{1/2}\left(P_r^{2/3} - 1\right)} \tag{A.2}$$

Here f is the Darcy friction factor,

$$f = \left(0.79\ln(R_{eD}) - 1.64\right)^{-2} \tag{A.3}$$

The Gnielinski correlation is valid for

$0.5 \le P_r \le 2000$

$3000 \le R_{eD} \le 5\times10^{6}$

Nusselt number is presented by

$$Nu = \frac{h_{liquid} D}{k} \tag{A.4}$$

Condensation heat transfer rate is calculated by

$$Q_{cond} = h_{total} \cdot A \cdot \Delta T_{lm} \tag{A.5}$$

$$T_{lm} = \frac{\Delta T_1 - \Delta T_2}{\ln\left(\frac{\Delta T_1}{\Delta T_2}\right)} \tag{A.6}$$

T_1 and T_2 are the inlet and outlet temperature. Experimental data can be calculated by

$$\frac{1}{h_{total}} = \frac{1}{h_{liquid}} \cdot \frac{1}{h_{tube}} \tag{A.7}$$

Film-wise condensation calculation,

$$h_{\mathrm{mod}el} = 0.729 \left[\frac{k_l^{\ 3} \rho_l^{\ 2} g L_{lv}}{\mu_l (T_{sat} - T_w) d} \right]^{1/4} \tag{A.8}$$

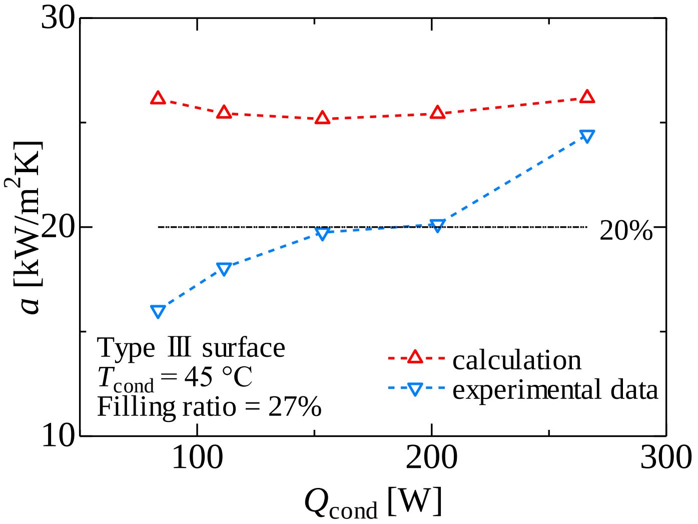

Fig. A.3. Comparison of the experimental condensation HTC with the prediction by the correlation.

The comparison of the experimental result and theoretical prediction for the condensation heat transfer coefficient at various heat input is shown in Fig. A.3. Due to the larger heat loss at low heat transfer rate (< 150 W), the relative error is higher than 20%. The temperature difference between the vapor and the condenser tube is very small, about 1K or 2 K. When the heat transfer rate is larger than 150 W, the error is within 20%.